AD NUMBER

**ADB032496**

NEW LIMITATION CHANGE

TO

**Approved for public release, distribution unlimited**

FROM

**Distribution authorized to U.S. Gov't. agencies only; Test and Evaluation; 27 DEC 1978. Other requests shall be referred to Commanding Officer, Naval Ocean Research and Development Activity, Attn: Code 600, NSTL Station, MS 39529.**

AUTHORITY

**CNO/N772 ltr N772A/6U875630 20 Jan 2006 & ONR ltr 31 Jan 2006**

LEVEL II

# NOSC

NOSC TR 276

NOSC TR 276



**Technical Report 276**

# COMBINED ACOUSTIC PROPAGATION IN EASTPAC REGION (EXERCISE CAPER): INITIAL ACOUSTIC ANALYSIS

MA Pedersen
RF Hosmer

June 1978

Research and Development Report: January - November 1977

Prepared for

Naval Ocean Research and Development Activity



NAVAL OCEAN SYSTEMS CENTER
SAN DIEGO, CALIFORNIA 92152

NAVAL OCEAN SYSTEMS CENTER, SAN DIEGO, CA 92152

AN ACTIVITY OF THE NAVAL MATERIAL COMMAND

RR GAVAZZI, CAPT, USN
Commander

HL BLOOD
Technical Director

## ADMINISTRATIVE INFORMATION

During August 1974 the Marine Physical Laboratory (MPL), the Naval Ocean Systems Center (NOSC), and the Hawaii Institute of Geophysics (HIG) conducted deepwater acoustic experiments off the coast of Southern California. These experiments are known as the Combined Acoustic Propagation in Eastpac Region (CAPER) Exercise. Exercise CAPER was supported by the Long Range Acoustic Propagation Project (LRAPP).

This report presents the initial acoustic analysis of CAPER. The work was conducted under Program Element 63795N, LRAPP Research Project 710119, (NOSC 730426). This report represents the completion of the NOSC analysis and modelling support for FY77, funded as Task 7 by LRAPP and entitled "Project CAPER Analysis." The report covers work from January to November 1977 and was approved for publication on 1 June 1978.

The assistance of all contributors who made Exercise CAPER a success is gratefully acknowledged. In particular the authors acknowledge the collaboration of G. B. Morris of MPL in designing the exercise. In addition the pre-exercise critique and recommendations made by J. S. Hanna, then of the Acoustic Environmental Support Detachment, were instrumental in improving the original design.

Released by
MR AKERS, Head
Systems Concepts and
Analysis Division

Under authority of
HA SCHENCK, Head
Undersea Surveillance
Department

UNCLASSIFIED

SECURITY CLASSIFICATION OF THIS PAGE (When Data Entered)

## REPORT DOCUMENTATION PAGE

READ INSTRUCTIONS BEFORE COMPLETING FORM

1. REPORT NUMBER: NOSC/TR-276
2. GOVT ACCESSION NO.
3. RECIPIENT'S CATALOG NUMBER

4. TITLE (and Subtitle): COMBINED ACOUSTIC PROPAGATION IN EASTPAC REGION (EXERCISE CAPER): INITIAL ACOUSTIC ANALYSIS

5. TYPE OF REPORT & PERIOD COVERED: Research and Development rept, January-November 1977

6. PERFORMING ORG. REPORT NUMBER

7. AUTHOR(s): M A Pedersen, R F Hosmer

8. CONTRACT OR GRANT NUMBER(s)

9. PERFORMING ORGANIZATION NAME AND ADDRESS: Naval Ocean Systems Center, San Diego, CA 92152

10. PROGRAM ELEMENT, PROJECT, TASK AREA & WORK UNIT NUMBERS: 63795N, LRAPP Project 710119

11. CONTROLLING OFFICE NAME AND ADDRESS: Naval Ocean Research and Development Activity, Code 600, NSTL Station, MS 29529

12. REPORT DATE: June 1978

13. NUMBER OF PAGES: 70

14. MONITORING AGENCY NAME & ADDRESS (if different from Controlling Office)

15. SECURITY CLASS. (of this report): Unclassified

15a. DECLASSIFICATION/DOWNGRADING SCHEDULE

Distribution limited to U.S. Gov't agencies only; Test and Re... 27 Dec 1978. Other requests for this document must be referred to ...

DISTRIBUTION STATEMENT (of this Report)

~~Distribution limited to initial recipients.~~ Other requests for this document must be referred to the Naval Ocean Research and Development Activity, Code 600, NSTL Station, MS 39529.

12 76p.

17. DISTRIBUTION STATEMENT (of the abstract entered in Block 20, if different from Report)

18. SUPPLEMENTARY NOTES

19. KEY WORDS (Continue on reverse side if necessary and identify by block number)

Underwater sound propagation
Acoustic ranging
Satellite navigation
Seamount shadowing
Sound-speed profiles

20. ABSTRACT (Continue on reverse side if necessary and identify by block number)

This report presents an initial acoustic assessment of Exercise CAPER, which was conducted during August 1974 in an area about 830 km west of San Diego, California. The principal objective of this exercise was to measure experimentally the interference of CW signals caused by a well-surveyed isolated seamount, in this case Stoddard Seamount. The report discusses the planning phase of the exercise as well as three major areas of analysis. The first area is the convolution of ray diagrams with the bathymetry of the seamount in order to delineate the shadow zones formed behind the seamount. The second area is the detailed comparison of acoustic ranges and satellite navigation ranges. The third area is to assess the effect of range-dependent profiles as measured on CAPER. →

DD FORM 1 JAN 73 1473 EDITION OF 1 NOV 65 IS OBSOLETE
S/N 0102-014-6601

UNCLASSIFIED
SECURITY CLASSIFICATION OF THIS PAGE (When Data Entered)

393 159

88 12 18 143

20. (Continued)

The design and execution of the various seamount shadowing runs well satisfy the goals of the exercise. The major effect of the seamount is to intercept the leading portion of the convergence zones.

Comparison of the differences between 52 acoustic and satellite ranges showed a mean difference of 117 m with a standard deviation of 272 m. The maximum difference was -726 m, while 88 percent of the differences fell within ±866 m.

There was propagation through four distinct near-surface water masses. A comparison of ray calculations for a single profile appropriate for the receiver with calculations utilizing all four profiles demonstrated the importance of horizontal change. Range differences of as much as 13.2 km were calculated for the eighth convergence zone. Sound speeds within 18 km of the seamount peak were about 0.22 m/sec higher than in the surrounding ocean for depths from 1000 to 2500 m. However the impact of this on acoustic propagation was nil, with estimated range differences of less than 200 m.

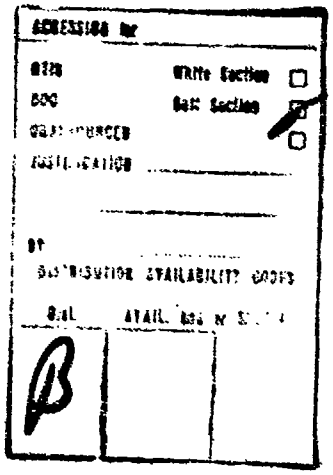

## SUMMARY

### PROBLEM

Make an initial acoustic assessment of exercise CAPER utilizing acoustic measurements and supporting environmental data. There are three major efforts in this assessment. The first is to convolve ray diagrams with the bathymetry of the seamount in order to delineate the shadow zones formed behind the seamount. The second is to make a detailed comparison of acoustic ranges and satellite navigation ranges. The third is to assess the effect of range-dependent sound-speed profiles (measured on CAPER) by a comparison with results of range-independent profiles.

### RESULTS

1. This initial acoustic assessment of CAPER demonstrates that the exercise was well conceived, planned, and executed and warrants further detailed analysis.

2. The design and execution of the various seamount shadowing runs well satisfy the goals of the exercise. The major effect of the seamount is to intercept the leading portion of the convergence zones.

3. Comparison of the differences between 52 acoustic and satellite ranges showed a mean difference of 117 m with a standard deviation of 272 m. The maximum difference was -726 m, while 88 percent of the difference fell within ±366 m. Statistical tests show no significant difference between the accuracy of ranges at satellite fixes and the accuracy of ranges interpolated between fixes.

4. There was propagation through four distinctive near-surface water masses. Comparison of ray calculations for a single profile appropriate for the receiver water mass were made with calculations which utilized all four profiles. The leading edge of the eighth convergence zone differed by 13.2 km, illustrating the importance of horizontal change in profile. Sound speeds within 18 km of the seamount peak were about 0.22 m/sec higher than in the surrounding ocean for depths from 1000 to 2500 m. However the impact of this on acoustic propagation was nil, with estimated range differences of less than 200 m.

### RECOMMENDATIONS

1. Further analysis of the CAPER data should be considered in the areas of comparison with sophisticated propagation loss models, evaluation of the surface decoupling effect, and investigation of the mechanisms of backscattering and reflection from a seamount slope.

2. Dispense with acoustic ranging on sea tests and rely upon careful satellite navigation unless range accuracies better than ±450 m are required.

3. The composite method of treating horizontal change in sound-speed profiles should be compared with more rigorous methods.

4. In experiments where the effect of seamounts or ridges is critical, the deep sound-speed profile should be well sampled to determine modification due to bathymetry.

5. Use a latitude-dependent geodetic parameter rather than the nominal 60 nautical miles per degree of latitude in calculating ranges based on satellite fixes since the accuracy of these fixes warrants use of this refinement.

## CONTENTS

## INTRODUCTION

During 21-31 August 1974 the Marine Physical Laboratory (MPL) of the University of California at San Diego, the Naval Undersea Center (NUC), now Naval Ocean Systems Center (NOSC), and the Hawaii Institute of Geophysics (HIG) of the University of Hawaii conducted deepwater acoustic experiments about 830 km west of San Diego, California. These experiments were conducted under the Long Range Acoustic Propagation Project (LRAPP) sponsorship and were called Exercise CAPER (Combined Acoustic Propagation in EASTPAC Region).

The objectives and test plan are discussed in detail in Ref. 1. The primary objective of the exercise was to measure experimentally the interference of CW signals caused by a well-surveyed seamount. Other objectives were to provide ambient sea-noise data, to investigate surface decoupling effects, and to obtain data in surface duct transmission characteristics.

This report is concerned only with the seamount-shadowing phase of the exercise, which is illustrated schematically in Fig. 1. Figure 1 is taken from Ref. 1 and presents the planned CW source tracks as they relate to the general bathymetry of the exercise. The receiving vessel, R/V FLIP (MPL), was to be emplaced with a three-point moor at 33°41′N, 125°28′W. The acoustic signals were projected from the source ship, the USNS DE STEIGUER, which proceeded along the tracks of Fig. 1. Run A was designed to open from FLIP, pass directly over Stoddard Seamount (peak estimated at 31°47′N, 126°17′W) at a range of about 225 km, and to continue to a maximum range of about 440 km. Run C was designed as an unobstructed closing run, covering the range interval from about 400 to 165 km. Runs D, E and B were traverses designed to measure the shadowing effect as the line of acoustic propagation cut across the deeper slopes of the seamount as well as across the peak. The center of Runs D, E, and B were designed to be about 27, 51, and 181 km, respectively, behind the peak of the seamount. Runs D and B represent geometries of predicted maximum shadowing, whereas Run E represents a geometry of predicted minimum shadowing.

The major objective of the report is to delineate the shadow zones formed behind the seamount, using ray theory together with measured bathymetry and sound-speed profiles as inputs. A second objective is the comparison of ranges obtained from measurements of acoustic travel time to ranges obtained from satellite navigation. A third objective is to assess the effect of range-dependent sound-speed profiles.

The remainder of the introduction is divided into two sub-sections. The first section treats the exercise planning phase while the second section discusses the execution phase and the supporting environmental data which is available in previous publications.

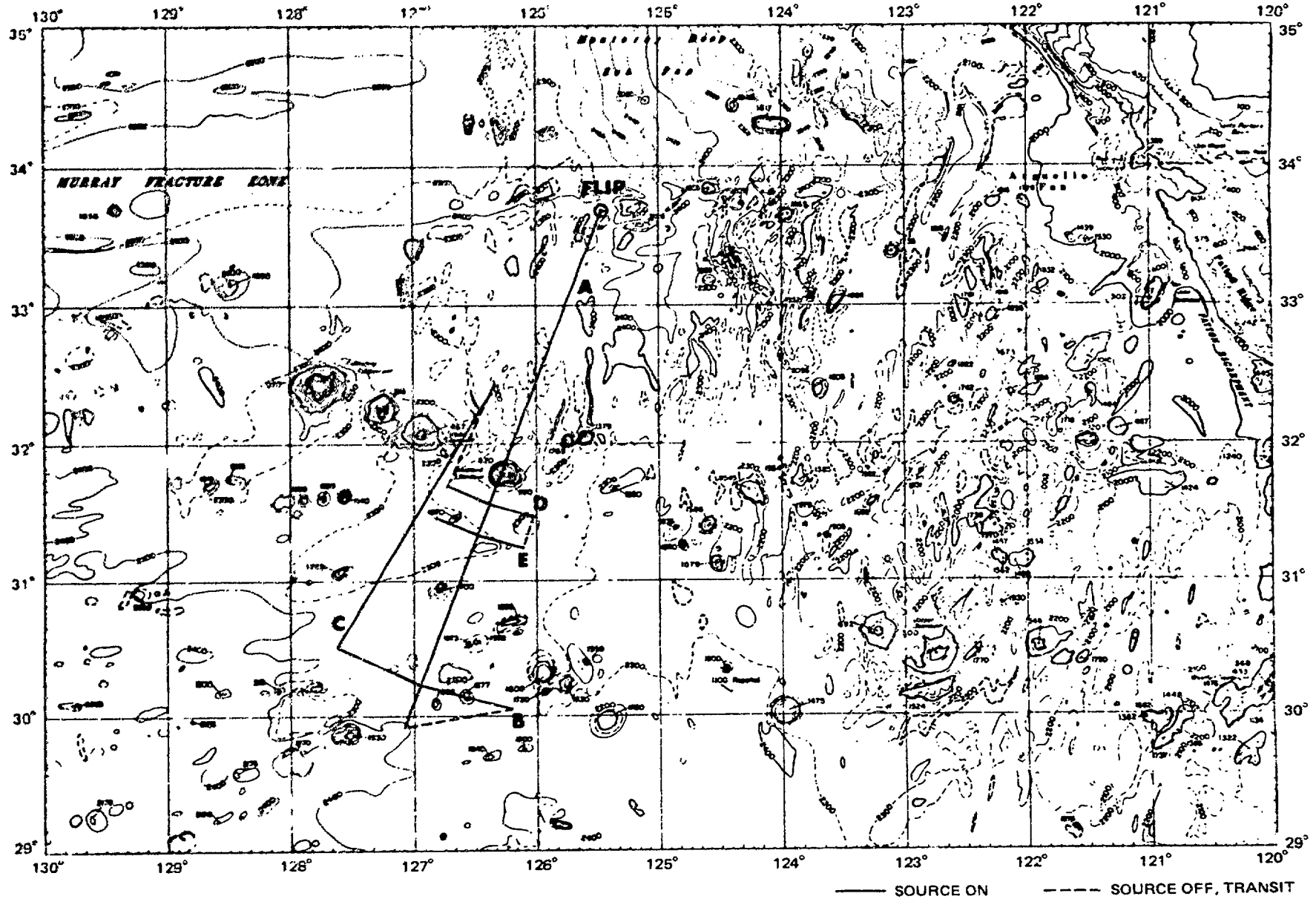


Figure 1. CW source tracks for the seamount shadowing experiment.

## EXERCISE PLANNING

A vital part of any major exercise is the planning phase. This phase is often inadequate and, even if adequate, is generally not presented in reports. We have chosen to be more explicit here because this phase was particularly important and evolved over a period of 6 months with inputs from many people.

The first task in planning was to select a suitable seamount. The general area for the FLIP moor was dictated by a requirement to provide ambient sea-noise data to supplement that taken during the CHURCH ANCHOR Exercise. The general area was chosen to have sufficient depth excess and to not lie directly on major shipping routes, where ships passing nearby would contaminate the measurements. Roughly speaking, FLIP was to be moored in an area bounded by 33–34°N and 125–126°W. On the basis of Fig. 1 the authors and Dr. G. B. Morris of MPL (the Chief Scientist of the exercise) examined the four seamounts lying about 220 km to the southwest of the FLIP mooring area. These all appeared as good initial candidates since there was little evidence of important bathymetric features between them and the FLIP location.

The center two seamounts were judged to be less desirable than Fieberling Tablemount or Stoddard Seamount. These center seamounts are closer together and we wished to minimize the possibility of out-of-plane reflections off a second seamount when shadowed by the seamount chosen for crossing. Fieberling Tablemount then became first choice because it was better surveyed than Stoddard.

The next step was to construct the ray diagram of Fig. 2 for the proposed source depths of 91 m and for a sound-speed profile appropriate for the area and season. The bottom profile across the peak of Stoddard Seamount (Fieberling Tablemount will be addressed later) was determined from the best bathymetric chart available and plotted on the scale of Fig. 2 at three locations: D, E, and B, with the seamount peak at ranges of 27, 55, and 183 km. These were the prospective ranges of the centers of the traverse runs D, E, and B of Fig. 1. As can be seen, all rays are intercepted by the seamount at positions D and B, whereas all rays clear the seamount at position E.

The next step was to determine at what range FLIP should be located from the peak of the seamount. This range was selected to be 224 km. The ranges of FLIP corresponding to the center of Runs D, E, and B are shown in Fig. 2 by the dashed vertical lines. There were to be 20 hydrophones on FLIP with the shallowest at a depth of 98 m and the deepest at a depth 4340 m. The 224-km position of FLIP was chosen so that on traverse D the entire set of hydrophones would be ensonified, once the traverse completely cleared the seamount. This would also be true of traverse B except for hydrophones deeper than 3840 m. On traverse E, hydrophones deeper than 3060 m would not be ensonified. This latter limitation was not regarded as serious because there would be enough hydrophones to determine that at position E there was no interference by the seamount. On the other hand it was felt more important that on traverse D, all hydrophones could receive the source if not blocked by the seamount.

We turn now to the question of Fieberling Tablemount, which was selected as first choice for the shadowing experiment. Figure 3 shows Fieberling centered at position E on the first position of the ray diagram of Fig. 2. The width at the top is about 7 km. There is no source range relative to Fieberling that would allow any rays to pass over without at least one bottom reflection. The problem is that Fieberling is not an ordinary seamount, but rather a guyot, i.e., a mountain that at some stage of history was planed off by wave action. Indeed if we extrapolate the side slopes of Fieberling, they intersect about 225 m above sea

level. Thus the effect on acoustic propagation by Fieberling is more like that of an island rather than a seamount. For this reason Fieberling was rejected and Stoddard was selected.

The discussion thus far represents the status of planning at the time of the April 1974 LRAPP site visit. The site visit team, particularly John Hanna, then of the Acoustic Environmental Support Detachment (AESD), had a number of reservations and suggestions as to the exercise plan.

The principal doubt stemmed from the inability to navigate at sea so as to pass directly over a seamount, which at the planning stage had not been adequately charted. Would the goals of the exercise fail if the source ship missed the seamount peak by a kilometer in Run A or if navigation on the traverse Runs D, E, and B were off by several kilometers relative to the seamount peak?

In order to answer these questions, Fig. 4 was prepared immediately after the site visit. Figure 4 presents the predicted shadow zone structure behind Stoddard Seamount. The hatched areas represent regions from which no rays from a 91-m source can propagate beyond the seamount without reflecting from the seamount.

The scales of Fig. 4 are made relative to the peak of the seamount, which is labelled P. The vertical scale represents the distance from the peak along Track A. The horizontal scale represents the normal distance to Track A. The calculations of Fig. 4 were based on the predicted sound-speed profile and on seamount cross sections taken at 1.8-km intervals from the peak cross section of Fig. 2 as estimated from the best bathymetry available at that time.

This plot clearly indicates that the basic exercise was not hypersensitive to imprecise navigation. For example, navigation on Track A could depart 1.8 km and the width of the first shadow zone would be decreased by only 17 percent of the possible maximum width corresponding to crossing the exact peak. As another example, navigation in Track D could depart 4.6 km and the length of the first shadow zone would be decreased by only 13 percent.

In addition to demonstrating that the experiment was feasible from the navigational aspect, Fig. 4 was used to adjust the range location of the traverse runs as initially laid out on the basis of Fig. 2. Track D was left unchanged at 27 km, Track E was moved from 55 to 51 km to provide for a more even split between the first two shadow zones, and Track B was moved from 183 to 181 km for improved centering in the fourth shadow zone behind the seamount.

The data from the exercise were to be provided to AESD for use in the strengthening and evaluation of acoustic propagation models. The acoustic data would not serve this purpose without adequate environmental measurements and without accurate range information. At the request of the site visit team the exercise plan was improved to meet these requirements.

A complete suite of measurements was scheduled to define the sound-speed profiles. These included XBT, CTD/SV, hydrocast, and surface temperature measurements. Similarly DE STEIGUER and MOANA WAVE were to maintain echo-sounder logs during the active phase of the exercise. In addition, MOANA WAVE was to make a detailed bathymetric survey of Stoddard Seamount prior to the start of Run A and was scheduled to be positioned at the seamount peak so that the DE STEIGUER could position on MOANA WAVE as DE STEIGUER approached the seamount on Track A.

During this bathymetric survey, MOANA WAVE was scheduled to take a special series of CTD/SV measurements which were to be made from the surface to 90 percent of the water depth within 18 km of the seamount peak. Previous measurements of seamount shadowing by Bannister (Ref. 2) hinted that sound-speed profiles may be influenced by the presence of

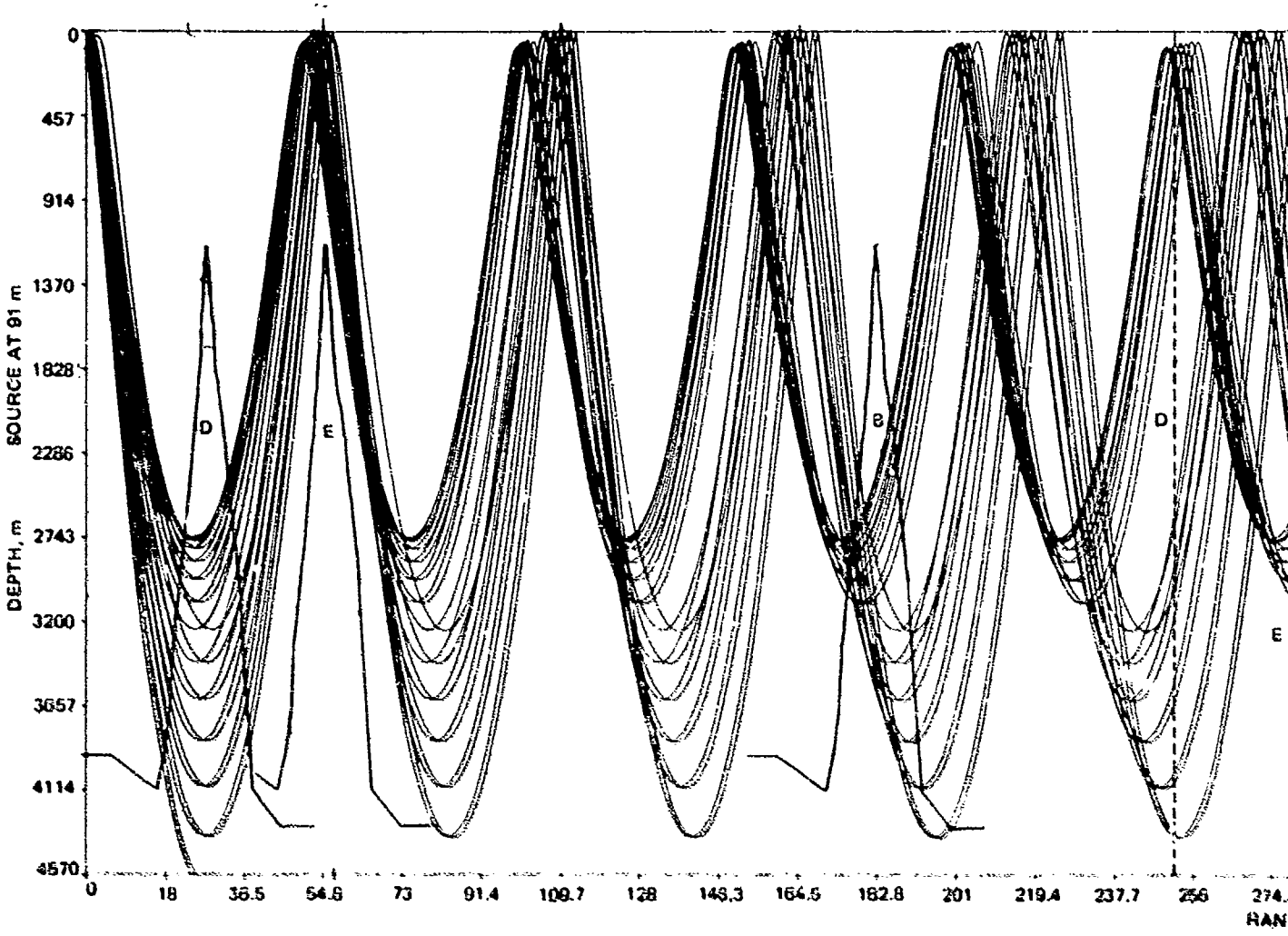
SOURCE AT 91 m
DEPTH, m
0
457
914
1370
1828
2286
2743
3200
3657
4114
4570
0
18
36.5
54.6
73
91.4
109.7
128
146.3
164.5
182.8
201
219.4
237.7
256
D
E
D
E
D
E

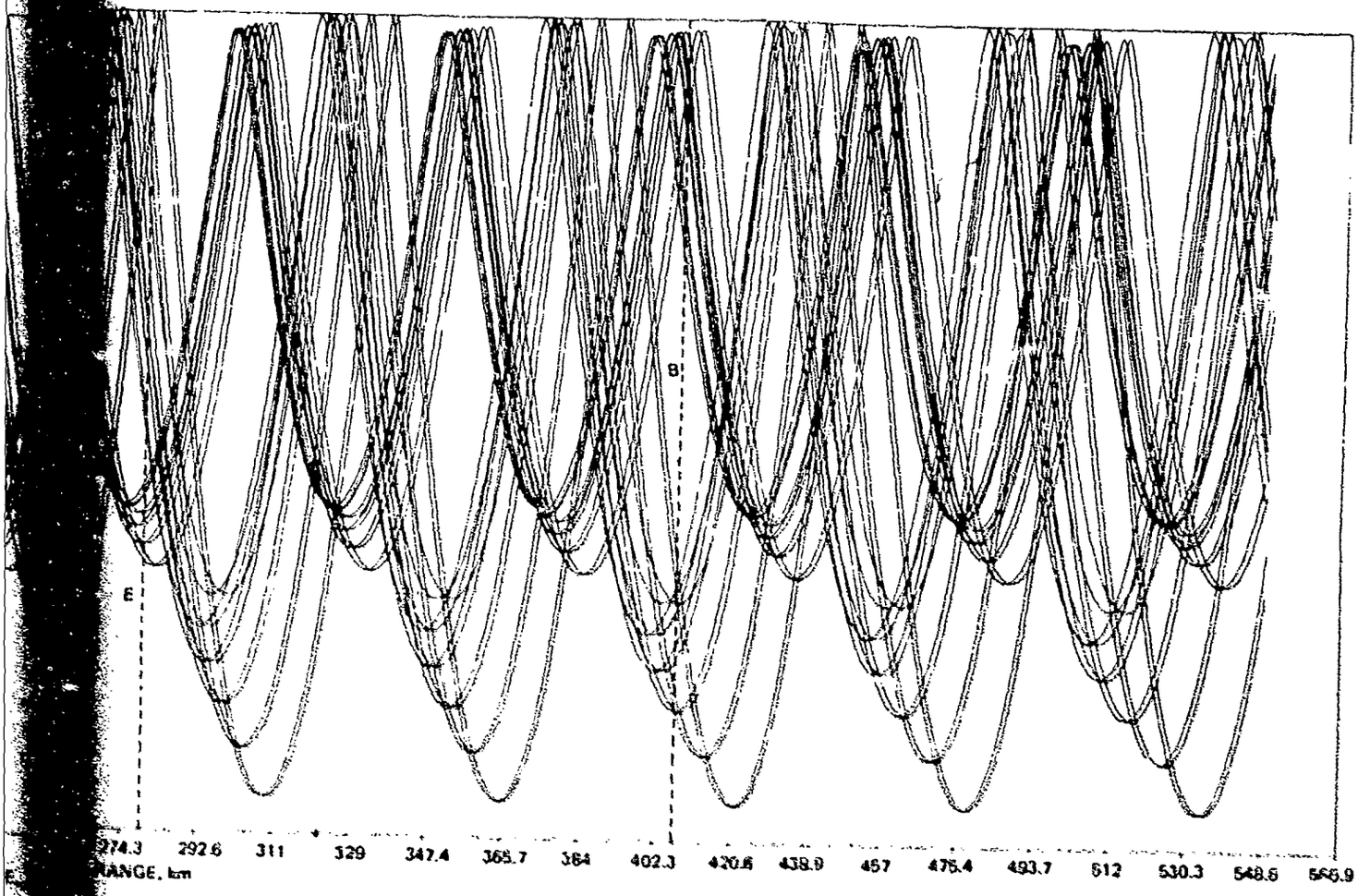


Figure 2. Ray diagram used in the planning phase of the exercise.

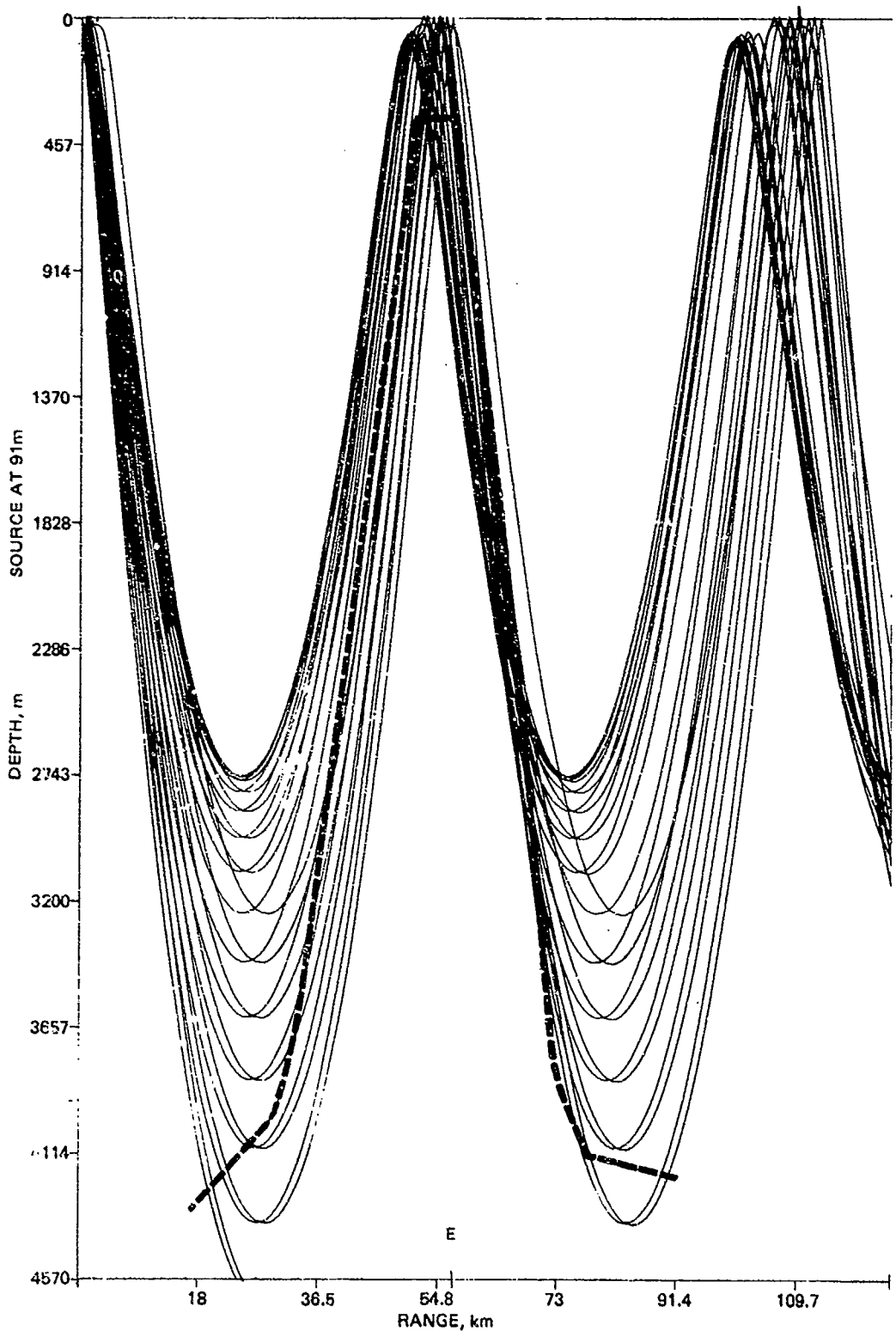


Figure 3. Ray diagram illustrating Fieberling Tablemount centered at position E.

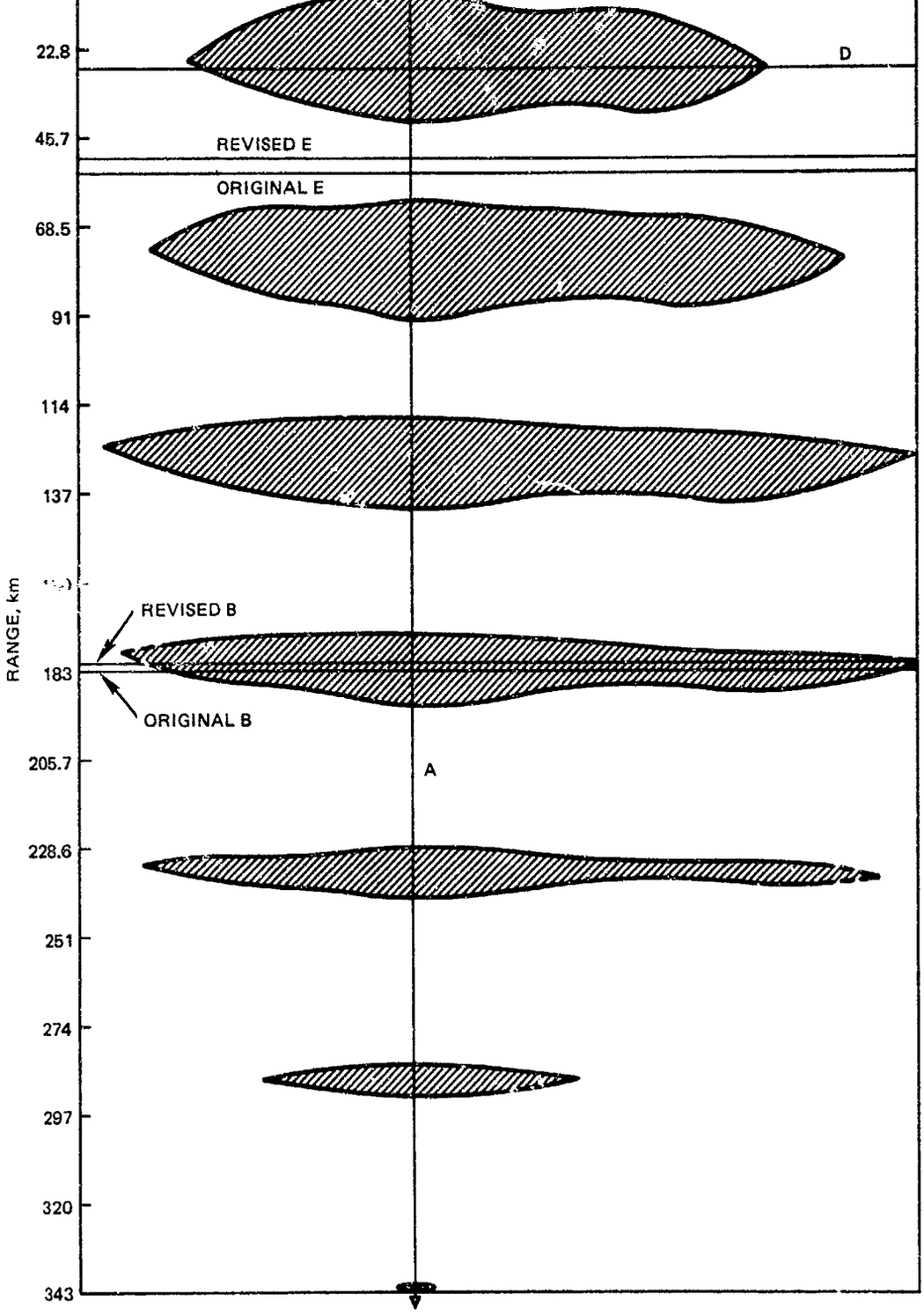


Figure 4. Predicted shadow zone structure behind Stoddard Seamount for a 91-m source depth.

seamounts. In this paper Bannister reported that propagation loss began to increase markedly about 160 km before crossing the Louisville Ridge, which lies east of New Zealand. Although the Louisville Ridge represents a more prominent bathymetric feature, Stoddard Seamount could influence the sound-speed profiles. Thus these special CTD/SV measurements were made to determine whether sound-speed profiles in the vicinity of seamounts differ significantly from those over the nearby abyssal hills.

A point of controversy arose within the site visit team as to how range should be determined, i.e., were ranges determined by satellite fixes adequate or should ranges be determined from acoustic travel times. In previous LRAPP exercises, ranges were often determined solely from satellite fixes, and on some occasions this procedure had lead to gross incongruities. The incongruities were attributed by some investigators to operator or analysis error and by others to basic defects in the satellite navigation system.

The exercise plan was modified to allow for both types of ranging (satellite and acoustic) so that the two types could be compared as well as ensuring that accurate ranges would be available for use in comparison with models. A special effort to obtain accurate satellite ranges was made under the direction of R. T. Bachman of NOSC. Implementation of the acoustic ranging posed some special problems. The MPL processing system required a CW output from the primary source, the HX-231F operating at 104 Hz. Moreover this processing would be contaminated if bomb shots were used for ranging purposes. Therefore the use of shots had to be ruled out.

The use of two pulsed sources was implemented. One was an HX-182A source at 140 Hz and the other was a C-42CJ source at 1 kHz. Both these sources were to project 1/2-sec pulses every 15 sec and both were to be towed 12 m deeper than the primary source. The chief purpose of two secondary sources was acoustic ranging. It was also anticipated that the 140-Hz pulses would be useful in resolving the multipath structure of arrivals at a frequency near that of the primary source. The 1-kHz pulses would allow investigation of possible frequency-dependent diffraction effects.

## EXERCISE EXECUTION AND ENVIRONMENTAL ANALYSIS

In general the exercise went according to plan. There were two equipment casualties which impacted the seamount shadowing experiment.

The first problem was with the DE STEIGUER winch used in towing the acoustic sources. Upon initial lowering of the sources, it was found that the winch could not be reversed to raise the sources. The sources towed deeper than anticipated and could not be adjusted because of the winch problem. (The winch controls had been modified in San Francisco just prior to this exercise and the plans for the modification were not aboard the DE STEIGUER.) As a result, all of the seamount shadowing runs were made with the primary source at a depth of 122 m rather than 91 m as called for in the exercise plan. Moreover the 1-kHz source did not work properly and could not be brought onboard to repair. As a result no data were obtained at 1 kHz. However, the source at 140 Hz provided the necessary travel time data.

The second problem was improper tension on the analog magnetic tape recorder aboard FLIP. This tape was used to record the 140-Hz pulse transmissions. This improper tension caused an oxide buildup on the recording heads. As a result, the recordings on the various tape channels successively deteriorated as Track A progressed, with complete failure ensuing at a range of about 334 km on Track A. This problem was not detected until the

tapes were processed in the laboratory. Therefore, there were no acoustic ranging measurements during the remainder of Track A or for any of the subsequent tracks. This was not a catastrophic failure for, as we shall presently see, there were enough travel time measurements during Track A to establish that satellite ranging was adequate for practical purposes.

In 1975 Refs. 3 and 4, containing a thorough treatment of the environmental measurements made on CAPER, were issued.

The sound-speed profiles are discussed in detail in Ref. 3, which determined that the test area could be characterized by four profile shapes. Figure 5, taken directly from Ref. 3, presents the source ship tracks for Runs A–E and the sound-speed profile shape boundaries. In this plot the numbered dots represent the location of XBT's taken from the DE STEIGUER. (The location of other sound-speed data taken from MOANA WAVE and FLIP can be found in Fig. 6 of Ref. 3.)

Figure 6 presents the upper 400 m of these four profiles and also the profile labelled "PRE," which was the predicted profile used in the initial planning work of Figs. 2 to 4. From the analysis of Ref. 3, profiles 1A and 1B are the same below 100 m, profiles 2A and 2B are the same below 400 m, and all four of these profiles are the same below 500 m.* Table 24 of Ref. 3 lists the sound-speed differences between adjacent profiles. The maximum difference in this table is 9.61 m/sec and occurs between 2B and 1B at a depth of 125 m. This maximum difference occurs almost at the primary DE STEIGUER source at 104 Hz, which is at 122 m depth. Thus this source was operating at a very critical depth as far as horizontal sound-speed changes are concerned. As a consequence, the geometry is almost ideal from the standpoint of assessing the effect of range-dependent sound-speed profiles.

The predicted profile (PRE) in Fig. 6 was based on NORPAC measurements made in the exercise area during late August and early September of 1955. Values are given in Table A-1 of Ref. 1. At depths shallower than 50 m, the predicted profile is significantly lower than the measured data. Table 3 of Ref. 3, developed in the post-exercise analysis, presents the average of 35 hydrographic casts made in 8 different years. This average falls very close to the four measured profiles. For example, the differences from the four measured profiles at the ocean surface lie between 2.55 and –1.13 m/sec and are well within 3.0 m/sec standard deviation of the average. Thus the CAPER data agree well with the average profile of Table 3. On the other hand, the surface sound speed of the predicted profile (PRE) is almost two standard deviations less than that of the average profile. Unfortunately, the NORPAC measurements do not appear to be typical. In the exercise area in August–September 1955 the surface temperatures were apparently somewhat lower than usual.

Figure 7 presents the entire sound-speed profile for profile 1A. This illustrates the structure for all four measured profile types that were the same below 500 m. Below this depth the PRE profile differed by at most 0.7 m/sec, which occurred at 600 m depth. Differences below 2000 m were less than 0.1 m/sec. The nominal bottom depth of the abyssal hills is 4200 m and is indicated in Fig. 7 by the hatched line.

Recall our earlier concern during the planning phase about the possibility of the seamount influencing the sound-speed profiles. A comparison between a deep-water profile well removed from the seamount and the average of profiles measured within a 18-km radius of the seamount peak is presented in the lower part of Table 22 of Ref. 3.

The discussion of Table 22 as presented in Ref. 3 needs to be expanded somewhat, with some additional information provided. We first note a numerical error in the table. The difference for 2500 m depth should be 0.22 m/sec rather than the 0.28 m/sec value presented. We next note that at 800 m the difference between profiles is less than one-fourth the

*Reference 3 uses roman numerals for profile designation.

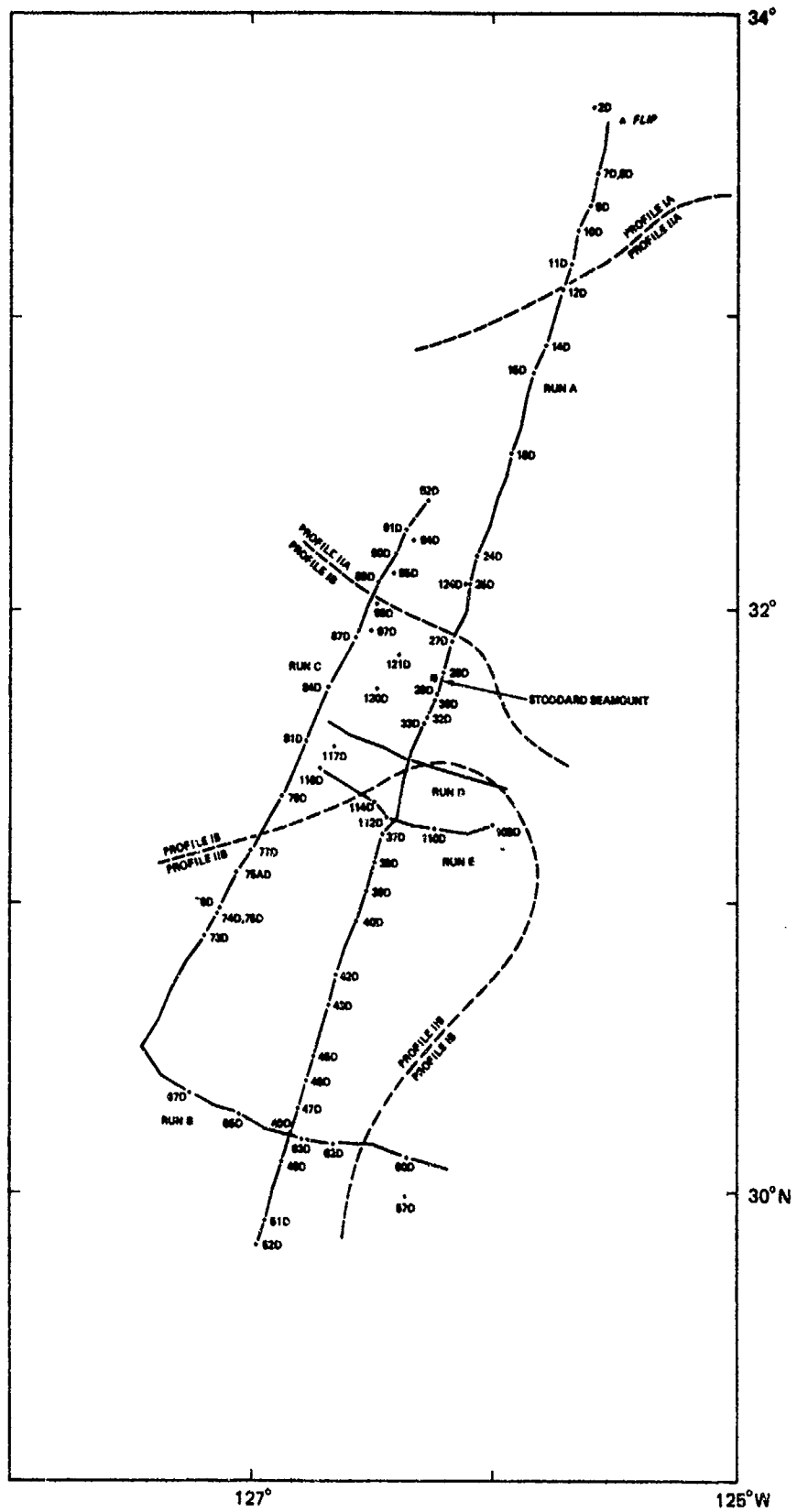


Figure 5. Location of DE STEIGUER XBT (•), Runs A-E source ship tracks, and sound-speed profile shape boundaries.

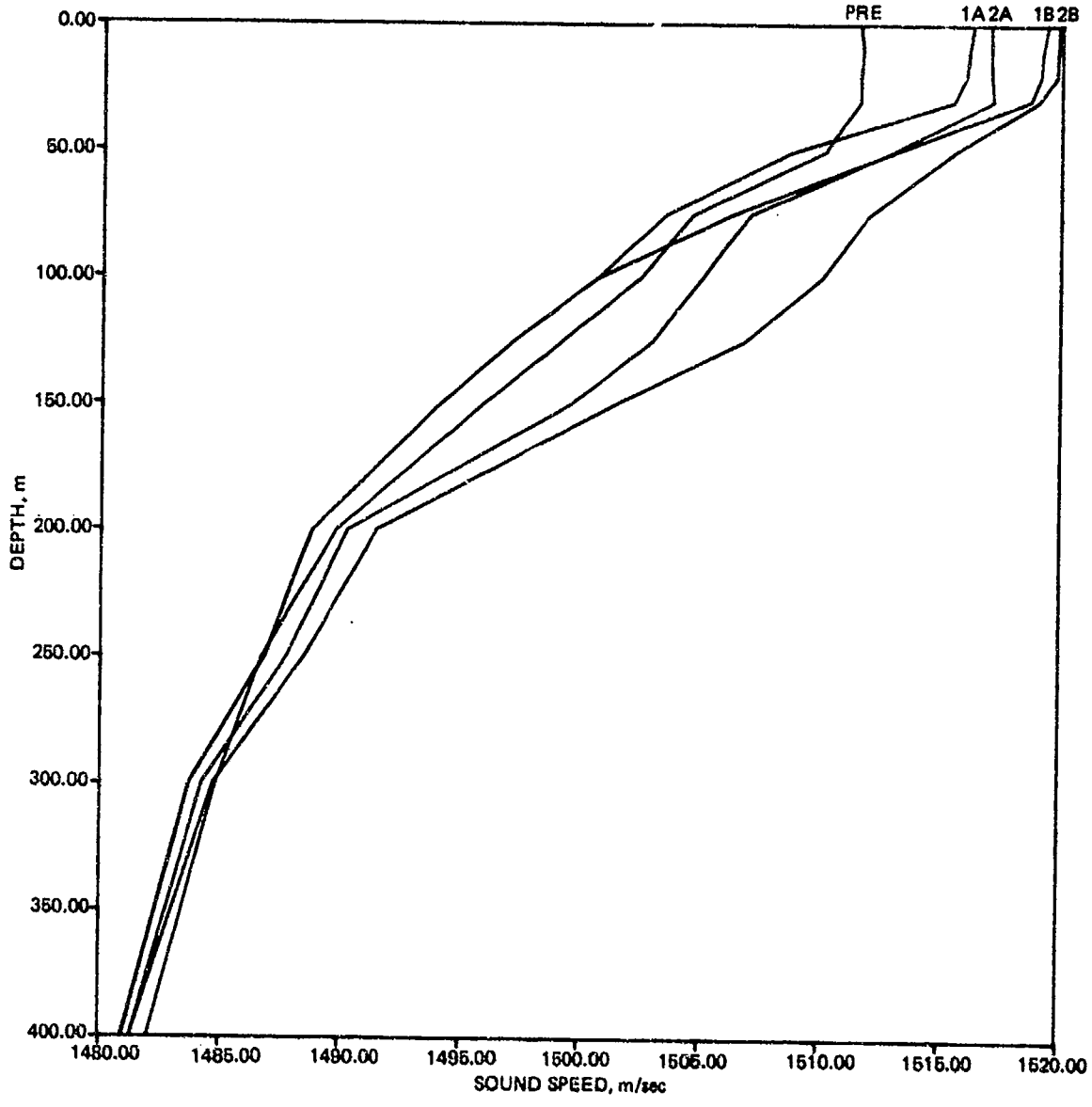


Figure 6. Near-surface sound-speed profiles illustrating the profile shapes referred to in Fig. 5.

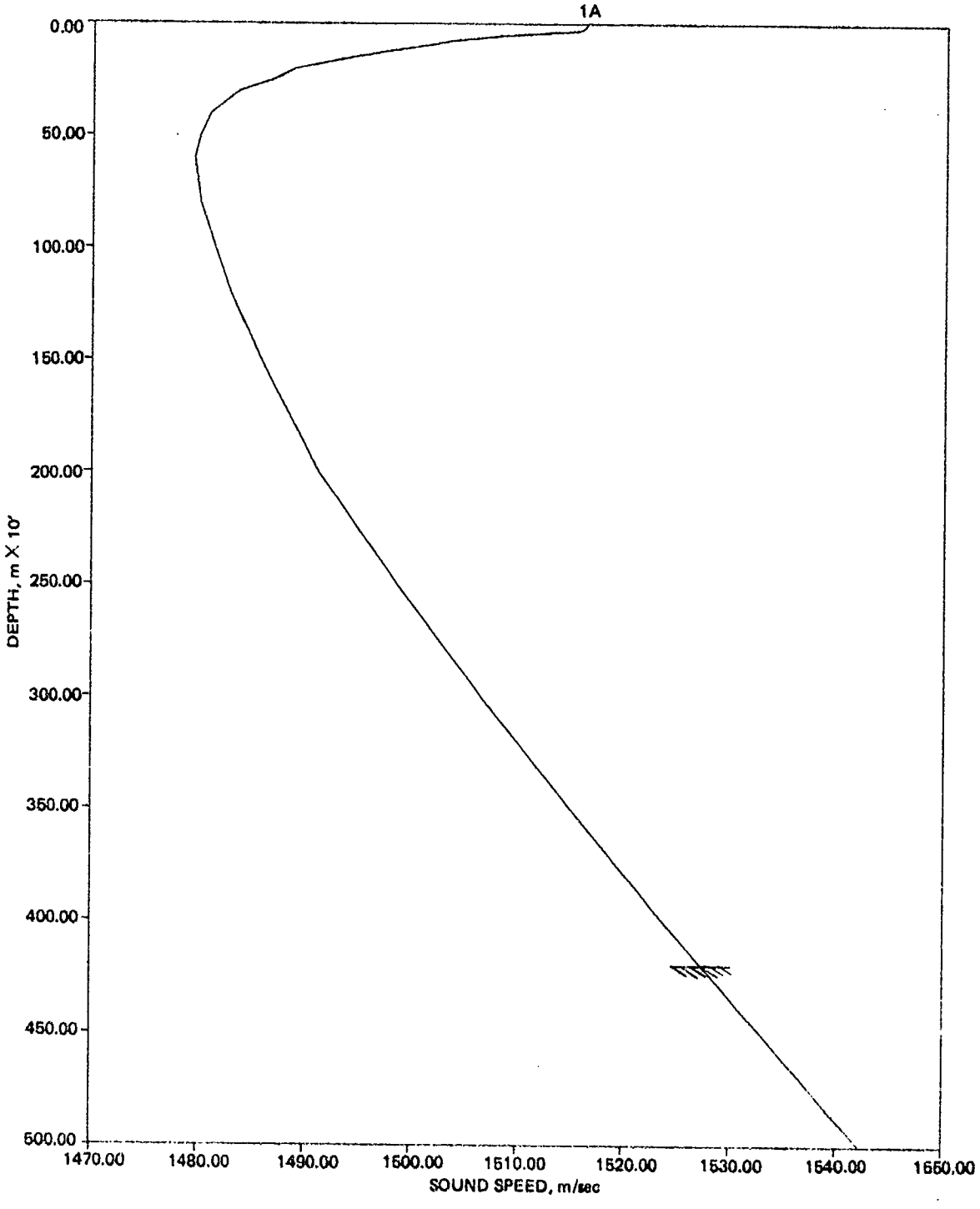


Figure 7. Complete sound-speed profile 1A. Values also apply to profiles 1B, 2A, and 2B below 500 m.

standard deviation. Thus the seamount has no apparent influence on sound speeds above a depth of 800 m. Finally we note the sequence of differences in Table 22. All of these differences for depths of 1000 to 2500 m lie between 0.21 and 0.24 m/sec with the exception of the value of 0.42 m/sec for 2000 m depth. In this case we surmise that the deepwater profile observation of 1491.25 m/sec is somewhat lower than typical. This hypothesis was checked by the data from two hydrographic casts made during CAPER and extending to 2000 m. These casts are presented in Table 6 of Ref. 3. The sound speeds at 2000 m depth were calculated to be 1491.35 and 1491.49 m/sec for Casts 1 and 2, respectively. Corresponding differences from the seamount profile are 0.32 and 0.20 m/sec, respectively. This tends to confirm our hypothesis. The significance of the seamount profile will be discussed in acoustic terms later.

Reference 4 presents the satellite navigation and bathymetric data for CAPER. One of the critically important measurements of Ref. 4 is the geographical coordinates of FLIP, since this FLIP position must be used to determine range for each satellite fix along the source tracks. The location of FLIP was determined on the basis of 15 satellite observations made by DE STEIGUER while within radar range of FLIP. This location was 33°37.92′N and 125°29.53′W. The standard deviation of this range position was 539 m. This location is 3.08′S and 1.53′W of the moor point called for in the exercise plan.

Reference 4 also contains a detailed bathymetric chart of Stoddard Seamount. The center of the peak is 31°44.8′N and 126°13.4′W. This location is 2.2′S and 3.6′E of the value quoted in Ref. 1. It was necessary for MOANA WAVE to change the planned schedule to complete other high-priority environmental measurements. Thus the MOANA WAVE did not position at the seamount peak as a guide for DE STEIGUER. Instead, the position of the seamount peak was radioed by MOANA WAVE prior to the start of Run A and the DE STEIGUER navigated toward this position. The DE STEIGUER crossed about 2.5 km east of the peak. About 5 min after noting a minimum depth of 1778 m, a satellite fix was taken. On the basis of this fix the ships course was adjusted to bring the ship closer to the bearing line between FLIP and Stoddard Seamount.

Reference 4 characterizes the operation area as "within a province of abyssal hills," characterized by low ridges (of 35 to 180 m relief), hills (of up to 730 m relief) and occasional seamounts or groups of seamounts (of up to 3 to 4 km relief). Other than in the vicinity of Stoddard Seamount the shallowest depth recorded was 3502 m.

## COMPARISON OF ACOUSTIC AND SATELLITE NAVIGATION RANGES

One of the secondary objectives was a comparison of range, as measured from acoustic travel time, with the range between source and receiver location as determined from satellite fixes.

The HX-182-A source was towed at a nominal depth of 133 m. It was operated at 140 Hz and emitted 1/2-sec pulses every 15 sec. The transmission of these pulses was controlled by a time code generator, which was checked periodically aboard DE STEIGUER with WWV. A radio pulse was transmitted simultaneously with each acoustic pulse.

The acoustic pulses were recorded on magnetic tape aboard FLIP for receiver depths of 94, 206, 732, 3508, and 4363 m. The radio pulses from DE STEIGUER and WWV time ticks were also recorded on this magnetic tape.

Upon return to the laboratory, the magnetic tape data were processed onto a six-channel Brush recorder. Not all receiver channels could be processed in the single pass made through the tapes. With a few exceptions, the most useful data came from the receivers at depths of 94 and 3508 m.

The strip chart recorder was normally run at a paper speed of 1 mm/sec. However every 15 min the paper speed was increased to a nominal 125 mm/sec to allow for an accurate measurement of travel time. The paper speed was also increased at the times corresponding to satellite fixes. The idea behind this procedure was that the range as determined by the satellite fixes should be most accurate at the time of the fix itself since ranges for other times would involve the additional error of interpolation between the ranges of successive fixes.

Considerable care was taken to eliminate or minimize various sources of error in the measurement of acoustic travel time. For example the paper speed was determined for each observation from the WWV time ticks. Successive values would run with consistency to about 0.1 mm/sec for a number of observations and then would jump to a completely different value. Paper speeds throughout the entire set of observations lay between 124.7 and 118.8 mm/sec. This is a variation of about 5 percent and, hence, represents a significant source of error if not determined for each observation.

Potential error was minimized by measuring on the recorder only the time difference between the radio pulse (or WWV minute pulse) and the nearest acoustic pulse received. This time difference never exceeds 15 sec. The acoustic pulse on which the measurement is based does not correspond to the radio pulse. However, the acoustic travel time can be obtained by adding in the appropriate multiple of 15 sec.

Whenever available, the radio pulse from the DE STEIGUER was used. When radio reception from DE STEIGUER was poor, without clean-cut pulses, the WWV minute pulse was used. This latter procedure requires that the time of transmission aboard DE STEIGUER be known accurately. Accuracy was ensured in this case by making a series of measurements of the time difference between the radio pulse from DE STEIGUER and the WWV minute pulse. A plot of these time differences over a 48-hour period during the acoustic run showed that the time code generator aboard DE STEIGUER drifted at a constant rate of about 28 msec/hour. Two jumps in the time code generator were also detected – one of 100-msec and the other of 400-msec. The drift and the jumps were factored in as corrections so that accurate acoustic travel times could be obtained when the DE STEIGUER radio pulse could not be used.

One other point should be noted. Since the source ship is moving and the receiver ship is fixed, the measured acoustic travel time is associated with the source position at the

time of transmission. The time of transmission was obtained by determining the time of reception aboard FLIP and then subtracting the acoustic travel time.

The next step of the process was to convert these measured travel times to acoustic ranges. At this point, the discussion of two ray diagrams will help illustrate how this conversion was done.

Figure 8 is a ray diagram for a source depth at 94 m. The horizontal line represents a receiver depth of 122 m. The ray treatment of a moving source in a range-variable environment is very complicated. Since in this exercise the receivers are fixed relative to the bottom topography and sound-speed profiles, in this and in all ray calculations to follow we will consider the rays to be emanating from the receiver aboard FLIP and will apply reciprocity. Thus the regions cut by the rays at 122 m depth in Fig. 8 represent ensonified regions corresponding in reality to a 122-m source depth and a 94-m receiver depth. (This was the shallowest of the FLIP receivers during the seamount shadowing phase of the exercise.)

The rays shown are at 1-deg increments from a source angle of 0° to ±9 deg. In addition the rays which graze a bottom depth of 4206 m are shown. This was chosen as the nominal bottom depth of the abyssal hills on either side of the seamount. The topography shown at the bottom of Fig. 8 is that measured along Run A, with the exception that the seamount profile itself (shown at a range of about 220 km) is the profile directly across the peak as determined from the seamount survey of Ref. 4. The nominal bottom depth of 4206 m was chosen on the basis of the minor bottom relief features of the abyssal hills. No attempt was made to take this minor relief into detailed account in the ray computations, because it is only indicative of what the true relief was between source and receiver. In short, as far as all ray computations are concerned, the bottom is assumed to be flat at 4206 m depth except for Stoddard Seamount.

The numbers set at various ranges along the horizontal line in Fig. 8 represent the convergence zone number and are positioned near the leading edge of a convergence zone for the 122-m receiver. The short dashed lines at the top of Fig. 8 represent the boundaries between the various sound-speed profiles as described in Ref. 3. They are labelled by the appropriate profile designator on each side of the dashed line. For example the boundary between profile 1A and 2A occurs at a range of about 61 km.

The ray theory used in this treatment is basically that presented in Ref. 5, for which the sound-speed profile has a continuous depth derivative. This treatment has been modified slightly to allow for horizontal changes in profile which take place near the surface. In this modification the horizontal change is programmed to take place so that there are no discontinuities in sound speed or in its depth derivative. In the example of Fig. 8, the rays are traced using profile 1A until they form the nadir between zone 1 and zone 2. At this point the ray trace proceeds using profile 2A. There are no discontinuities produced at this juncture, because profiles 1A and 2A are identical at the nadir depths. The ray trace continues then to use profile 2A until the rays form the nadir between zones 3 and 4. At this point the ray trace proceeds using profile 1B until the nadir between zones 5 and 6, at which time the remainder of the ray trace uses profile 2B.

The boundaries between 1A/2A and 2A/1B are geometrically well-positioned for this scheme of ray tracing. This is not true for the boundary between 1B/2B. This boundary falls in the middle of convergence zone 5. However, the ray tracing scheme assumes that profile 1B applies for all of zone 5. Thus this simple approach is only approximate. However it should accommodate most of the horizontal change in profile and should introduce relatively minor errors compared to ignoring horizontal change altogether.

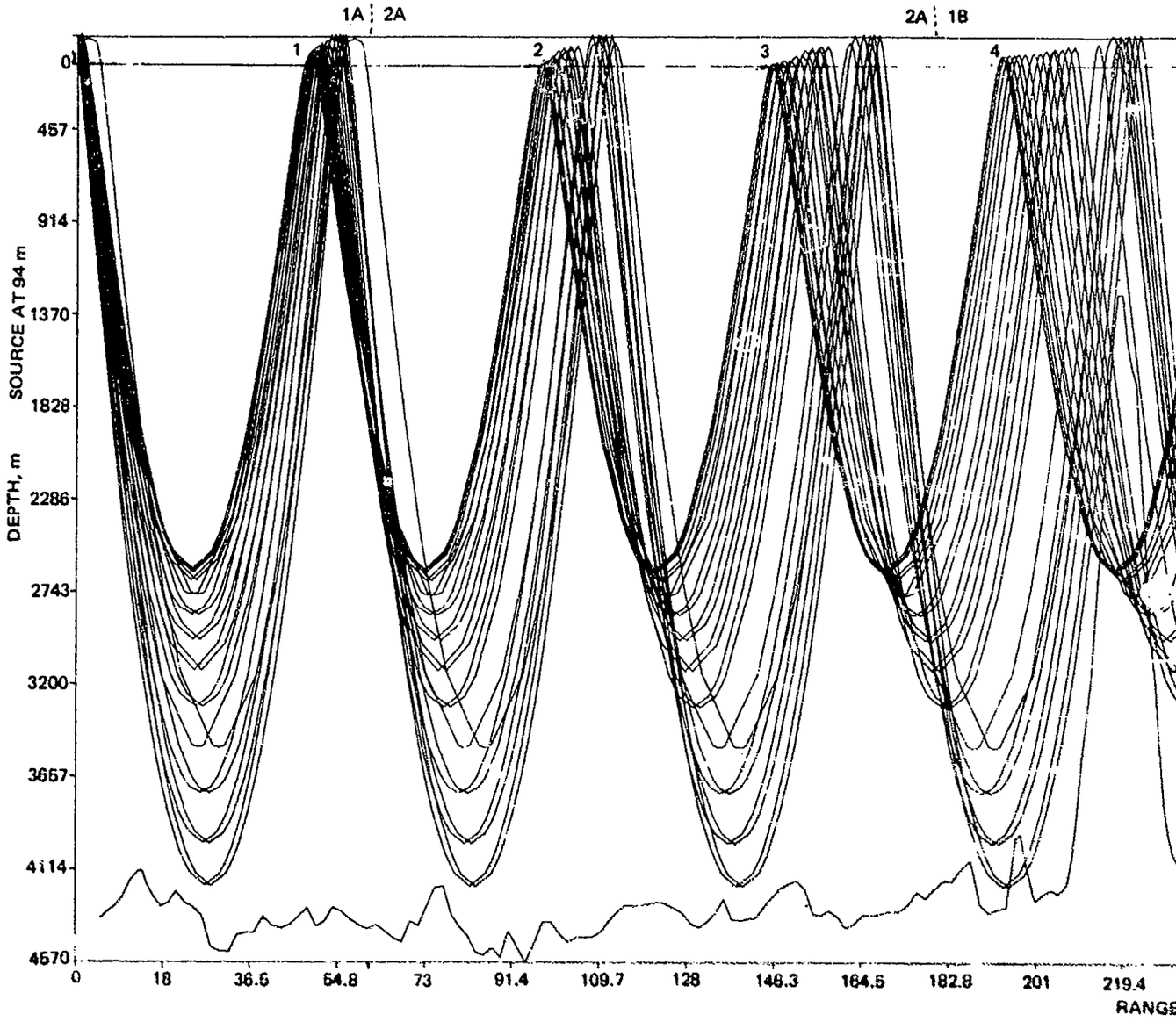
1A
2A
2A
1B
1
2
3
4
0
457
914
1370
1828
2286
2743
3200
3657
4114
4570
DEPTH, m
SOURCE AT 94 m
0
18
36.5
54.8
73
91.4
109.7
128
146.3
164.5
182.8
201
219.4
RANGE

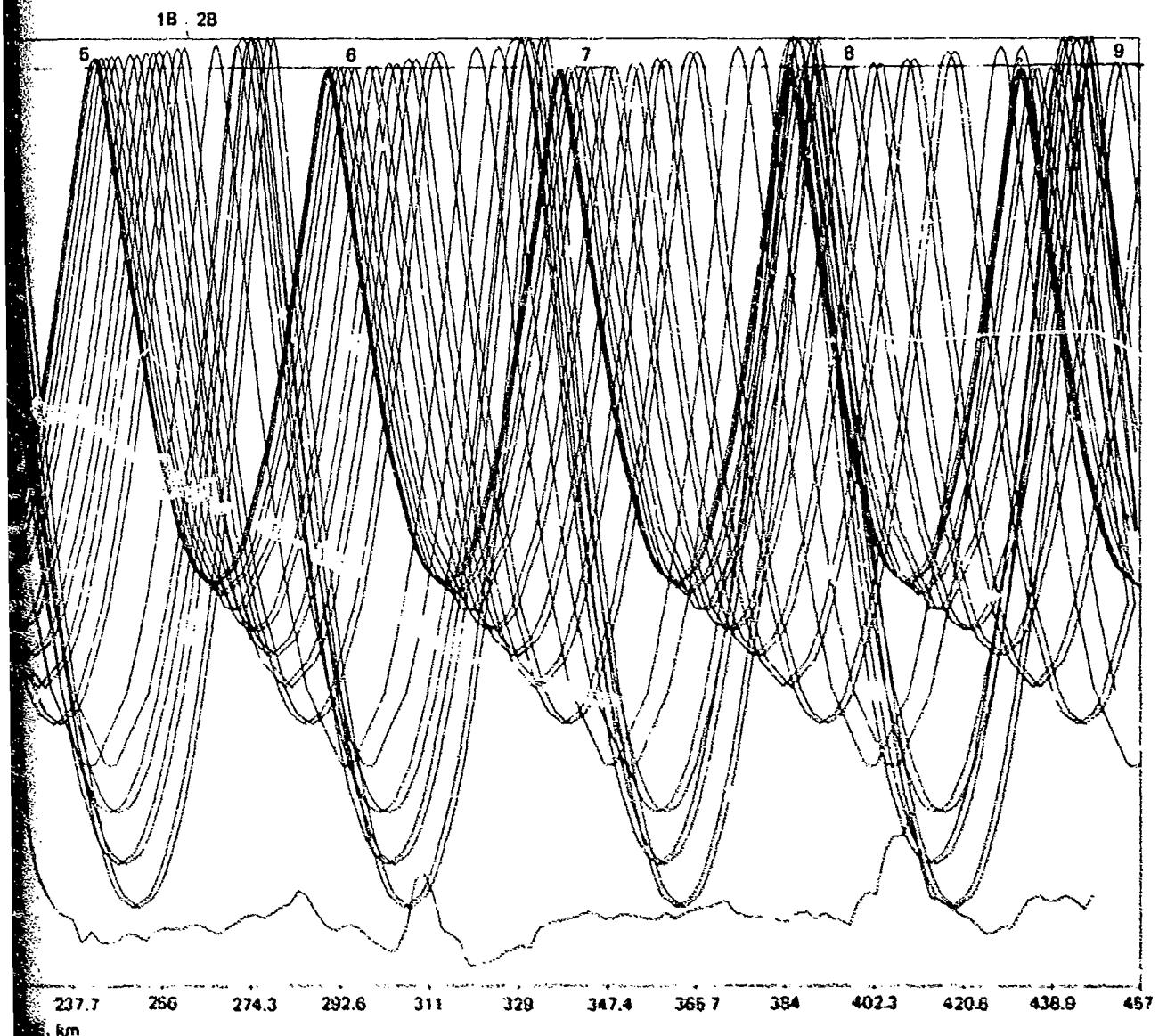


Figure 8. Ray diagram for a source depth of 94 m.

The effect of horizontal change is quite apparent in the ray diagrams. For example the 0-deg ray at the source barely reaches the 122-m receiver in zones 2 and 3, extends well above this receiver in zones 4 and 5, and falls well below this receiver for zones 6 to 9.

If one looks at the nadirs of the rays between zones 4 and 5, one can readily determine that absolute values of source angles less than 6 deg intersect the seamount, whereas those greater than 7 deg clear the seamount. Those clearing the seamount generally reflect from the ocean surface, although there is a small bundle which does not reflect from the ocean surface.

Figure 9 is the counterpart of Fig. 8 for a source depth of 3508 m. This corresponds to the deep receiver at FLIP, for which most travel time measurements were recorded. In this case the nomenclature for the various convergence zones does not necessarily conform to convention. We designate the initial region of surface ensonification as zone 0 because it consists in part of the direct field. (Others may consider this as zone 1, at least in part.)

In this calculation profile 1A is used to calculate zone 0, profile 2A is used to extend through zones 1 and 2, profile 1B is used to extend through zones 3 and 4, and profile 2B is used to extend beyond zone 4. In this example the geometrical position of the boundaries makes these profile-zone choices clear cut. As can be seen, all rays leaving the source intersect the seamount.

Now that the ray diagrams have been introduced, we may return to the problem of converting travel time measurements to range. In the case of travel time measurements, a receiver depth of 134 m applies rather than the 122-m depth shown in Figs. 8 and 9.

Travel times were computed consistent with the manner in which the ray diagrams of Figs. 8 and 9 were generated. It should be noted, however, that in the travel time computation and in propagation loss computations to be presented later, a much greater density of rays was computed than the few rays shown in the ray diagram.

In all measurements of travel time, the first (fastest) arrival was used. Each measured travel time was compared to the corresponding theoretical travel time and converted to range by means of three-point Lagrangian interpolation on the theoretical set of travel time and range computations.

If the ray calculations indicated that there was no non-bottom-reflected ray which had the measured travel time, the observation was omitted from the data set. These omitted observations could either result from bottom-reflected rays or from diffraction arrivals in the shadow zone. Those resulting from bottom reflections were omitted because the range accuracy depends on the exact depth of the bottom from which the reflection took place. This was not known precisely enough for this exercise, which was conducted in a region of abyssal hills rather than plains. The diffraction arrivals were omitted because it is not clear how these travel times should be converted to ranges.

There were 70 measurements of acoustic travel time, covering ranges from 3.7 to 333 km. There were 23 satellite fixes applicable to this range interval. The time period corresponding to this interval is from 1825 of one day to 0045 two days later. Thus this interval should contain 133 measurements of acoustic travel time: 110 measurements at 15-min intervals plus 23 measurements made at satellite fixes.

The first item to note is that only about 52 percent of the prescribed number of measurements were actually made. Causes for missed measurements are: all signals below noise, ragged leading edge of acoustic or radio pulse or WWV time ticks, missing radio pulse and time tick, and operator error. No doubt some of these missed measurements could be

obtained by careful replay of the tapes. Only one acoustic pulse and one radio or time tick measurement was recorded on fast speed. On replay an adjacent set could be recorded on fast speed. These adjacent sets might have better signal-to-noise ratios and clear-cut leading edges. Also on replay other receiver depths might be investigated. If one wished to, one could conceivably attempt to measure acoustic travel times for every pulse. Fortunately for our purposes replay does not appear necessary. As we shall see presently, the 70 measurements provide an adequate data set.

The limitation of acoustic data points to travel times corresponding to non-bottom-reflected rays reduced the 70 observations to 58. These 58 acoustic ranges and the 23 satellite ranges were subjected to another test to further weed out erroneous observations. In this test the ship's apparent speed as determined by two adjacent measurements of range is calculated.

These speeds as determined for all adjacent pairs of acoustic ranges are plotted as diamonds in Fig. 10. The speed is plotted at the range corresponding to the greater range of the two adjacent pairs. A similar procedure was performed for the ranges as determined by satellite fixes. Those are plotted as X's in Fig. 10. For general reference, the speeds as determined by ship's log are plotted as triangles in Fig. 10.

In Fig. 10 observations associated with the points labelled A to E are considered suspect because they produce unrealistic excursions in apparent ship speed. Consider first satellite point A. This point is in actuality way off scale at a value of 10.1 knots. Investigation showed that in this case the two satellite fixes were only 4 min apart. With so short a time baseline, a small error in range produces a large error in ship speed. The best of these two adjacent satellite fixes was accepted and the other rejected. This is the only satellite fix which was rejected. The other 22 satellite fixes were all used in the analysis to follow.

Investigation of the acoustic ranges associated with points B to E lead to the rejection of three acoustic ranges associated with points B to D. Reference 4 notes a steering casualty at a time which affects point E. Thus point E represents a true reduction in ship speed. Examination showed that one of the acoustic pulses associated with point B had a dubious leading edge and should be rejected. In contrast, the acoustic pulses associated with points C and D were clean cut. There was no apparent reason for error. Nonetheless a range point associated with C and D was rejected.

The rationale for these rejections is illustrated in Fig. 11. Figure 11 is the counterpart of Fig. 10 after the rejection of erroneous measurements associated with points A to D. Observe that this rejection results in a significantly smoother curve. Consider, for example, the rejection associated with point D. One erroneous range point always produces two erroneous ship speeds. In the case of point D the measured acoustic range at D was too small. Thus the ship speed calculated from this range and the preceding range will be too small. In contrast the ship speed as calculated from the range at D and the following range will be too large. Thus the one erroneous range at point D produces two glitches (one negative and one positive) in the plot of Fig. 10.

Observe how these two glitches are removed in Fig. 11. Comparison of Figs. 10 and 11 show removal of two glitches at each of the points A through D. In any case this removal of significant glitches appears to be sufficient grounds for rejecting observations even if no other basis is evident. The number of acoustic observations accepted was 55.

The next step in the process was to compare the acoustic ranges with those determined from the satellite observations. The difference between acoustic ranges and satellite ranges is plotted versus acoustic range in Fig. 12. The Y's represent differences associated with

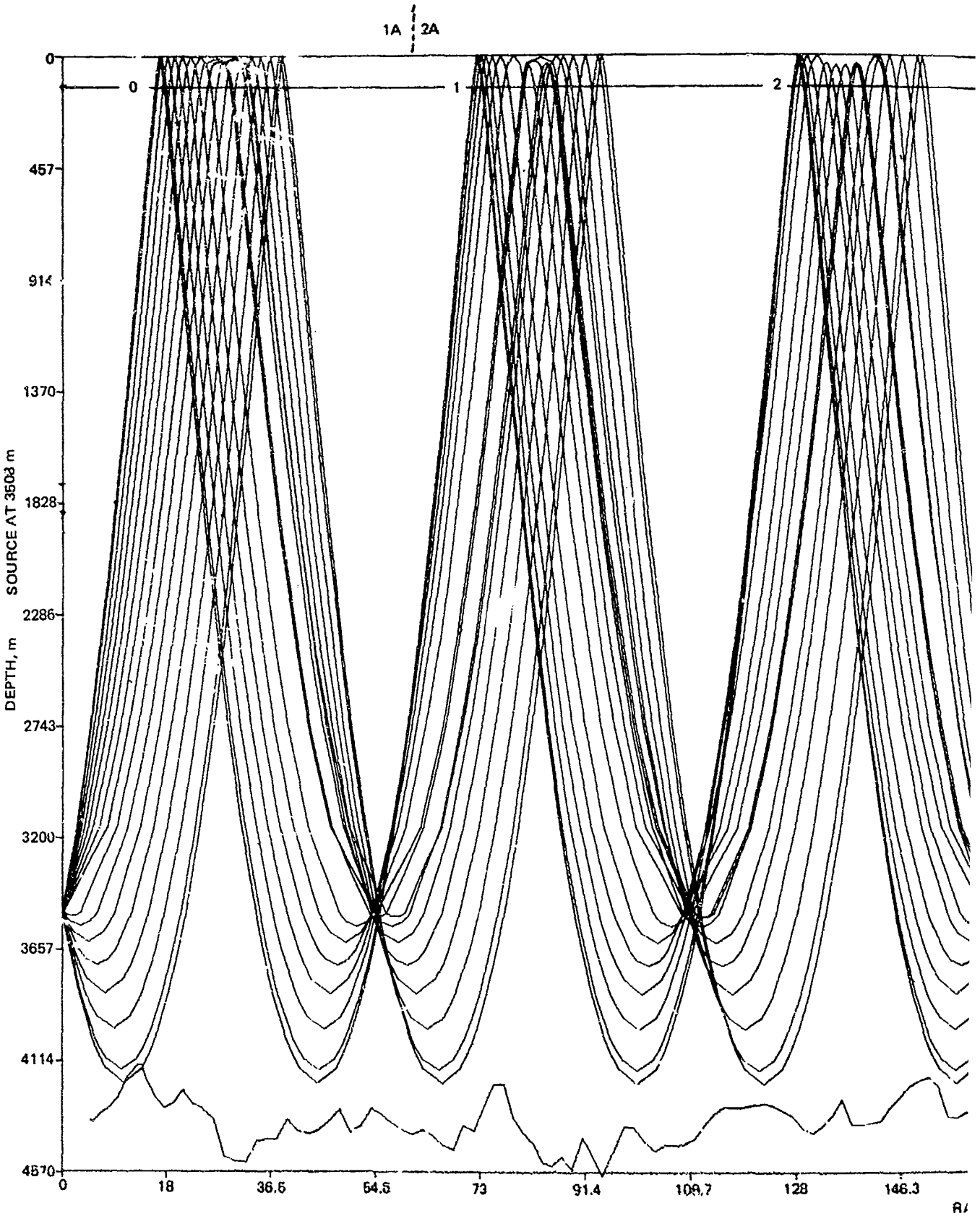
1A
2A
0
1
2
0
457
914
1370
1828
2286
2743
3200
3657
4114
4570
DEPTH, m
SOURCE AT 350 m
0
18
36.5
54.5
73
91.4
109.7
128
146.3

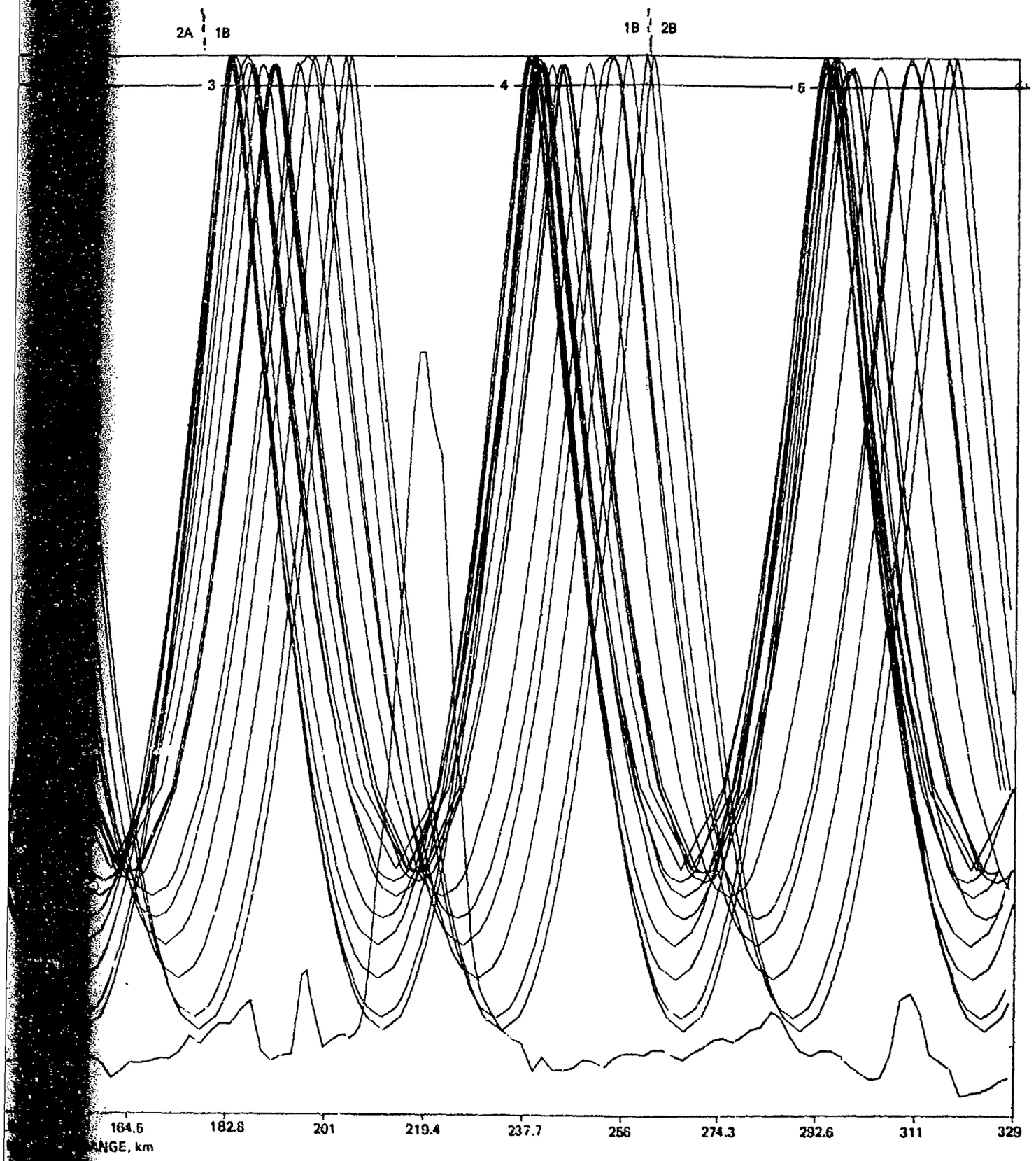


Figure 9. Ray diagram for a source depth of 3508 m.

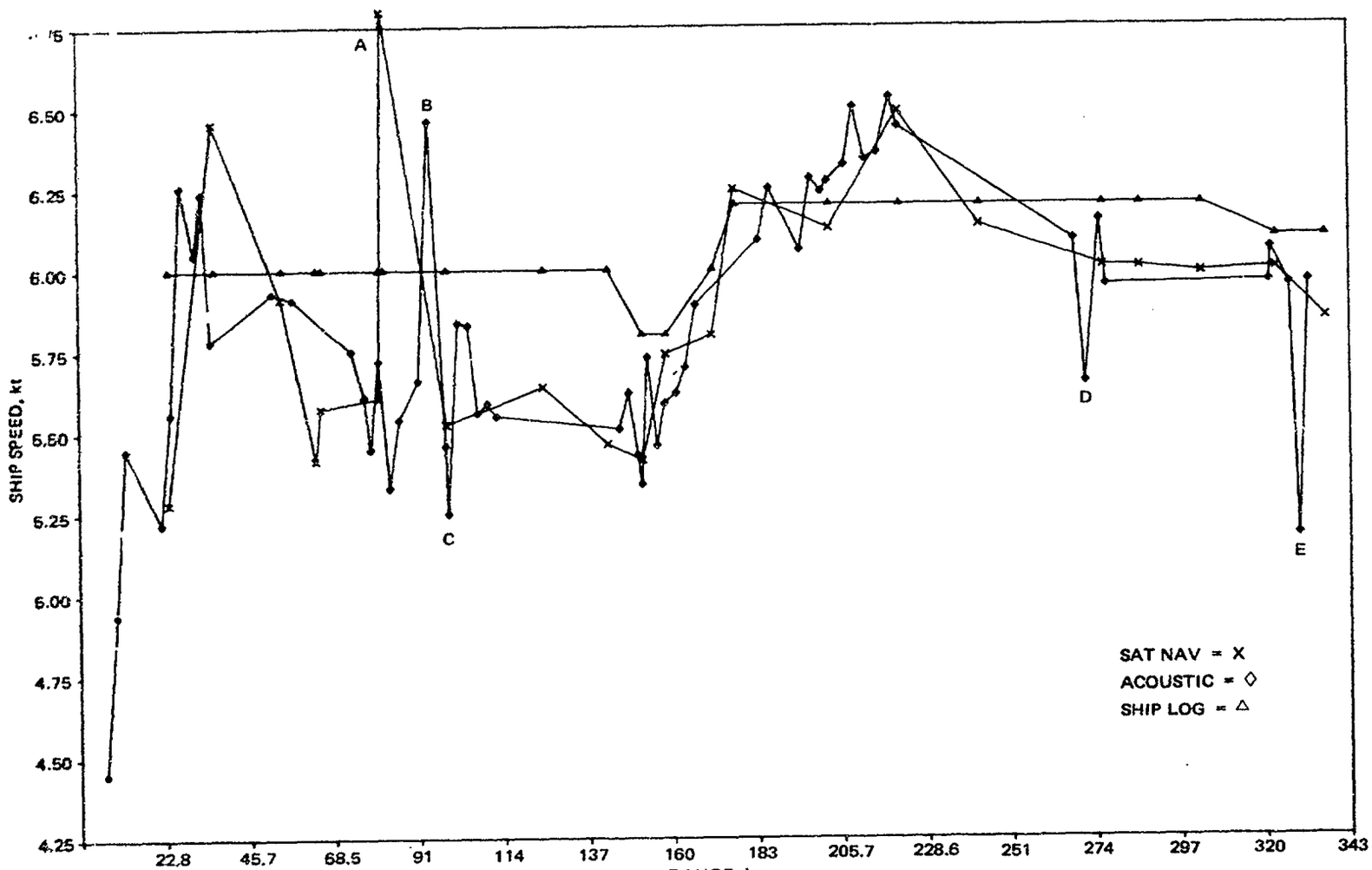


Figure 10. Ship speed as calculated from adjacent range observations. Points A to E are suspect.

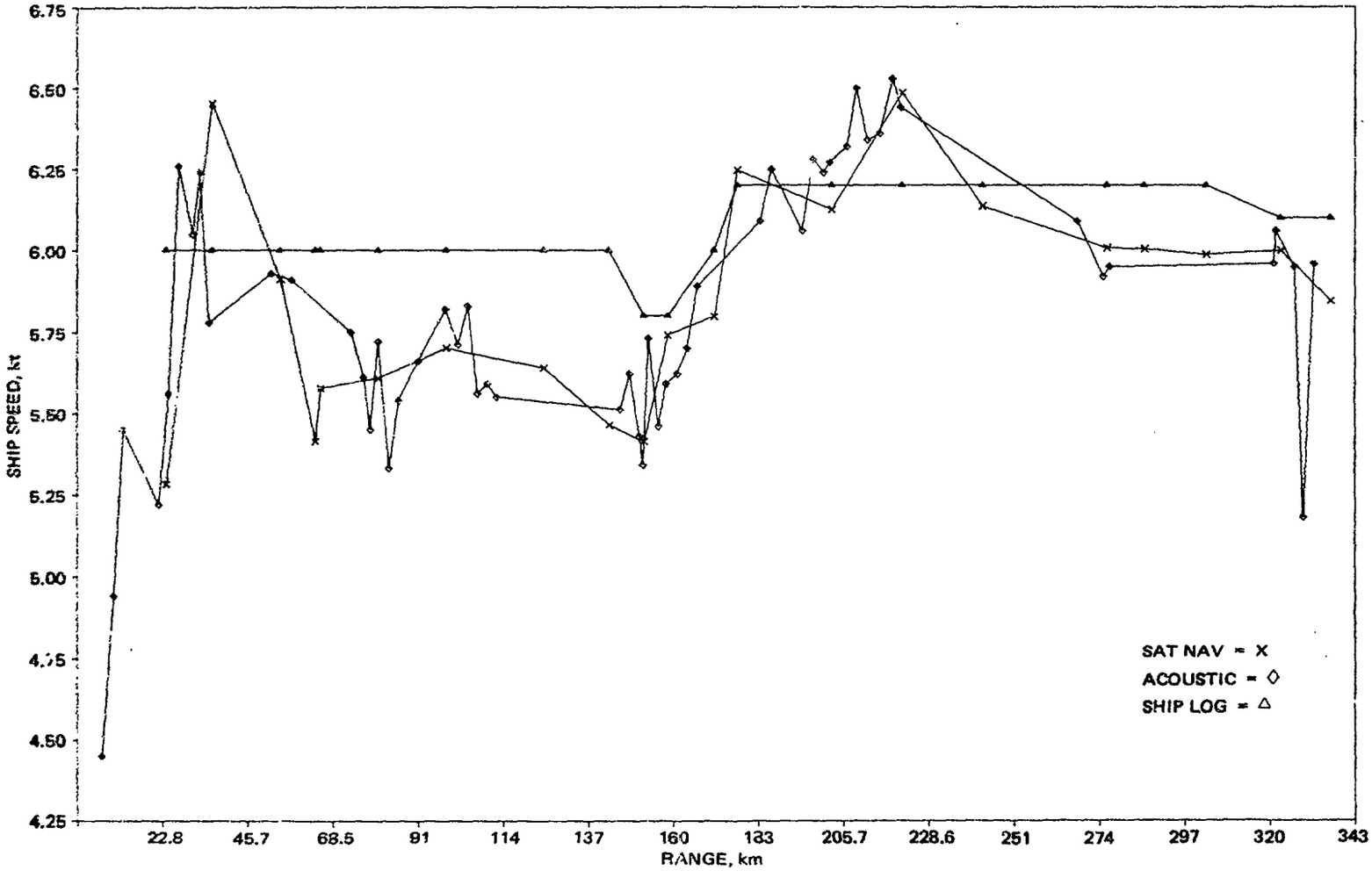


Figure 11. Ship speed as calculated from adjacent range observations after removal of points A to D of Fig. 10.

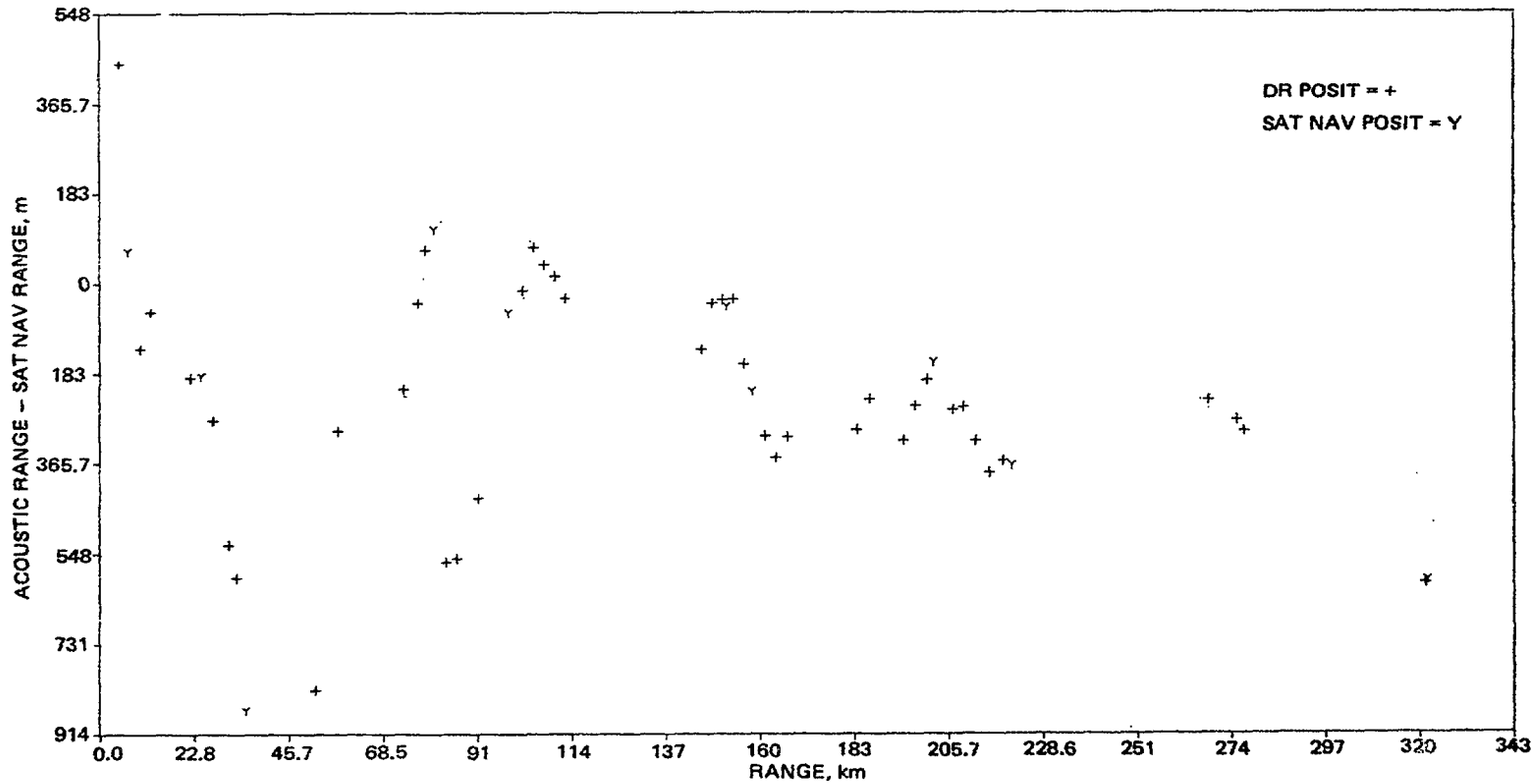


Figure 12. Difference between acoustic ranges and satellite navigation ranges (before correction).

simultaneous satellite and acoustic ranges, whereas the X's represent differences associated with interpolations between satellite ranges. There are 52 data points in Fig. 12. The last three of the acoustic observations accepted in Fig. 11 and covering ranges between 327 and 333 km could not be compared in Fig. 12. Because of the steering casualty there was no way to properly interpolate between satellite fixes. Thus there was no satellite range available for comparison.

As can be seen in Fig. 12, the differences are strongly biased to the negative side. This is illustrated in Fig. 13, which represents a histogram of the data of Fig. 12 divided into 91.4-m bins. The mean difference is -234 m, with a standard deviation of 240 m. Seventy-one percent of the 52 data points fall within the standard deviation. The standard error of the mean difference is 33 m.

We next applied a test to determine if the bias in Figs. 12 and 13 could be attributed to the statistical error in the position of FLIP. Student's t test applied to the data of Fig. 12 and to the FLIP position data of Ref. 4 yielded a value of t = 2.38, which is significant at better than the 1-percent significance level for the 65 deg of freedom involved in the test. Thus there is a significant bias in the data of Figs. 12 and 13.

Various sources of error which could introduce a bias in the data were investigated. The first source uncovered was the difference between the position of the satellite antenna and the acoustic source. The satellite antenna was mounted on the aft mast about 25 m from where the tow cable entered the water. The cable length to the pulsed source was 140 m. For a 25-deg wire angle this cable length was estimated to result in the source being about 47 m aft of the point where the tow cable entered the water. Since the source was towed on a radial from the receiver, the satellite range should be reduced by 25 + 47 m (72 m).

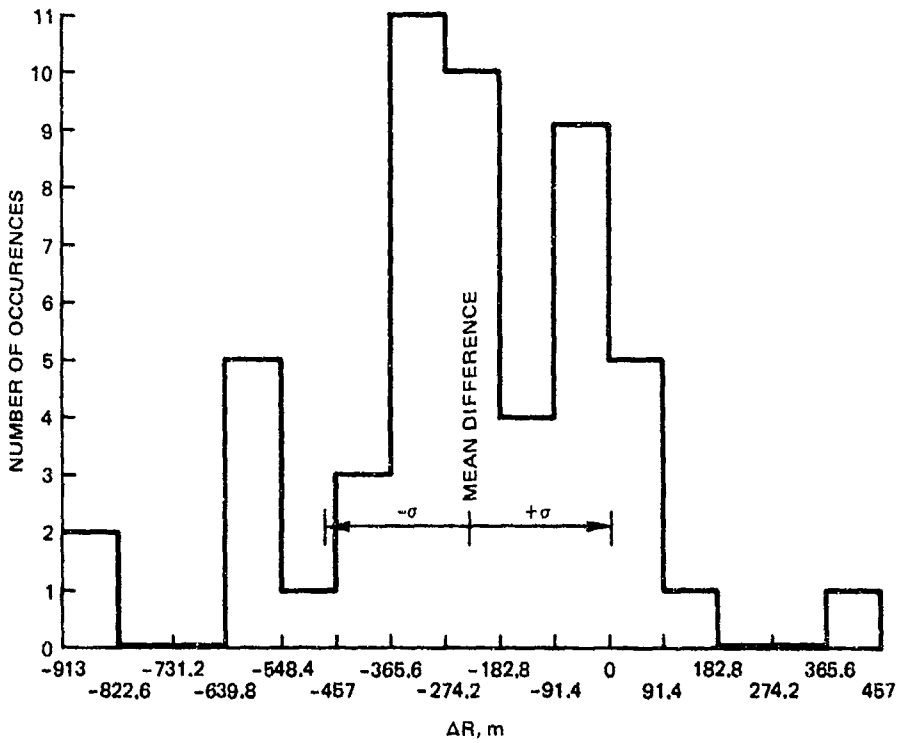


Figure 13. Histogram corresponding to Fig. 12. Mean difference = -234 m, $\sigma$ = 240 m.

This factor reduces the bias from -234 to -162 m. Student's t test now yields a value of t = 1.64, which corresponds to the 5-percent significance level. Thus although this correction reduces the bias, the significance level is still small enough to suggest other sources of systematic error in the data.

R. T. Bachman of NOSC then examined other possible sources of systematic error in the satellite ranges. He soon determined that in calculating these ranges in Ref. 4 he used a geodetic constant appropriate for a latitude of 45°. The geodetic constant decreases by about 1 percent from pole to equator and the use of the 45° value results in an error of about 0.5 percent at most. Heretofore this error has been considered acceptable in connection with satellite navigation at sea. However in this case it represents a significant source of error. The median range of Fig. 12 is about 155 km and corresponds to a latitude of about 32.4°. The geodetic constant at this latitude is 0.217 percent less than that at 45°. This error would then translate into a satellite range that is about 350 m too great. Thus it is significant in terms of Fig. 12.

Bachman then recomputed all the satellite ranges by means of a geodetic constant which varies appropriately with the mean latitude. The counterpart of Fig. 12 for these newly computed ranges is presented in Fig. 14, which also takes into account the 72-m displacement between acoustic source and satellite antenna. The differences are now biased on the positive side. This is illustrated by Fig. 15. The mean difference is 117 m with a standard deviation of 272 m.

Student's t test applied to the data of Fig. 14 and to the FLIP position data of Ref. 4 yielded a value of t = 1.124. This corresponds to a significance level of about 13 percent.

Thus our corrections have decreased the significance level of the bias. We also note by comparing Figs. 14 and 12 that the correction due to the improved geodetic constant has removed a slight dependence on range. In Fig. 14 the differences appear to be quite independent of range beyond 69 km. Observe, however, that the standard deviation has increased somewhat in Fig. 15 as compared to Fig. 13. This is explained by the points on the left tail of the distribution. Examination of the data shows that the four observations with differences to the left of -366 m are all affected by a satellite observation at 36.1 km. We believe this to be a poor satellite fix. Removal of this poor fix would reduce the standard deviation considerably, but would also increase the mean difference.

Although we cannot prove it, we strongly suspect there remains a significant bias in the data of Fig. 15. The fact that 67 percent of the data points lie between 91 and 366 m strongly suggests that this is the case. Possible reasons for this bias are only speculative. However a likely cause is some bias in the location of FLIP.

One assumption made throughout is that the FLIP position is fixed. Reference 6 discusses the excursions of FLIP on a three-point moor in 4110-m water as measured during a 5-week period. The average excursion was on the order of 229 m. However a total spread of some 1100 m was noted. These extreme excursions occurred when wind and current were in the same direction. Thus there is no doubt that the meanderings of FLIP on its moor contribute to the scatter of Fig. 14. Indeed the somewhat cyclical nature of the data in Fig. 14 beyond a range of 69 km suggests the influence of wind and currents. It is also conceivable that wind and currents were such that the mean set of FLIP differed by several hundred meters during the determination of the FLIP location and during Run A.

Thus far we have investigated only the satellite ranges as a possible source of bias. There is a good possibility that some of the bias can be attributed to the acoustic ranges. The acoustic ranges were based on Anderson's sound speeds (Ref. 3). A recent analysis by

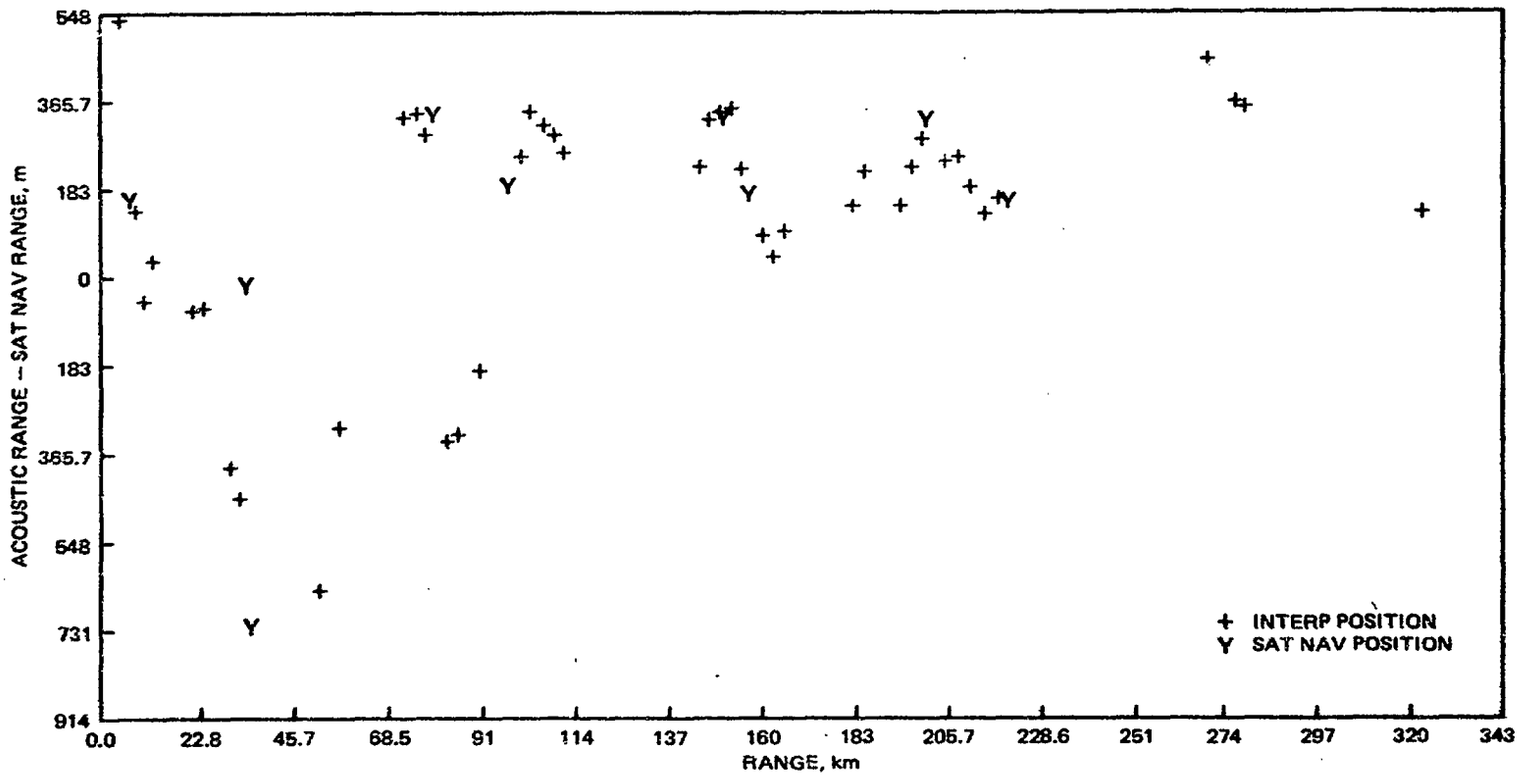


Figure 14. Counterpart of Fig. 12 after correction for geodetic constant and acoustic source position.

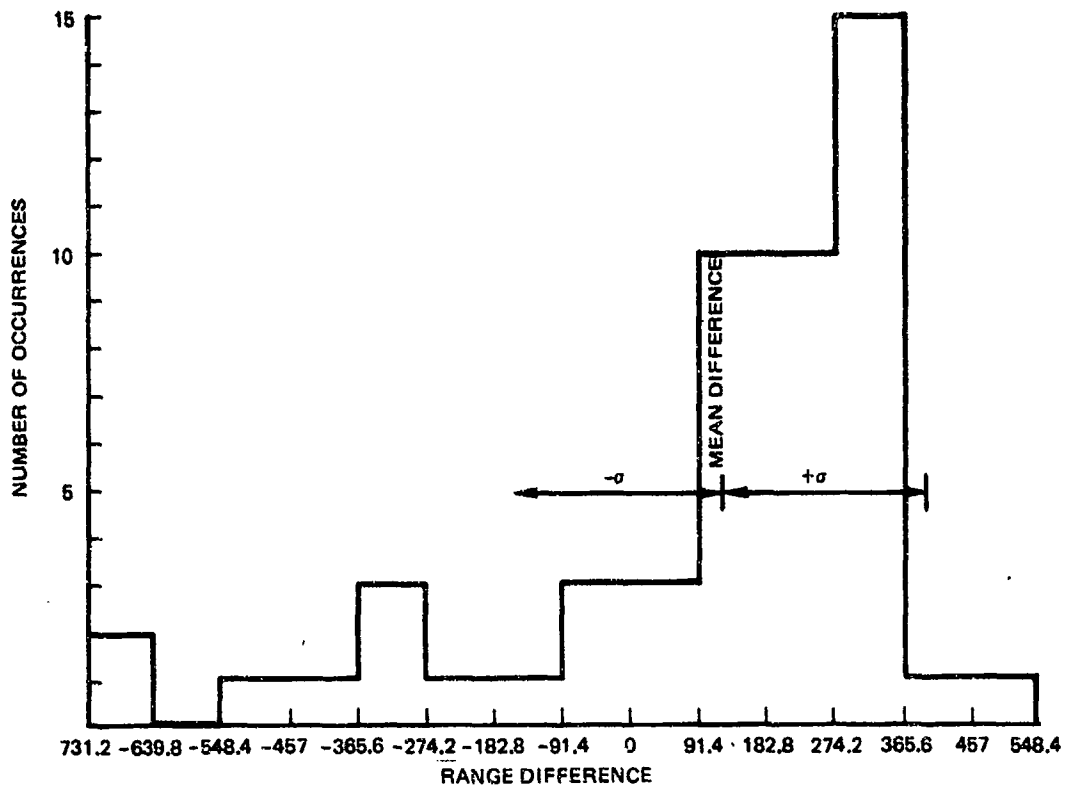


Figure 15. Histogram corresponding to Fig. 14. Mean difference = 117 m, $\sigma$ = 272 m.

Lovett (Ref. 7) indicates that the Anderson sound speeds are between 0.3 and 0.4 m/sec too high. The first-order effect of this is to make the group velocity of ray theory 0.3 to 0.4 m/sec too high. The acoustic travel time at the median range is about 105 sec. Thus if we lower the group velocity by 0.35 m/sec we decrease the median acoustic range by 37 m. This estimate would reduce the bias in Fig. 15 from 117 to 80 m.

Note in Fig. 15 that 88 percent of the acoustic ranges lie within ±366 m of their corresponding values determined by satellite navigation. Thus if a 366-m error is tolerable, satellite navigation is an acceptable method for ranging between a fixed and moving ship.

The CW signals which MPL processed during CAPER were averaged over a time interval of 3 min and 36 sec. At a nominal speed of 6 knots this corresponds to averaging over a range interval of 667 m. Thus the integration interval is about twice the value of the possible range error attributable to satellite navigation. This supports MPL's contention from the inception of the planning of Exercise CAPER that satellite navigation was adequate in this application.

Four other items on the navigational aspects of CAPER are of interest. Let us first consider the distance between FLIP and Stoddard Seamount. This range as determined from the satellite positions was 219.9 km. The acoustic range from the DE STEIGUER at the shallowest point logged on the echo sounder was 220.1 km. On the basis of the bathymetric charts the actual peak of Stoddard Seamount was estimated to be at about 457 m greater range. Thus our best acoustic estimate is 220.6 km. This is not an independent acoustic estimate because it depends on the details of the seamount bathymetry, which relies on satellite navigation. In any case both the 219.9 and 220.6 km values are reasonably close to the distance of 224 km upon which the exercise was designed.

A second item is that Ref. 4 reports a relative satellite navigational error of about 457 m based on the agreement between bathymetry on track crossings.

A third item is that the range scales on the bathymetry of Figs. 8 and 9 and similar figures to follow are based on acoustic ranges out to a range of about 330 km and are based on satellite ranges beyond. A final item concerns the data of Fig. 14. The data set of Fig. 14 was divided into two subsets. There were nine data points for which differences corresponded to satellite observations. The mean difference of this first set was 122 m with a standard deviation of 310 m. There were 43 data points for which differences correspond to interpolation between satellite range observations. The mean difference of this second set was 116 m with a standard deviation of 264 m. The difference between these means (6 m) is not statistically significant. (Student's t test yields a value of t of 0.056.) Thus there is no significant difference in accuracy between the satellite ranges and the interpolated satellite ranges. The additional error introduced by interpolation between fixes is small compared to the error in the fixes themselves. In other words, for practical purposes the interpolated ranges are as accurate as those corresponding to the actual satellite fixes.

## ASSESSMENT OF SEAMOUNT SHADOWING

The first topic to consider in the assessment of seamount shadowing is the receiver depths at FLIP. These are given in Table 1 and are numbered from deepest to shallowest. The depths for numbers 1 through 15 were determined acoustically, whereas those for 16 to 20 are shallow enough that the wire depths were accurate. The bottom depth at FLIP as measured acoustically was 4528 m. The receivers flagged with the asterisks are those that were recorded on magnetic tape for the travel time analysis discussed in the preceding section.

The FLIP receivers were grouped in four sets of five each. Numbers 1 to 5 were selected to be near the ocean bottom. Numbers 6 to 10 are just shallower than the critical depth (depth where sound speed equals surface sound speed). Numbers 11 to 15 were selected to straddle the sound-speed axis. Numbers 16 to 20 are positioned in the thermocline.

The first item to note is that whereas hydrophones 1 to 5 are positioned well with respect to the 4528-m bottom depth at FLIP, they are not positioned well from the standpoint of the bottom relief as illustrated in Figs. 8 or 9. A nominal vertexing depth of 4206 m was chosen for the steepest angle ray which would likely clear the bottom relief. Hydrophones 1 to 5 are all deeper than this value. Thus we are reasonably certain that, except for very short ranges, most of the acoustic arrivals reaching receivers 1 to 5 have reflected from the bottom even before the seamount was traversed. These receivers are not well suited to investigate seamount shadowing. This also explains why only one useful acoustic travel time was obtained from receiver number 1.

Unfortunately as far as receivers 1 to 5 are concerned, the effect of the abyssal hills was underestimated. The bathymetric chart of Fig. 1 gave no hint as to the presence of this relief. As a matter of fact, that chart suggests corrected bottom depths of between 4300 and 4480 m for at least the first 91 km of Run A. Although these receivers were not located well from the standpoint of Run A, they appear to be in excellent locations for northern or western directions.

Let us consider now hydrophones 6 to 10. Figure 9 presents the ray diagram for number 6; Fig. 16 presents the ray diagram for number 10. It is obvious from Figs. 9 and 16 that all arrivals from beyond the seamount must reflect from the seamount for hydrophones 6 to 10. Thus there are no non-bottom-reflected arrivals from beyond the seamount for these hydrophones.

Table 1. Receiver Depths at FLIP.

| Hydrophone # | Depth, m | Hydrophone # | Depth, m |
|---|---|---|---|
| 1* | 4363 | 11 | 844 |
| 2 | 4335 | 12 | 816 |
| 3 | 4307 | 13 | 788 |
| 4 | 4279 | 14 | 760 |
| 5 | 4251 | 15* | 732 |
| 6* | 3508 | 16* | 206 |
| 7 | 3480 | 17 | 178 |
| 8 | 3452 | 18 | 150 |
| 9 | 3424 | 19 | 122 |
| 10 | 3396 | 20* | 94 |

Figure 17 presents the ray diagram for hydrophone number 11. (In order to simplify the plot, rays which do not reach a depth of 304 m are excluded from this figure.) In this case there are rays which pass over the seamount without reflection. Thus hydrophones 11 to 20 can receive rays which emanate from beyond the seamount and which do not reflect from the seamount.

One can estimate from Fig. 16, the deepest receiver depth for which a ray can clear the seamount. We note that the first ray that can clear the seamount is the bottom-limited ray that starts initially downward at the receiver depth. The critical point of clearance on the seamount profile is the point where the slope breaks on the far side at a depth of about 1714 m. The horizontal displacement of the bottom-limited ray in Fig. 16 at this point is about 8 km. We now determine the depth which corresponds to 8 km range for the bottom-limited ray that starts initially upward in Fig. 16. This depth was determined to be 1746 m. For a receiver at this depth the bottom-limited ray that starts initially downward will just clear the seamount. Thus for receivers shallower than 1746 m, some rays will always clear the seamount without bottom reflection.

We now turn to a more detailed examination of the extent of shadowing for a particular receiver. In this case we have chosen the shallowest receiver, i.e., number 20 at a depth of 94 m. The source depth in this case was 122 m.

Figure 18 presents a summary of this study. The format is similar to that of Fig. 4 in that distances are relative to the peak of the seamount, which is labelled P. The vertical scale represents the distance from the peak along the bearing line joining FLIP to P. The horizontal scale represents the normal distance from this bearing line.

The solid horizontal lines designate the various ray-theory convergence zones (assuming no seamount interference). Convergence zones 5, 6, and 7 and portions of zones 4 and 8 are shown. The shadow zones between them are labelled SZ.

The hatched areas represent regions where no rays can pass from a 122-m source to a 94-m receiver without reflecting from the seamount. These areas represent regions where the seamount "shadows" the propagation paths that would exist without the seamount. The leading edge of these regions coincides with the leading edges of the convergence zones because the seamount cannot shadow ray paths that do not exist without the seamount. Maximum lateral shadowing occurs at the leading edge. Maximum shadowing in range occurs at zero lateral displacement because this represents maximum interception by the seamount peak. Other displacements represent decreases shadowing by the lower slopes of the seamount.

The dashed lines represent the various ship tracks based on the navigational data of Ref. 4. Time of day corresponding to satellite fixes are labelled along the tracks. Track A passed about 2.7 km from the seamount peak. At more distant ranges the track meandered about the exact bearing line with maximum lateral displacement of only 1.8 km. As can be seen, Run A corresponds very closely to maximum possible shadowing.

Traverse Run D was also well positioned. Along traverse Run D shadowing occurs for a total lateral distance of about 14.6 km. Traverse Run E was also well positioned. Along this track rays can always pass over the seamount.

Unfortunately, from an analysis standpoint, traverse Run B fell at the most complicated position possible as far as the 94-m receiver is concerned. This track "lies on the ragged edge" of or falls within the thin shadow zone between the convergence zones 7 and 8. The problem of shadow zone diffraction when the ensonified region is intercepted by a seamount is very difficult from an analysis standpoint.

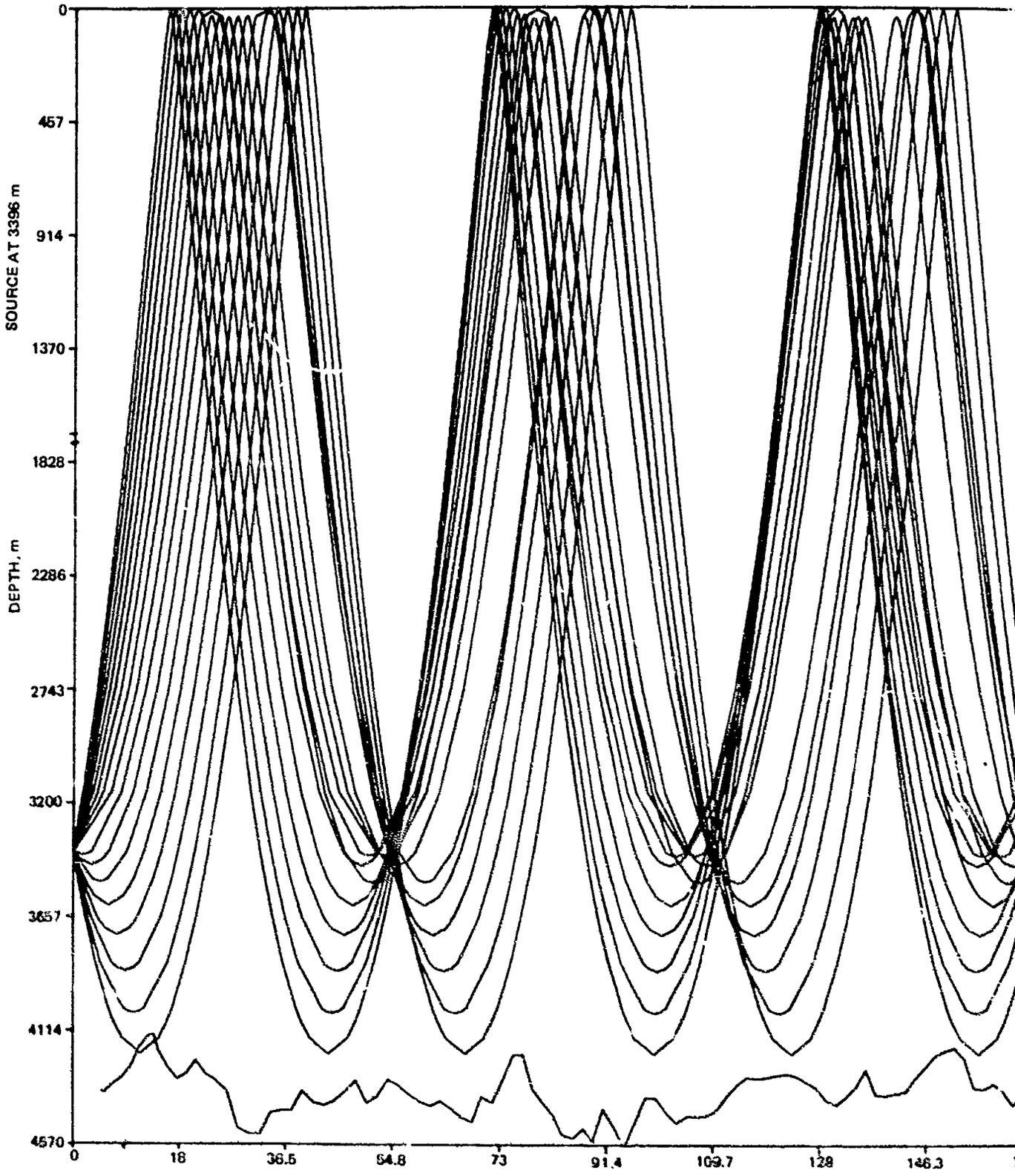
SOURCE AT 3396 m
DEPTH, m
0
457
914
1370
1828
2286
2743
3200
3657
4114
4570
0
18
36.5
54.8
73
91.4
109.7
128
146.3
RAN

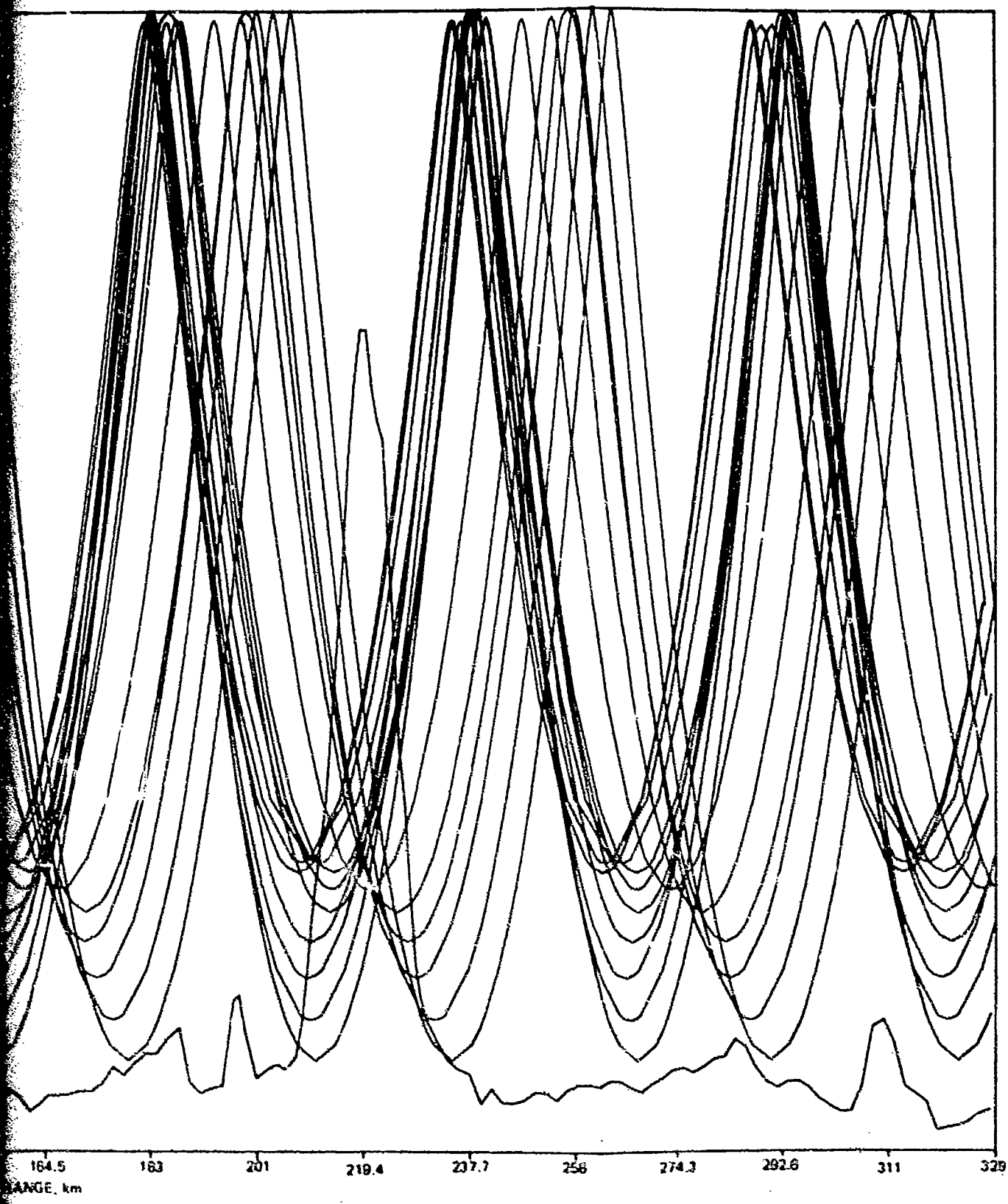


Figure 16. Ray diagram for a source depth of 3396 m.



2

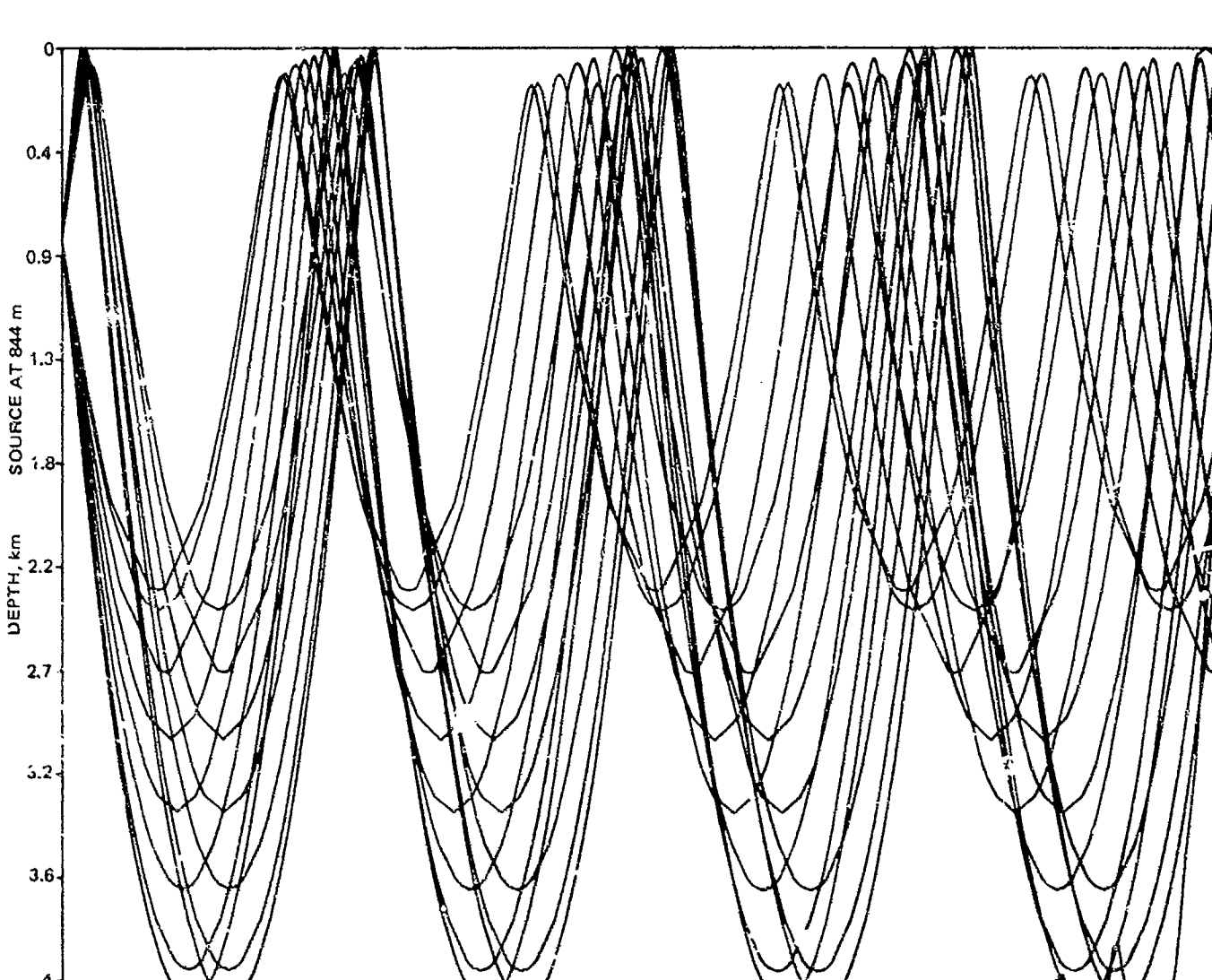
SOURCE AT 844 m
DEPTH, km
0
0.4
0.9
1.3
1.8
2.2
2.7
3.2
3.6
4
4.5
0
18
36.5
54.8
73
91.4
109.7
128
146.3
164.5
182.8
201

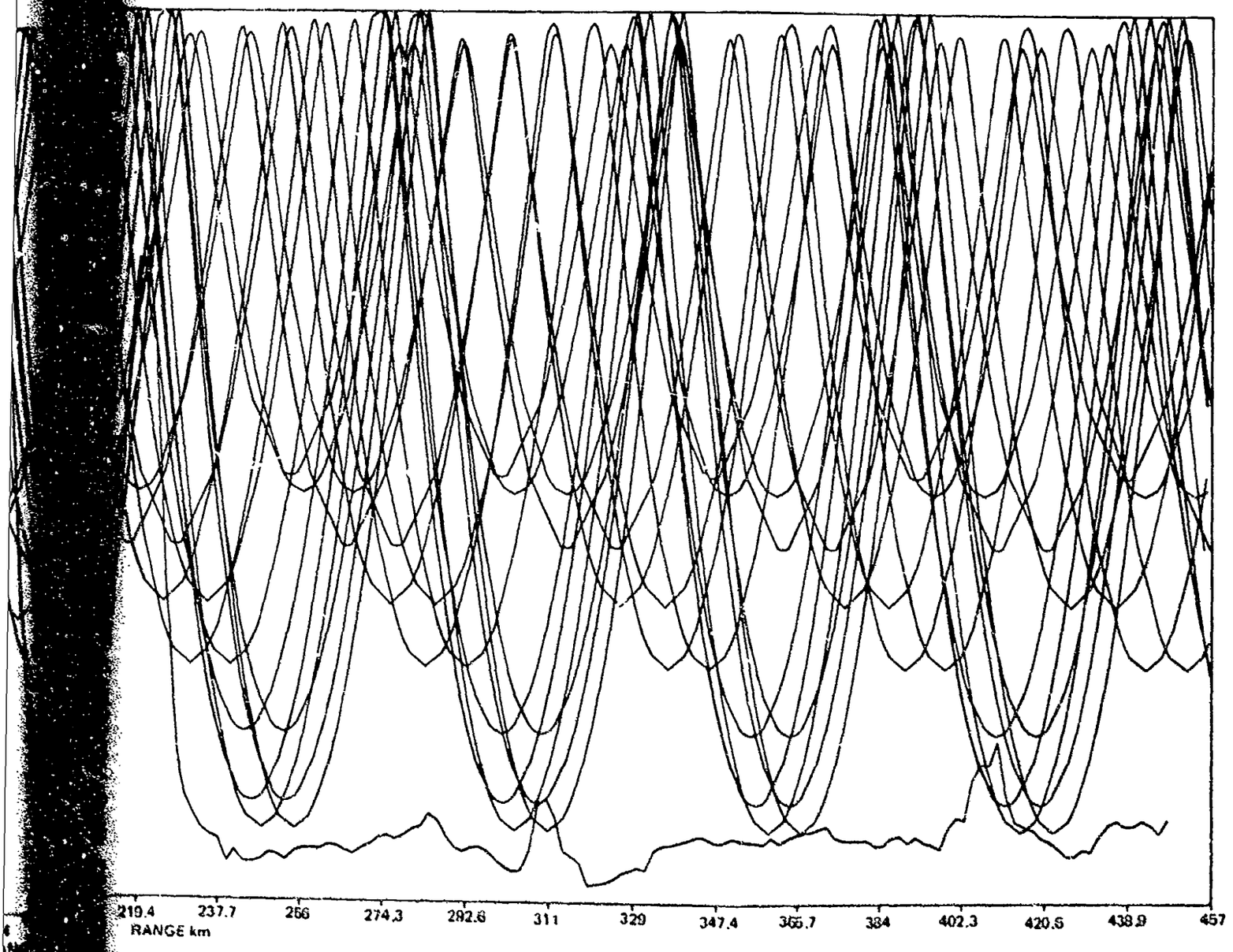


Figure 17. Ray diagram for a source depth of 844 m.

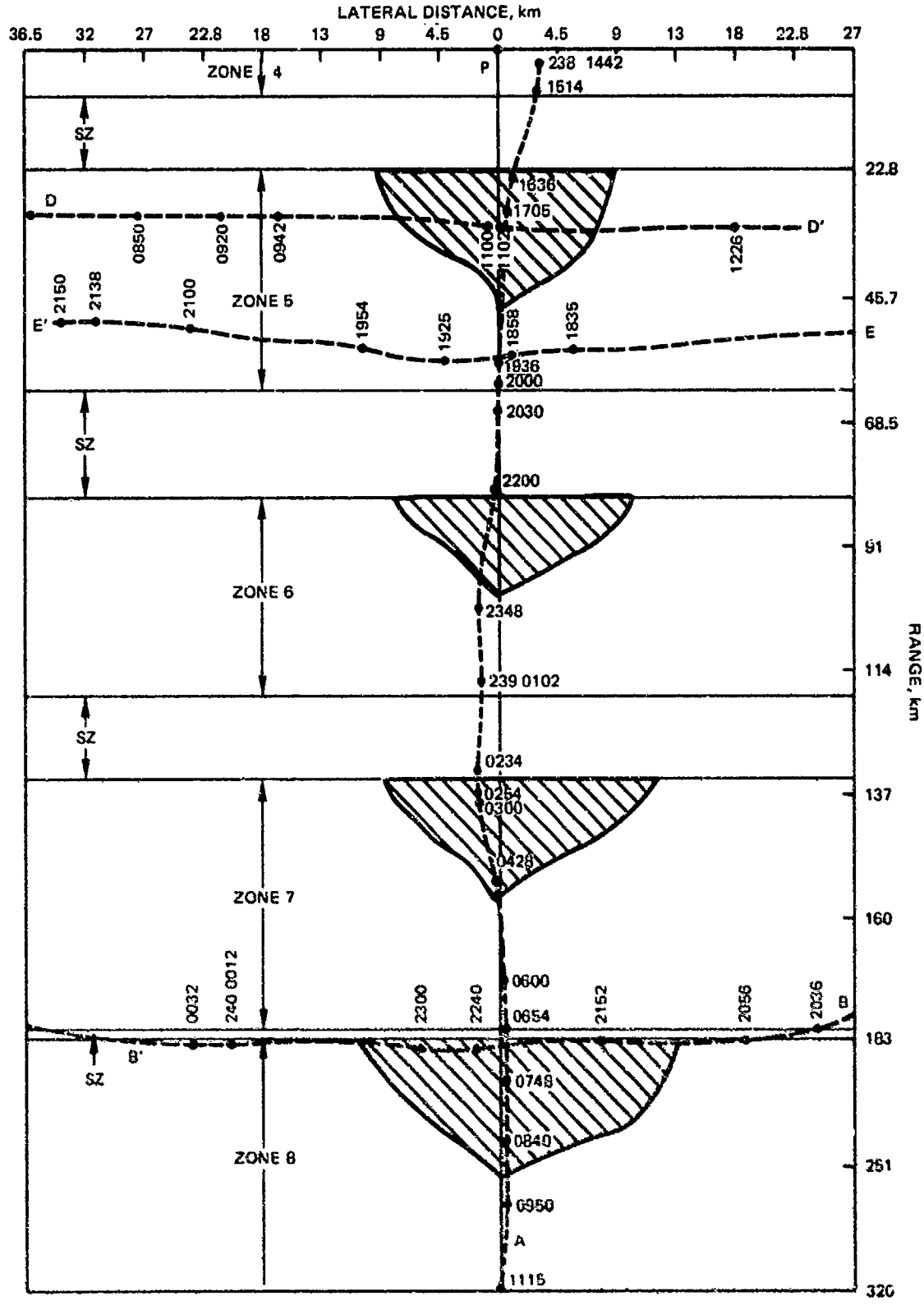


Figure 18. Shadow zone structure behind Stoddard Seamount for a 121-m source depth and a 94-m receiver depth.

The analysis of Run B may be more clear-cut for somewhat deeper receivers at FLIP. For example, in Fig. 15, for the receiver at 844 m, the source at 122 m is ensonified for the range of Run B at a nominal 400 km.

It should be noted that although similar to Fig. 4, Fig. 18 is conceptually different. Figure 4 represents the shadow zones produced by the blockage of a 91-m source irrespective of receiver depth. Figure 18 represents shadow zones produced by the blockage for a 122-m source for a particular receiver depth, i.e.; 94 m at a particular range. This basic difference is the reason that the plots of Fig. 4 and 18 look different. It is not because Fig. 4 is based on a single predicted profile and Fig. 18 based on multiple measured profiles.

Before leaving Fig. 18 we should comment on the excellent job of navigation and ship handling done by the DE STEIGUER in following the exercise plan. This becomes even more noteworthy in light of the fact that at times the currents were such that the ship had to crab 15 deg to maintain the proper course.

It is of interest to look at seamount shadowing from the standpoint of propagation loss. Figure 19 is the propagation loss counterpart of the shallow-receiver ray diagram of Fig. 8. The leading portions of the convergence zones beyond 237 km are labelled "intercepted." These represent the portions of the convergence zones that are intercepted by the seamount. Thus if we remove these portions, we have the propagation loss plot which applies to Run A, assuming that bottom-reflected paths do not contribute. If we retain these portions we have the propagation loss plot which applies to Run C, representing an unobstructed run.

Figure 20 is the propagation loss counterpart of the deep-receiver ray diagram of Fig. 9. In this case the entire convergence zone is intercepted for all zones beyond 219 km. Again if these zones are retained we have the propagation loss plot which applies to Run C.

Recall that in our previous analysis we determined that the rays from all receiver depths below 1747 m would be intercepted by the seamount. At first sight it would appear that this was a result of poor planning, for FLIP could have been positioned at a range from the seamount at which at least some rays would not be intercepted by the seamount. However such a positioning would have resulted in complete interception for shallow receivers.

This result is related to the fact that shallow and deep receivers complement each other. If we compare Figs. 19 and 20 we see that the shadow zones for the shallow receiver are covered in large part by the convergence zones for the deep receiver.

This is the reason why these two receiver depths were so useful in obtaining travel times for ranges. When one was in a shadow zone the other was in a convergence zone and vice versa. This feature breaks down after the seamount is crossed. As illustrated in Fig. 11, beyond a range of 221 km only eight measurements of acoustic range were made. Three of these measurements were between 269 and 277 km. Comparison with Fig. 19 shows that these all fell in the nonintercepted trailing portion of the fifth convergence zone. The other five measurements were between 321 and 332 km. These all fall in the trailing portion of the sixth convergence zone. It is evident then why there were so few measurements of travel time beyond the seamount. The deep receiver was completely blocked, while the convergence zone width for the shallow receiver was reduced to about half its unobstructed width.

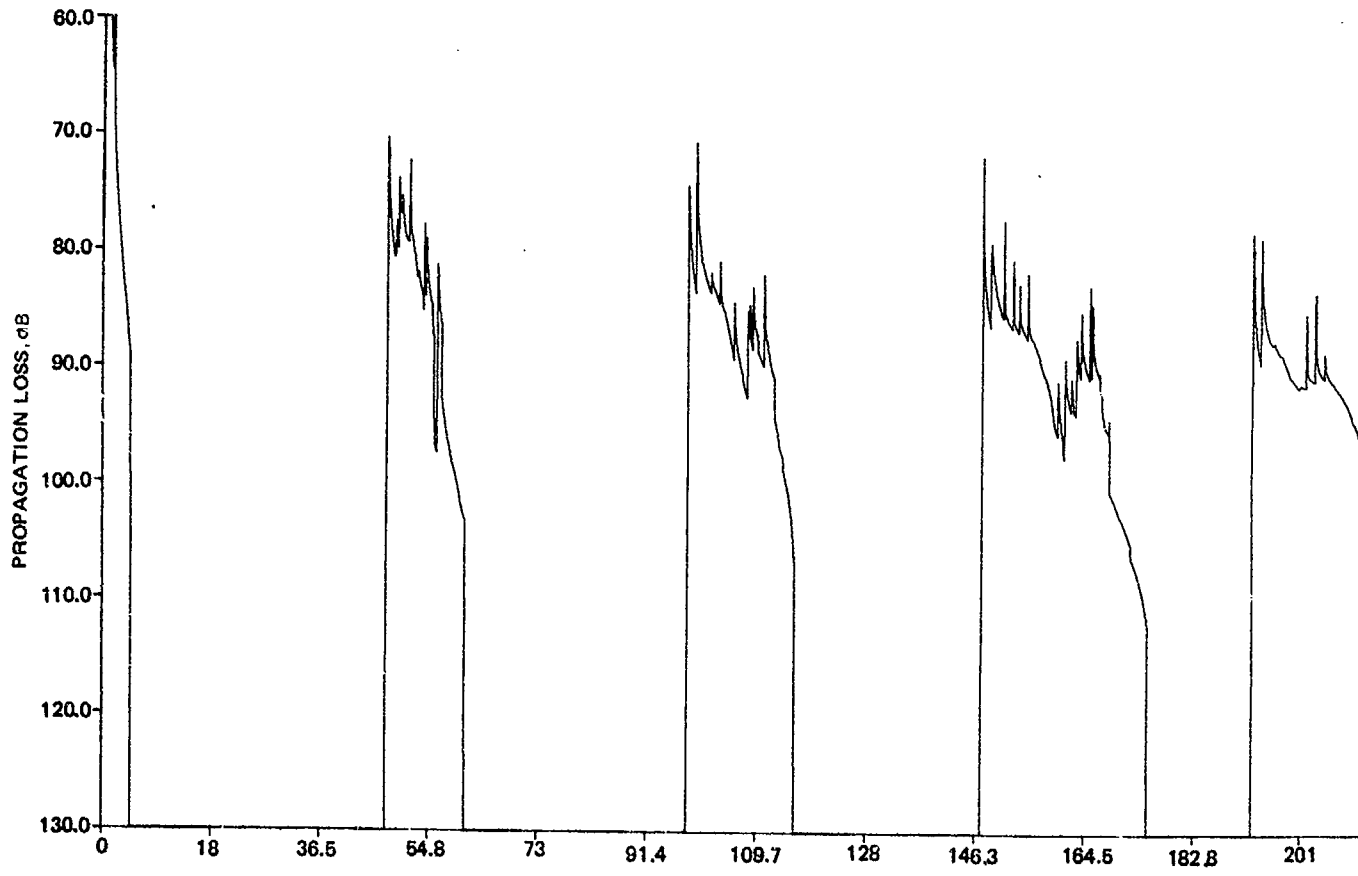
60.0
70.0
80.0
90.0
100.0
110.0
120.0
130.0
PROPAGATION LOSS, dB
0
18
36.5
54.8
73
91.4
109.7
128
146.3
164.5
182.8
201

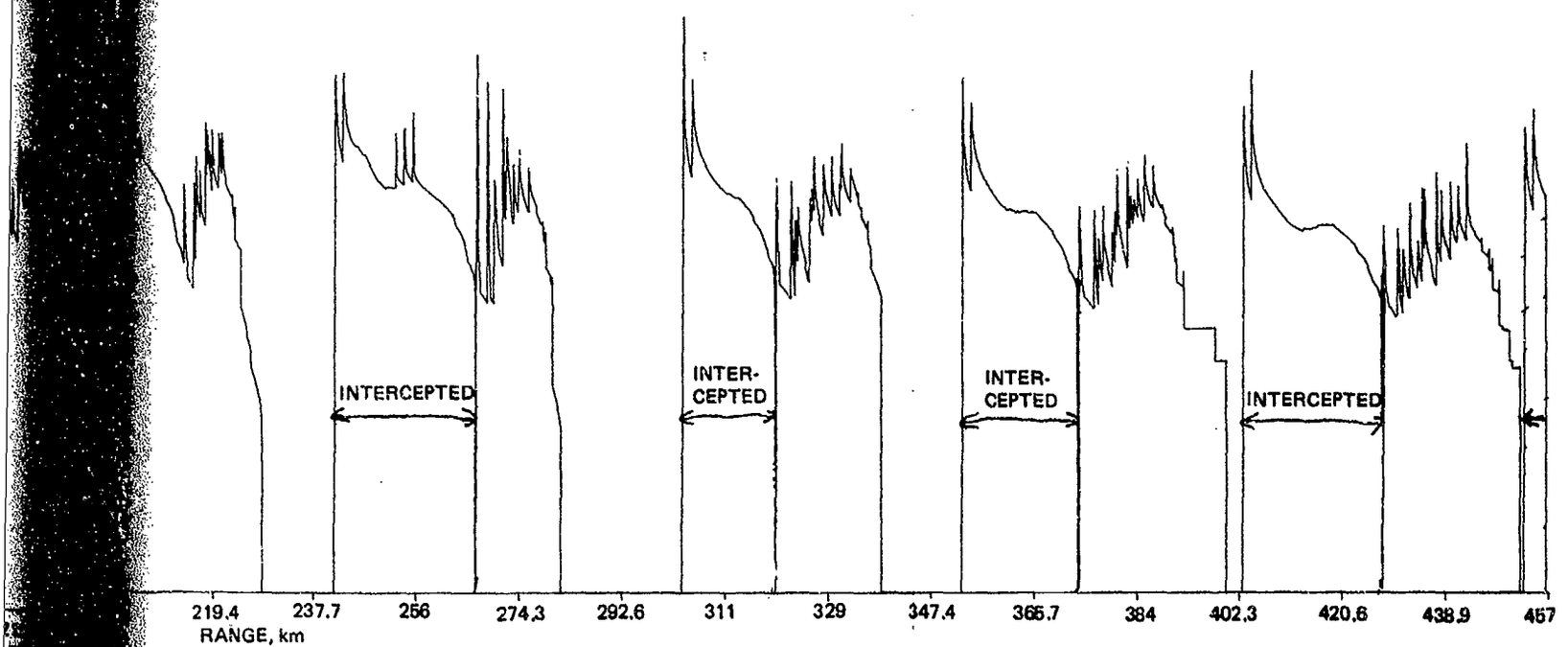


Figure 19. Propagation loss for a source depth of 122-m and a receiver depth of 94-m.

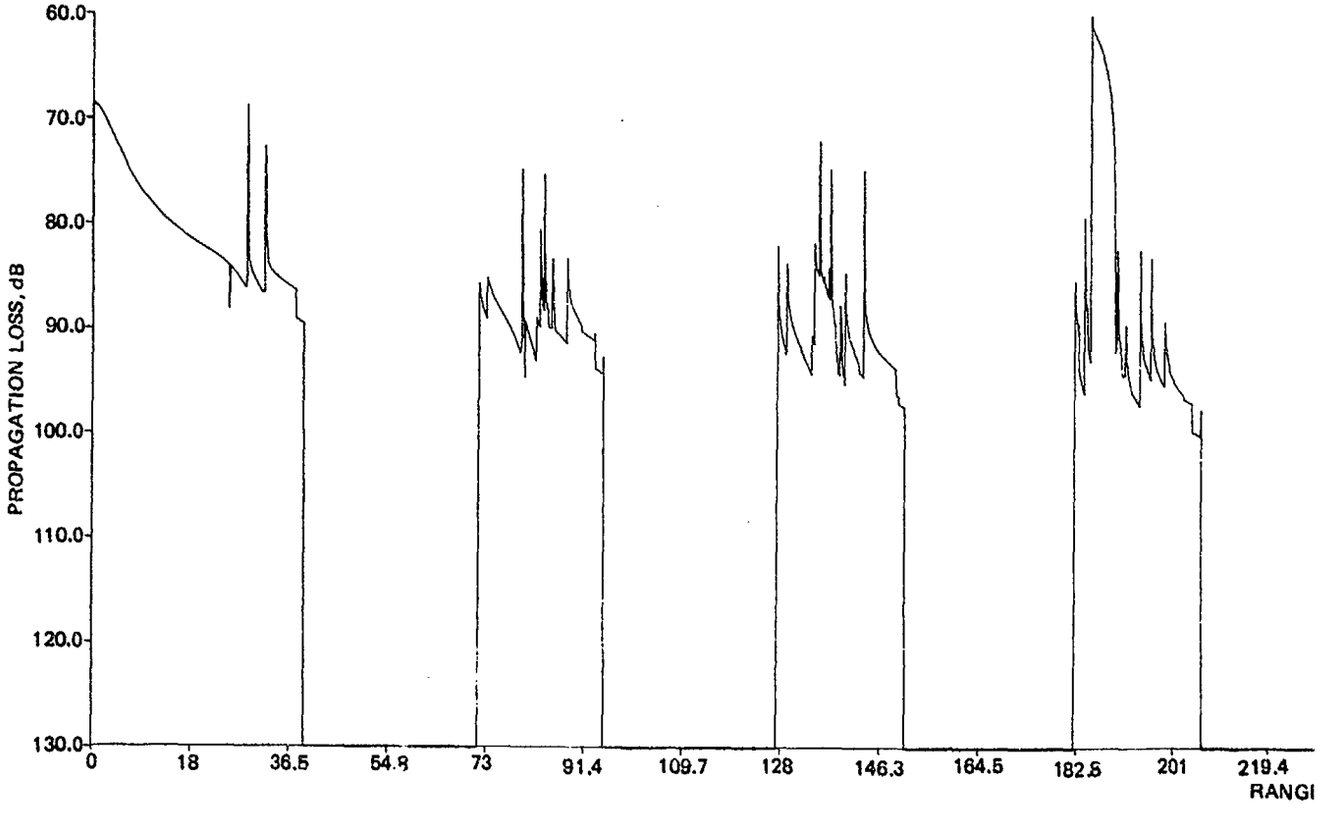
60.0
70.0
80.0
90.0
100.0
110.0
120.0
130.0
PROPAGATION LOSS, dB
0
18
36.5
54.9
73
91.4
109.7
128
146.3
164.5
182.8
201
219.4
RANGI

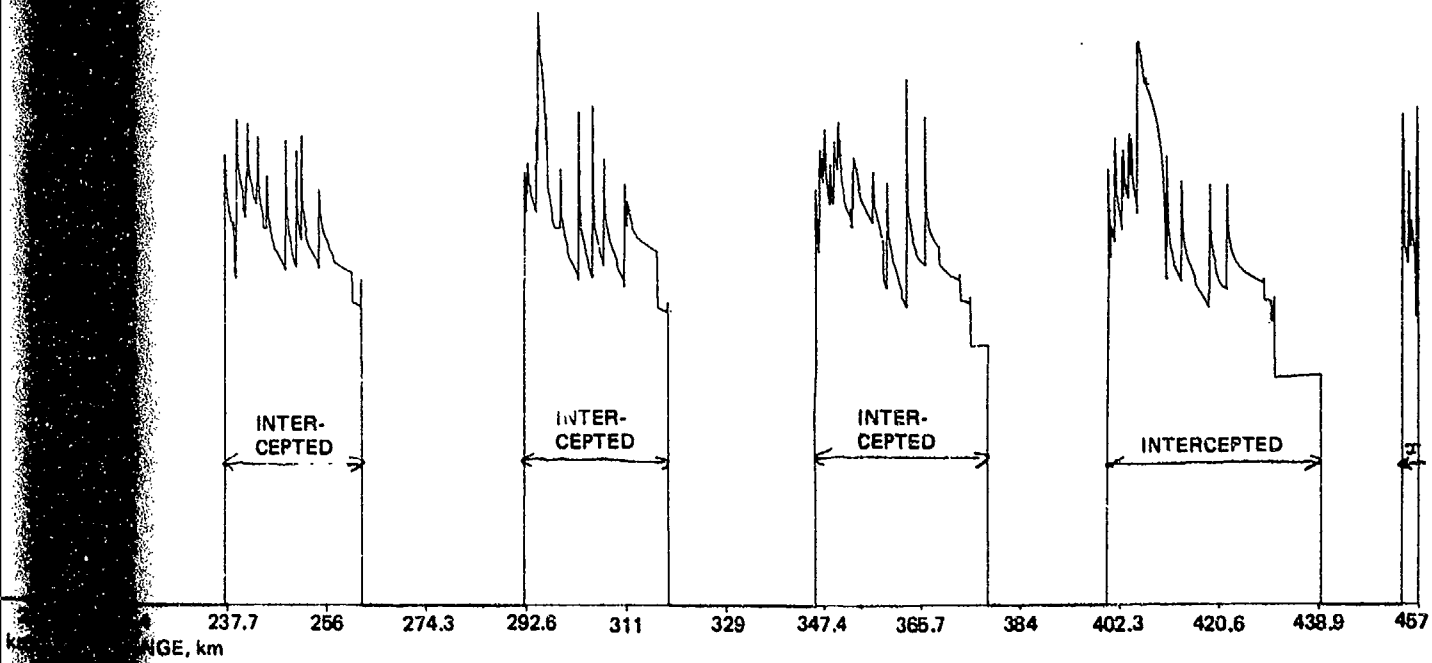


Figure 20. Propagation loss for a source depth of 122-m and a receiver depth of 3508-m.

## EFFECT OF HORIZONTAL CHANGE IN PROFILE

This section presents a brief study of the effect of horizontal change in sound-speed profile to determine if these are important to the acoustic results. In order not to confound effects of profile change and seamount blockage, all these examples ignore the effect of blockage.

The first step in this study was to compare the propagation loss for the composite profile, i.e., the computations of Figs. 19 and 20, with the propagation losses for various profiles with no horizontal change. The other profiles used in this study were profiles 1A and PRE of Fig. 6 and another profile referred to as an average profile. This average profile was obtained by a weighted average of profiles 1A, 1B, 2A and 2B. The weights used were 1 for profile 1A, 2 each for profiles 2A and 1B, and 3 for profile 2B. These weights are consistent with the ray tracing scheme used for the composite profiles in Figs. 8 and 9, i.e., the profile is weighted according to how many zones are traversed in the particular profile. This average profile should then be a profile which might apply for computations in the eighth convergence zone.

The comparisons of propagation loss for the 122-m source depth and 94-m receiver depth are given in Figs. 21A to C. In each of these three figures the solid curve is the same, i.e., the propagation loss of Fig. 19. The dashed curve is the propagation loss for the other profile under consideration.

Figure 21A compares the result of the composite profile with that of the profile at the receiver, i.e., the dashed curve assumes that the receiver profile holds at all ranges. Zones 0 and 1 are identical in Fig. 21A because the same profile applies. The differences between the two computations are reasonably small for zones 2 through 5; however, for zones 6 through 8 the dashed curve falls at significantly smaller ranges. The reason for this is apparent in Fig. 6. Both source and receiver are in the thermocline region where there is the greatest difference between profiles. Profile 1A has the lowest sound speed. Profile 2B, which becomes a factor at zone 6, has the highest sound speed. This increase in sound speed when profile 2B is encountered shifts the convergence zone out in range much further than if the low sound speeds of profile 1A had prevailed.

Figure 21B compares the results of the composite profile with those of the predicted profile. This was the profile which was used in designing the exercise. Surprisingly enough, the results of the predicted profile agree better with those of the composite profile than do the results of profile 1A. Results are comparable for zones 1 to 3, somewhat better for profile 1A for zones 4 and 5, but much better for the predicted profile for zone 6 and higher order zones. This feature can again be explained from Fig. 6. The sound speeds for the predicted profile are greater than those of profile 1A for depths below 50 m. Thus in the critical thermocline region where the source and receiver are, the predicted profile is a better measure of the influence of fast profiles 2A and 2B than slow profile 1A is. Thus the average profile agrees better in zone 2 and 3 where profile 2A begins to dominate and better in zones 6 to 8 where profile 2B begins to dominate. For this source and receiver configuration, the low near-surface sound speeds of the predicted profile appear to have little effect, i.e., the predicted profile appears better than profile 1A despite the low surface sound speeds.

Figure 21C compares the results of the composite profile with those of the weighted average profile. Recall that the average profile was weighted for zone 8. Note that the agreement for zones 6 and 7 as well as zone 8 is much better in Fig. 21C than in Fig. 21A or B. Thus our system of weighting the profiles appears to have some merit. However, the agreement for zones 1 to 5 is worse in Fig. 21C than in Figs. 21A or B. This is not too surprising

because profile 11B is heavily weighted in the average profile, but does not even enter into the computation for zones 1 to 5 for the composite profile.

Figures 22A to C are the counterparts of Figs. 21A to C for the 3508-m receiver. Agreement with the results of the composite profile is generally much better than in Figs. 21A to C. For this deep receiver depth only steep rays are involved and the sound-speed structure is not as important.

Table 2 presents some quantitative results for zone 8 for the various profiles. Columns 1–4 pertain to the 94-m receiver. Column 1 is the leading edge of the convergence zone, Column 2 gives the range of the bottom grazing ray, Column 3 presents the difference between the leading edge of the composite profile and that of other profiles. Column 4 is the counterpart of Column 3 for the bottom grazing ray. Columns 5 to 8 are the corresponding values for the 3508-m receiver.

The results are similar to those discussed for Figs. 21 and 22. Features associated with lower angle rays are generally more sensitive than those with higher angle rays. Differences for the bottom grazing ray are generally smaller than those for the leading edge, while differences for the leading edge are smaller for the 3508-m receiver than for the 94-m receiver. There is only one feature of Table 2 which cannot be explained qualitatively from consideration of the sound-speed profiles. It is not at all evident why the agreement in the leading edge for the 3508-m receiver is poorer for the average profile than it is for profile 1A or the predicted profile. This feature also shows up in Fig. 22 in zones 6 and 7.

There remains the problem of assessing the effect of the seamount sound-speed profile, which has thus far been ignored. The simple scheme used to treat near-surface changes in sound speed cannot be used because here we are treating changes in the deep profile, where the rays form nadirs.

An estimate of the effect of the seamount profile was made from ray calculations for two profiles. The quantities calculated were the cycle range, i.e., the range between successive apexes and the corresponding group velocities, i.e., the cycle range divided by the cycle travel time.

Figure 23 presents cycle range versus ray parameter (i.e., phase velocity) for profile 1B with the deepwater profile appended. (This is the profile which was used to progress from zone 4 to zone 5 in Fig. 8.) The smallest phase velocity corresponds to the axial ray, whereas the largest value corresponds to the ray which grazes the nominal bottom depth of 4206 m.

The computations corresponding to Fig. 23 were then made for profile 1B with the seamount profile appended. Differences between these computations and those of Fig. 23 are too small to compare directly. Hence the values of cycle range were subtracted from those of Fig. 23. These differences are plotted in Fig. 24. The maximum difference occurs for the axial ray. The profile near the axis at about 600 m depth should be the same for both profiles since the seamount profile only applies to 1000 m and deeper. However the procedure by which the profiles are fit by curvilinear segments depends on the entire deepwater structure, and thus the fits at the axis can be different for the two profiles.

In any case the region of near-axial rays of Fig. 24 is not important. The sound speed at the primary source depth (122 m) limits the rays of interest. These are labelled on Fig. 24 as $C_1$ for profile 1B and $C_2$ for profile 2B. Thus we can ignore values of phase velocity less than these values. The conclusion that we come to is that the ray trace ranges can differ at most by only ~201 m. This value is conservative because it assumes that the seamount profile applies for a full loop length, when in reality it probably applies for less than a full loop length.

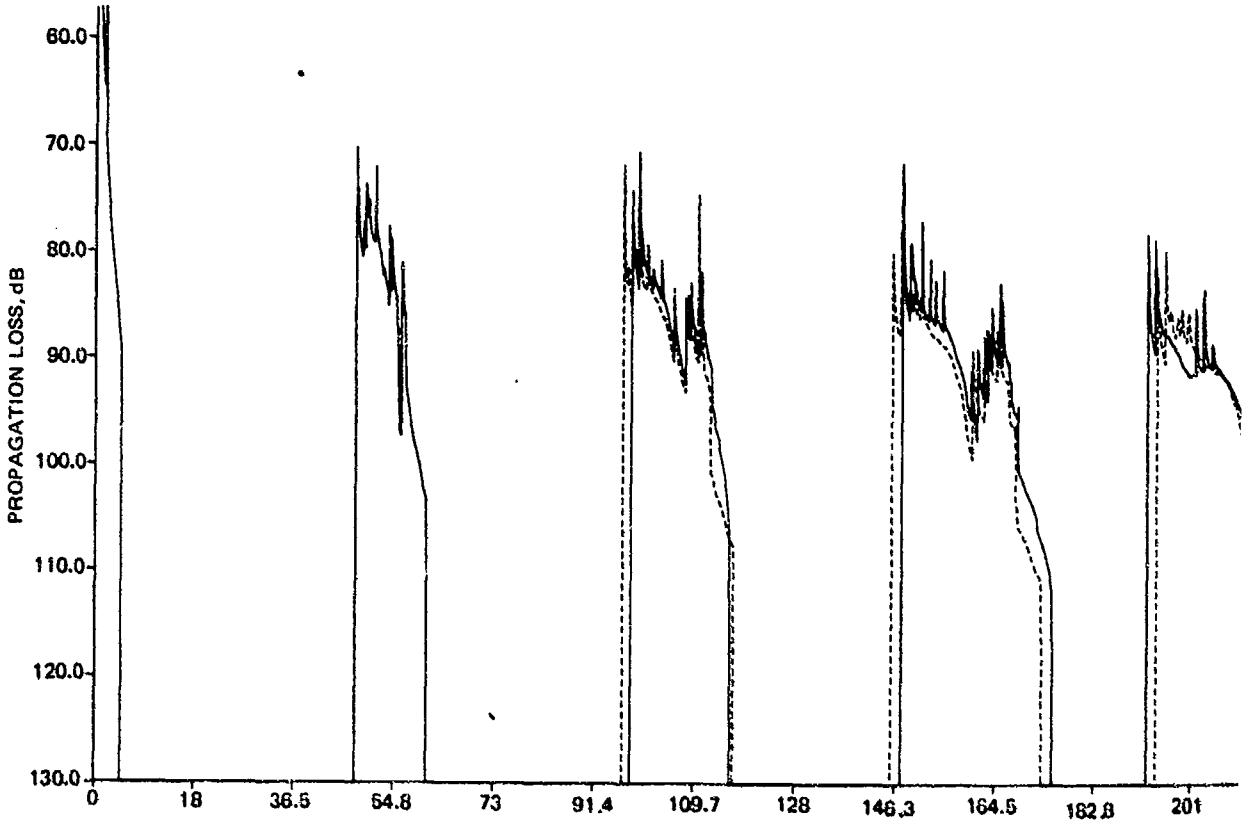
PROPAGATION LOSS, dB
60.0
70.0
80.0
90.0
100.0
110.0
120.0
130.0
0
18
36.5
54.8
73
91.4
109.7
128
146.3
164.5
182.8
201

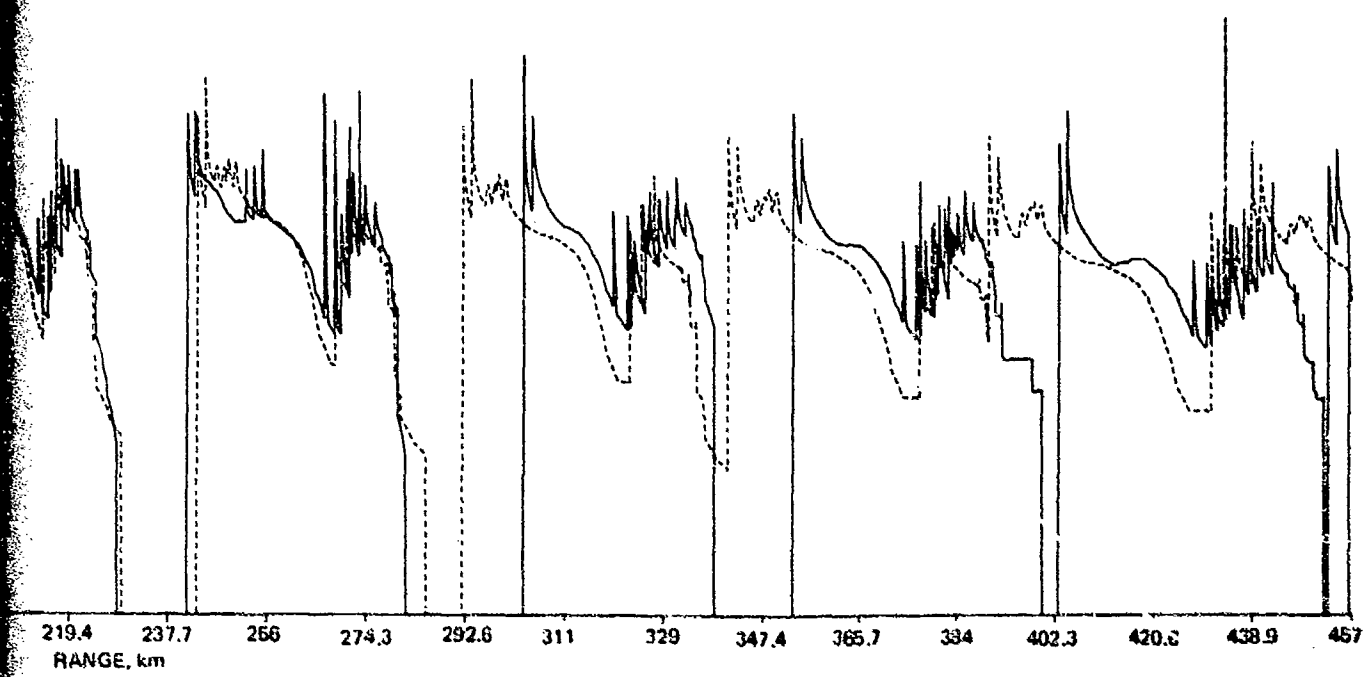


(A)

Figure 21. Comparisons of propagation loss for the 122-m source and 94-m receiver and the composite profile with: (A) those of Profile 1A; (B) those of the predicted profile; (C) those of the average profile.



2

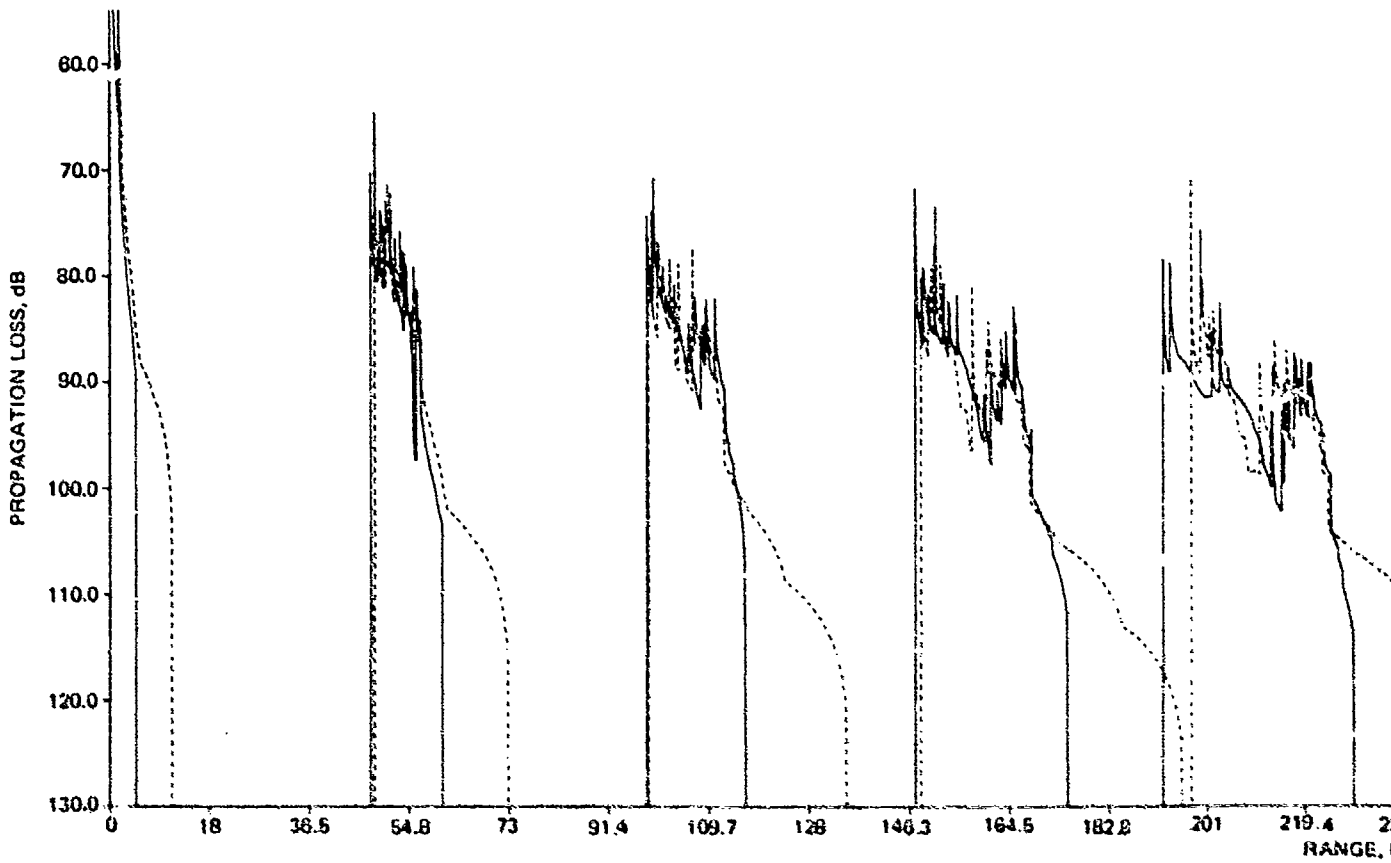
PROPAGATION LOSS, dB
60.0
70.0
80.0
90.0
100.0
110.0
120.0
130.0
0
18
36.5
54.8
73
91.4
109.7
128
146.3
164.5
182.8
201
219.4
RANGE,

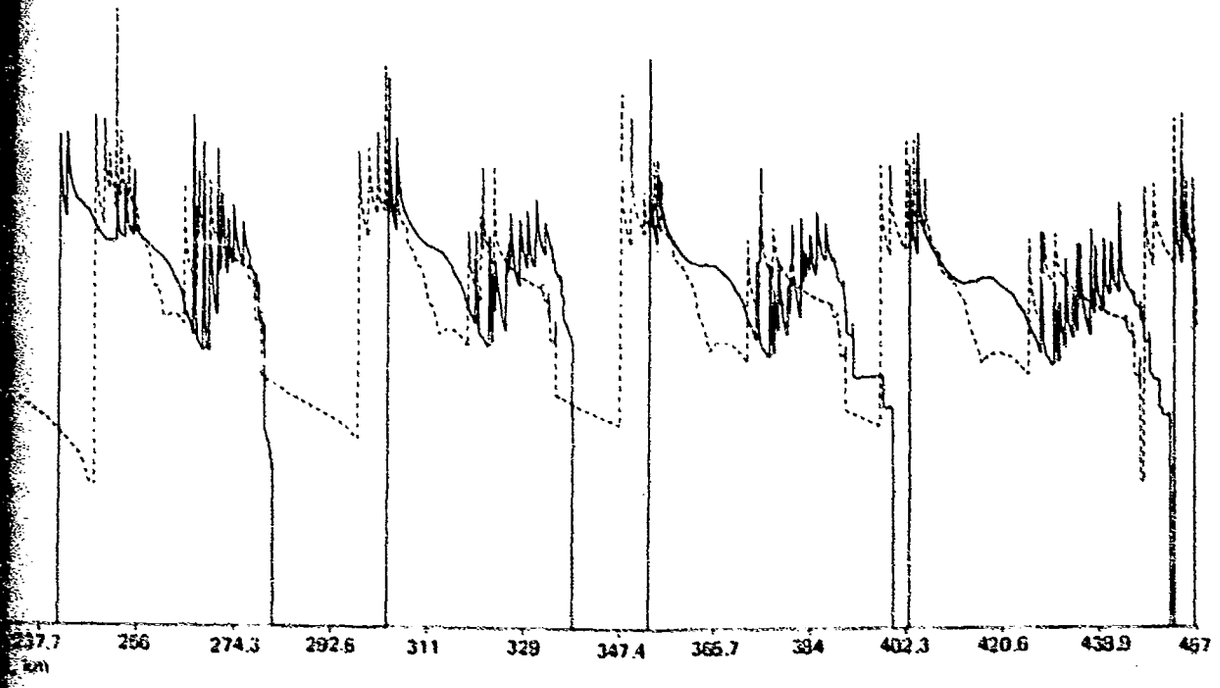


(B)

Figure 21. (Continued).

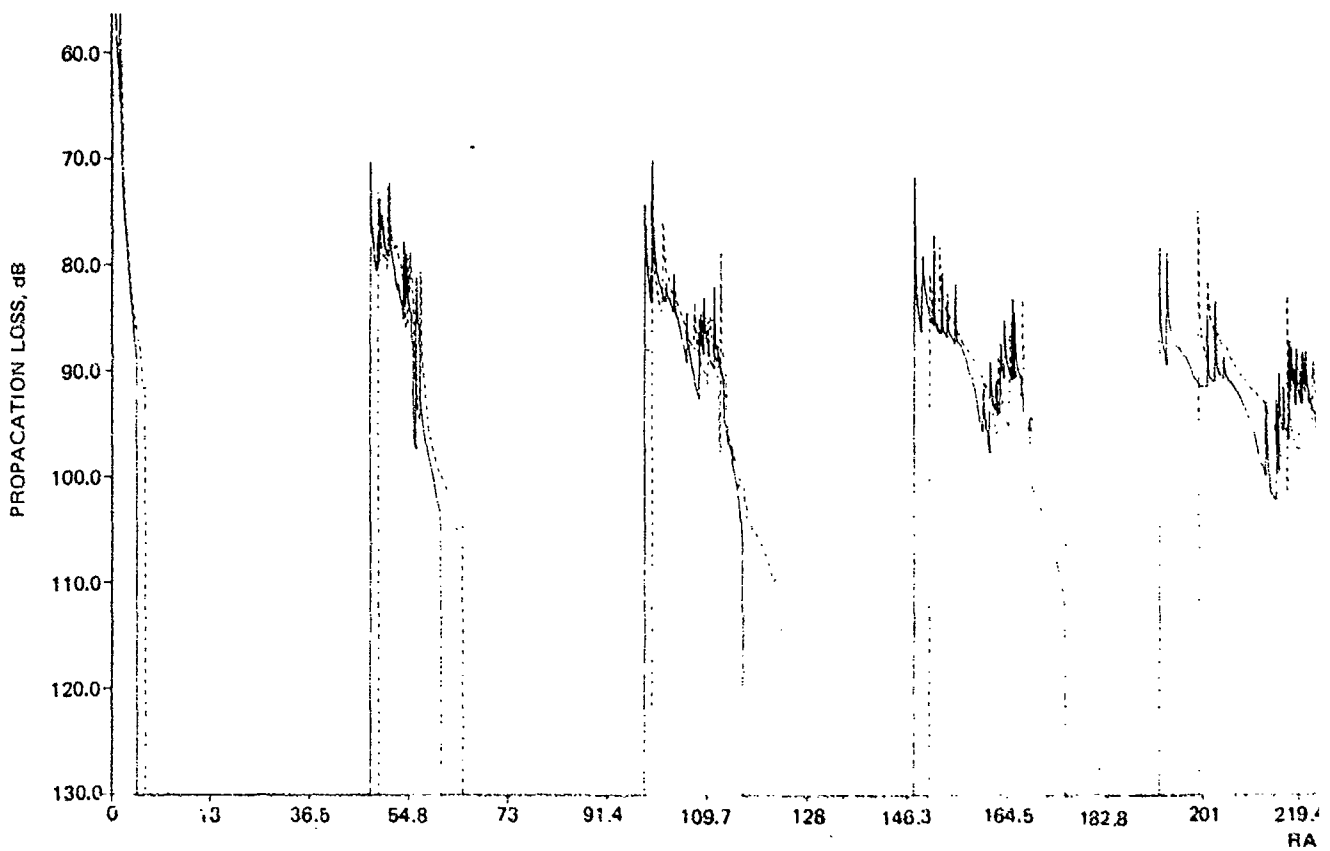
PROPACATION LOSS, dB
60.0
70.0
80.0
90.0
100.0
110.0
120.0
130.0
0
36.5
54.8
73
91.4
109.7
128
146.3
164.5
182.8
201
RA

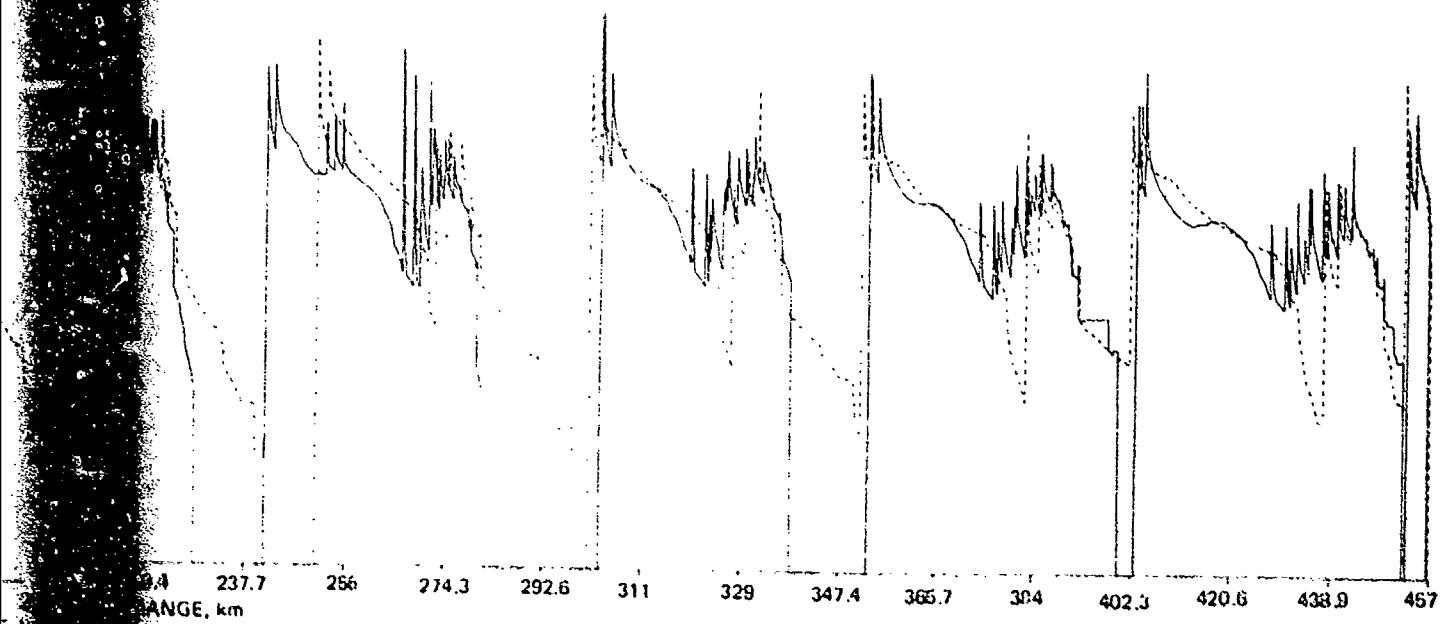


(C)

Figure 21. (Continued)

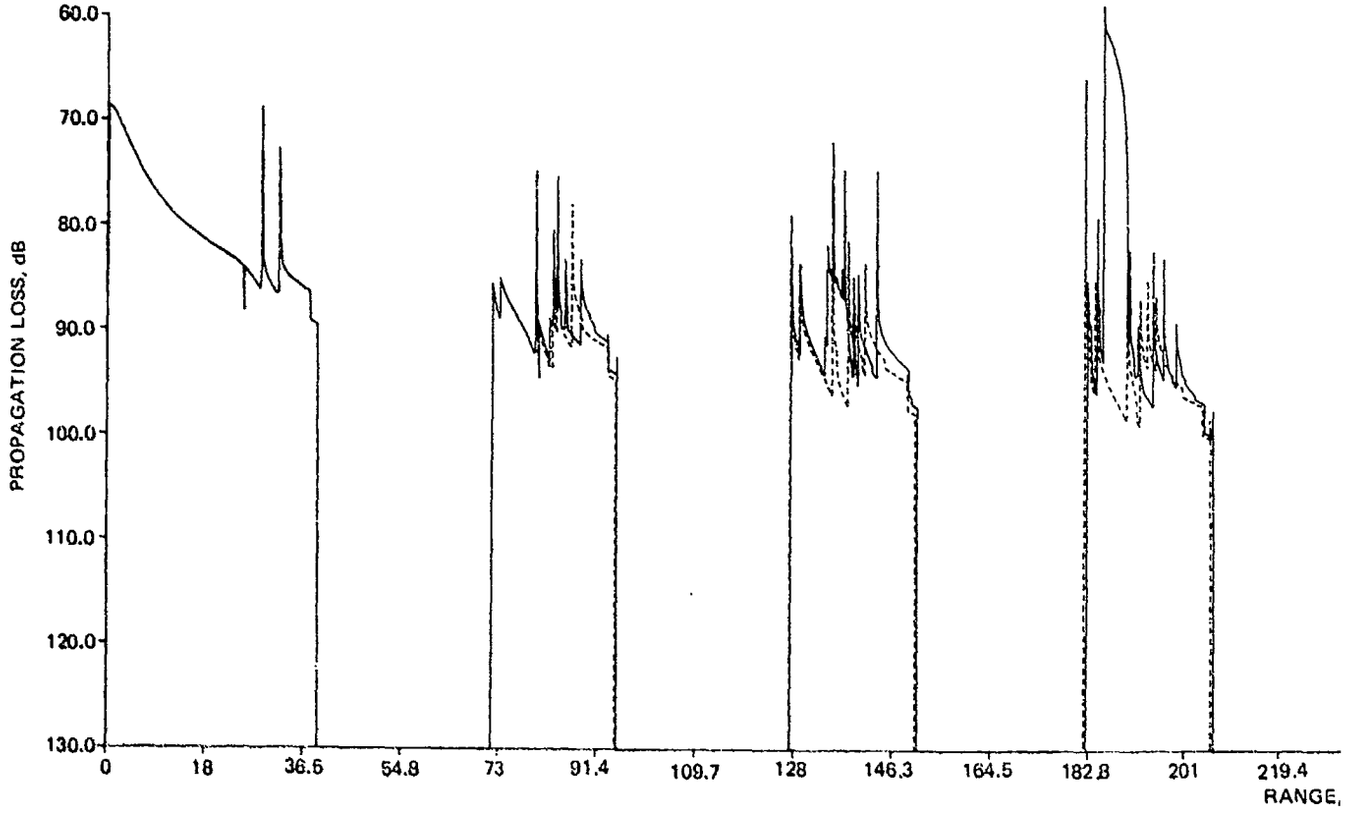
60.0
70.0
80.0
90.0
100.0
110.0
120.0
130.0
PROPAGATION LOSS, dB
0
18
36.6
54.8
73
91.4
109.7
128
146.3
164.5
182.8
201
219.4
RANGE,

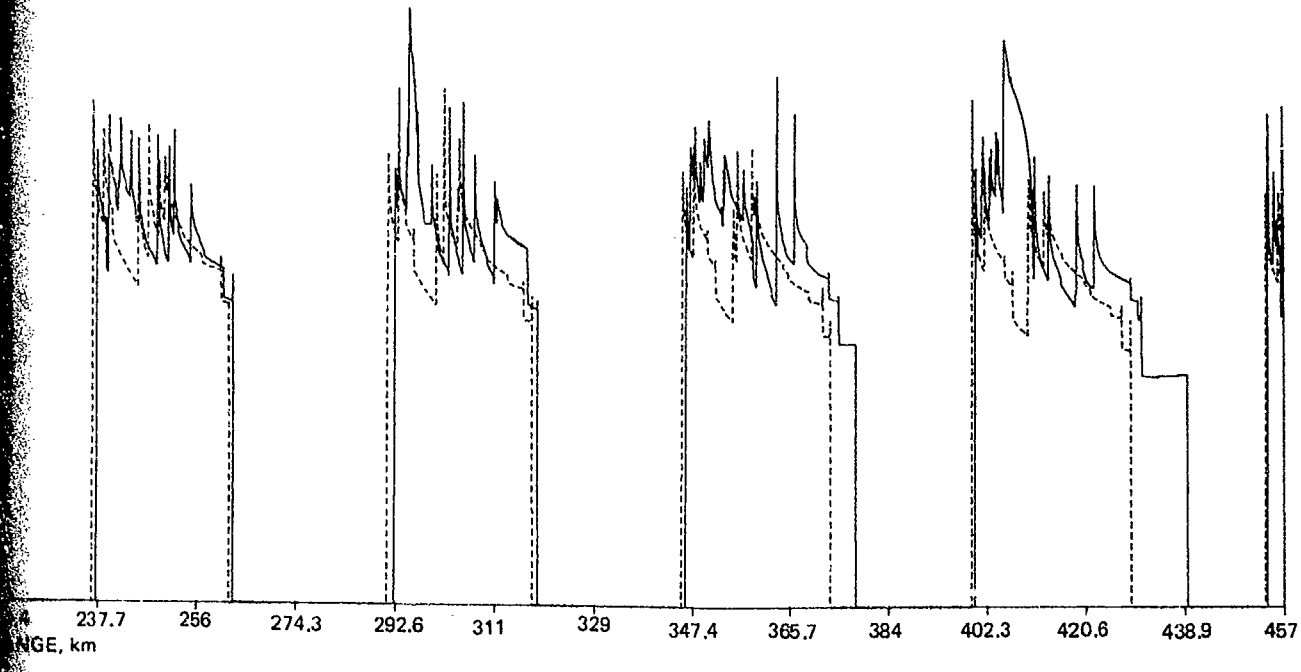


(A)

Figure 22. Comparison of propagation loss for the 122-m source and 3508-m receiver and the composite profile with: (A) those of profile 1A; (B) those of the predicted profile; (C) those of the average profile.

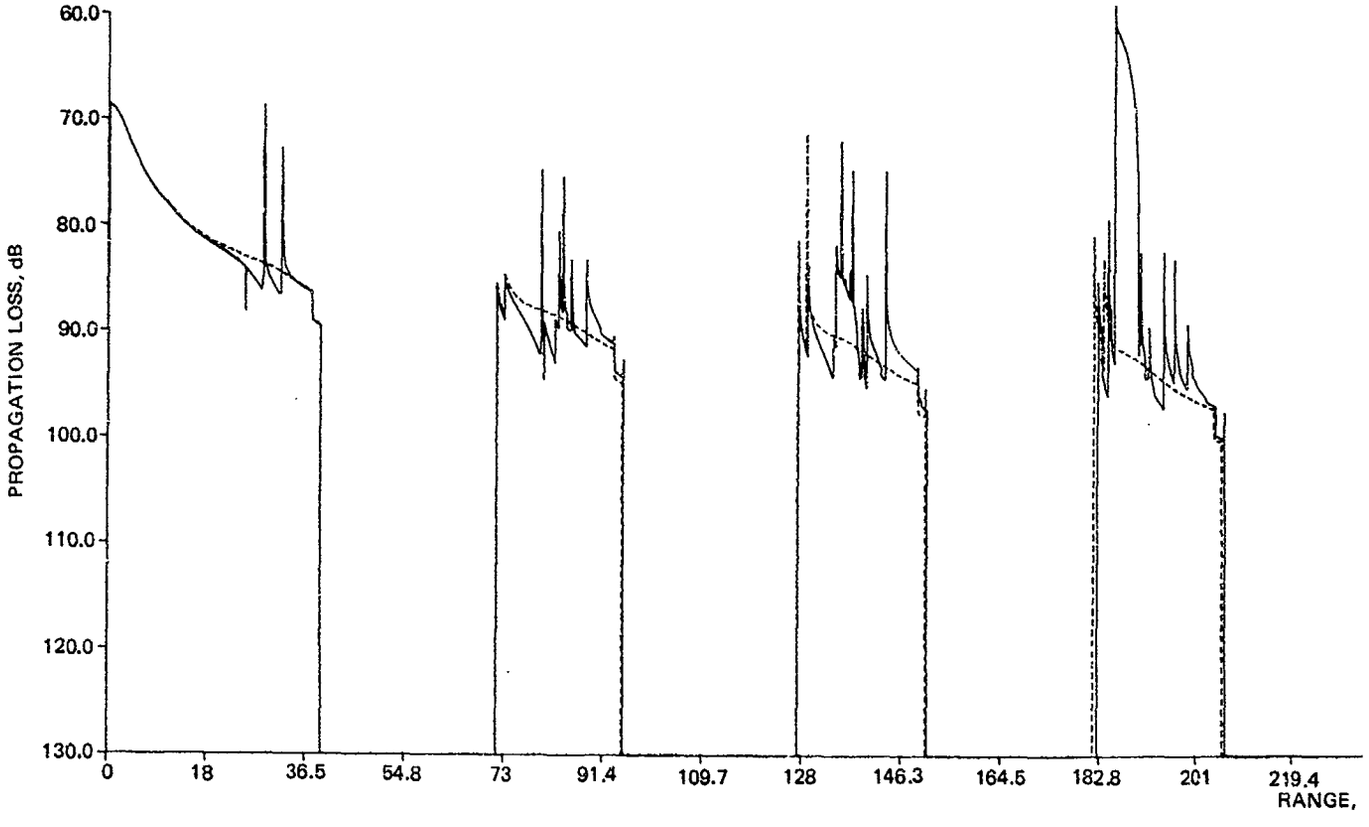
60.0
70.0
80.0
90.0
100.0
110.0
120.0
130.0
PROPAGATION LOSS, dB
0
18
36.5
54.8
73
91.4
109.7
128
146.3
164.5
182.8
201
219.4
RANGE,

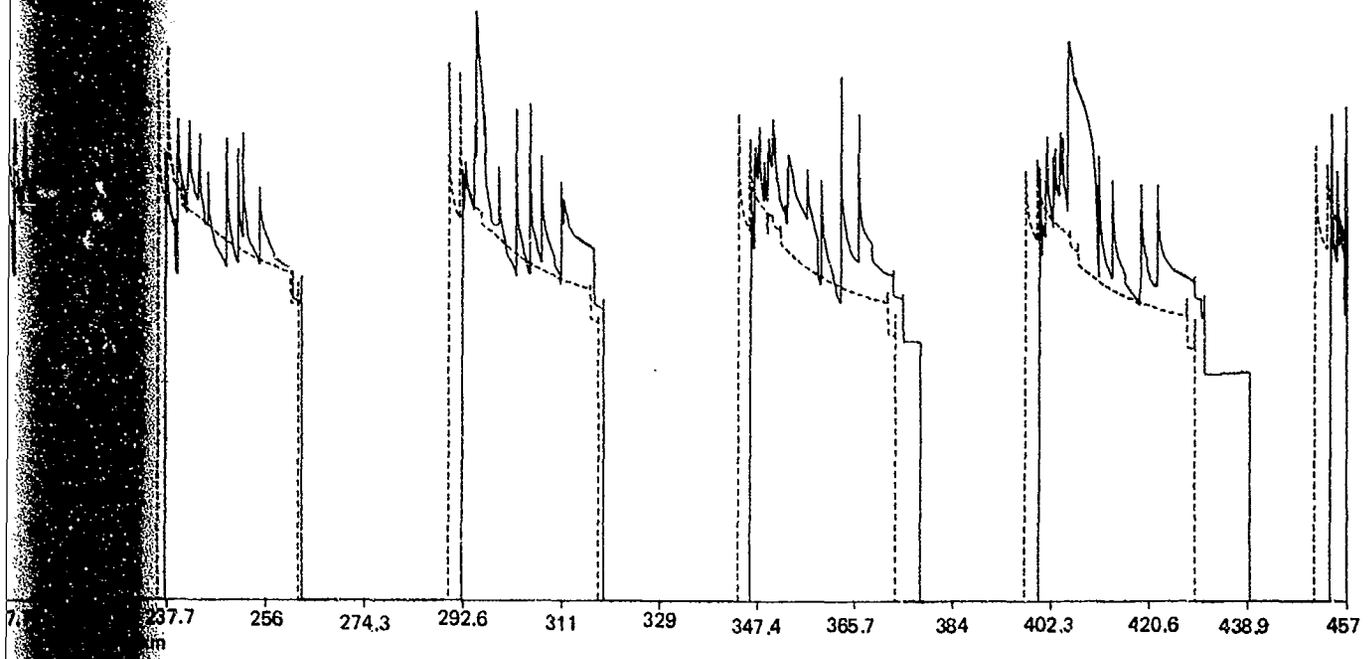


(B)

Figure 22. (Continued).



2

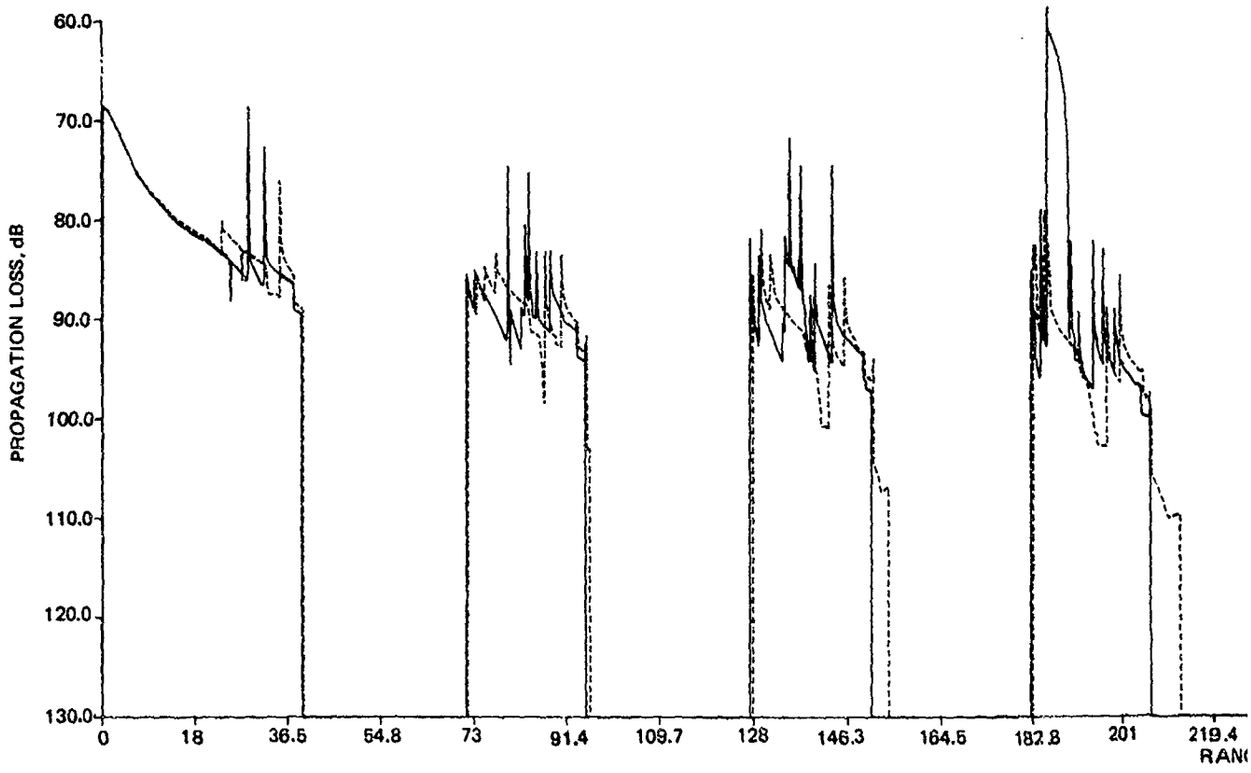
PROPAGATION LOSS, dB
60.0
70.0
80.0
90.0
100.0
110.0
120.0
130.0
0
18
36.5
54.8
73
91.4
109.7
128
146.3
164.5
182.8
201
219.4
RAN

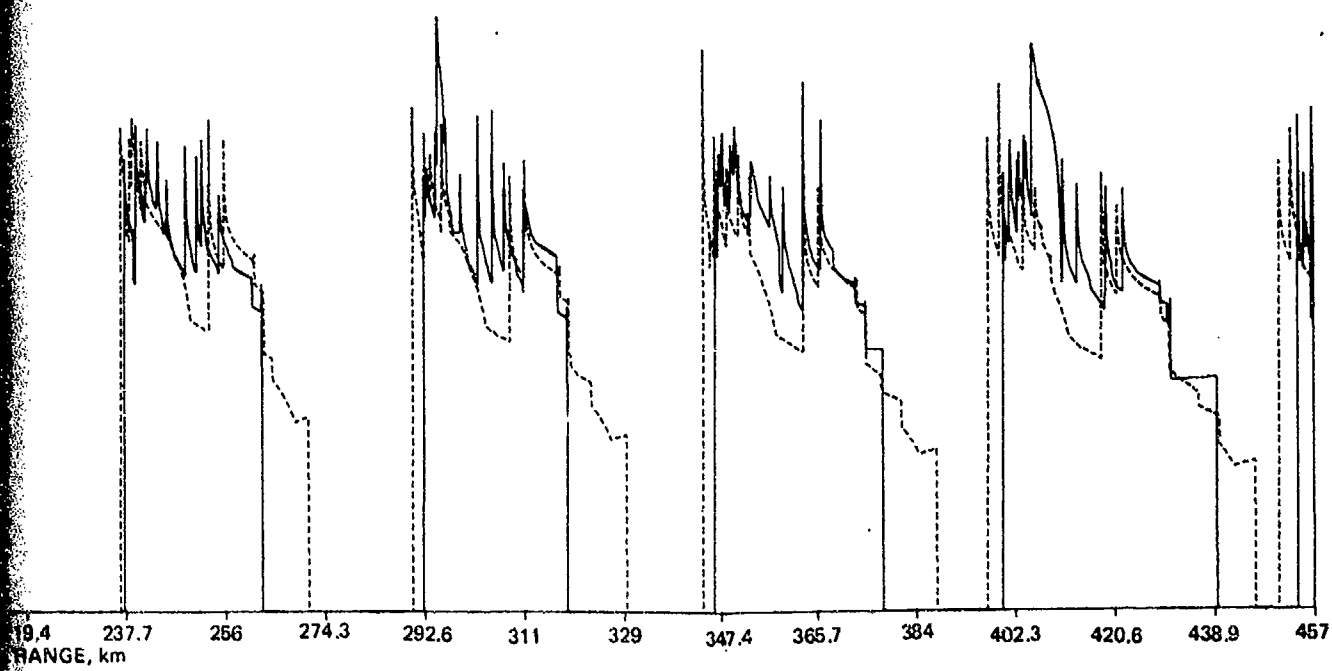


(C)

Figure 22. (Continued).

Table 2. Zone 8 Ranges and Differences from Composite Profile for Various Profiles.

| Receiver Depth | 94 m | | | | 3507 m | | | |
|---|---|---|---|---|---|---|---|---|
| Profile | Leading Edge, km | Bottom Grazing, km | Δ Leading, km | Δ Grazing, km | Leading Edge, km | Bottom Grazing, km | Δ Leading, km | Δ Grazing, km |
| Composite | 403.1 | 448.4 | 0 | 0 | 454.2 | 464.8 | 0 | 0 |
| 1A | 389.9 | 446.5 | 13.2 | 1.9 | 453.9 | 462.9 | 0.3 | 1.9 |
| Predicted | 397.5 | 446.5 | 5.6 | 1.9 | 451.3 | 463.0 | 2.9 | 1.8 |
| Average | 402.1 | 448.4 | 1.0 | 0 | 450.8 | 464.9 | 3.4 | -0.1 |

The counterpart of Fig. 23 for the group velocity is presented in Fig. 25, while the counterpart of Fig. 24 for the differences in group velocity is presented in Fig. 26.

Note in Fig. 26 that the differences are all negative. This should be expected because higher sound speeds lead to higher group velocities and the sound speeds for the seamount profile were higher than the deepwater profile. We note that the maximum difference in Fig. 26 is about -0.28 m/sec. This number is comparable to the differences between the deepwater profile and seamount profile given in Table 22 of Ref. 3.

Since group velocity is of principal concern in converting acoustic travel times to range, we need to analyze Fig. 26 from this standpoint. First of all the sound speed at the pulsed source depth (134 m) limits the rays of interest. These are labelled in Fig. 26 as $C_3$ for profile 1B and $C_4$ for profile 2B. We can ignore phase velocities less than these values. In contrast to Fig. 24, this limitation does not decrease the maximum difference. This maximum difference represents -0.28 m/sec as compared to a group velocity of about 1481 m/sec. Thus this maximum represents a percentage difference of only 0.0188 percent. For a nominal cycle range of 50 km this difference represents an associated acoustic range error of only 9 m. We see then that the seamount profile can only have a very slight effect on ranges determined from acoustic travel times.

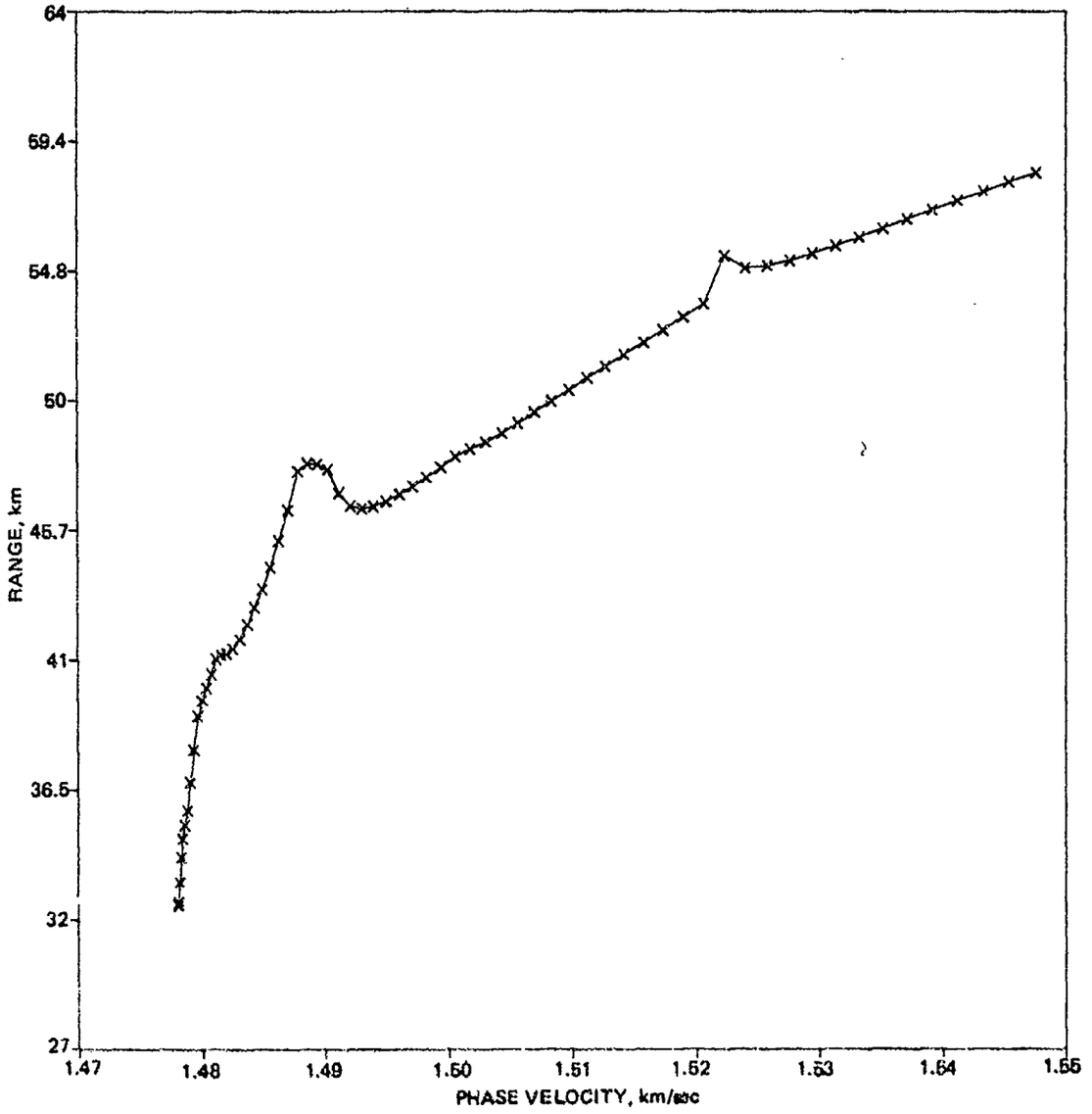


Figure 23. Cycle range vs phase velocity for profile 1B with deepwater profile appended.

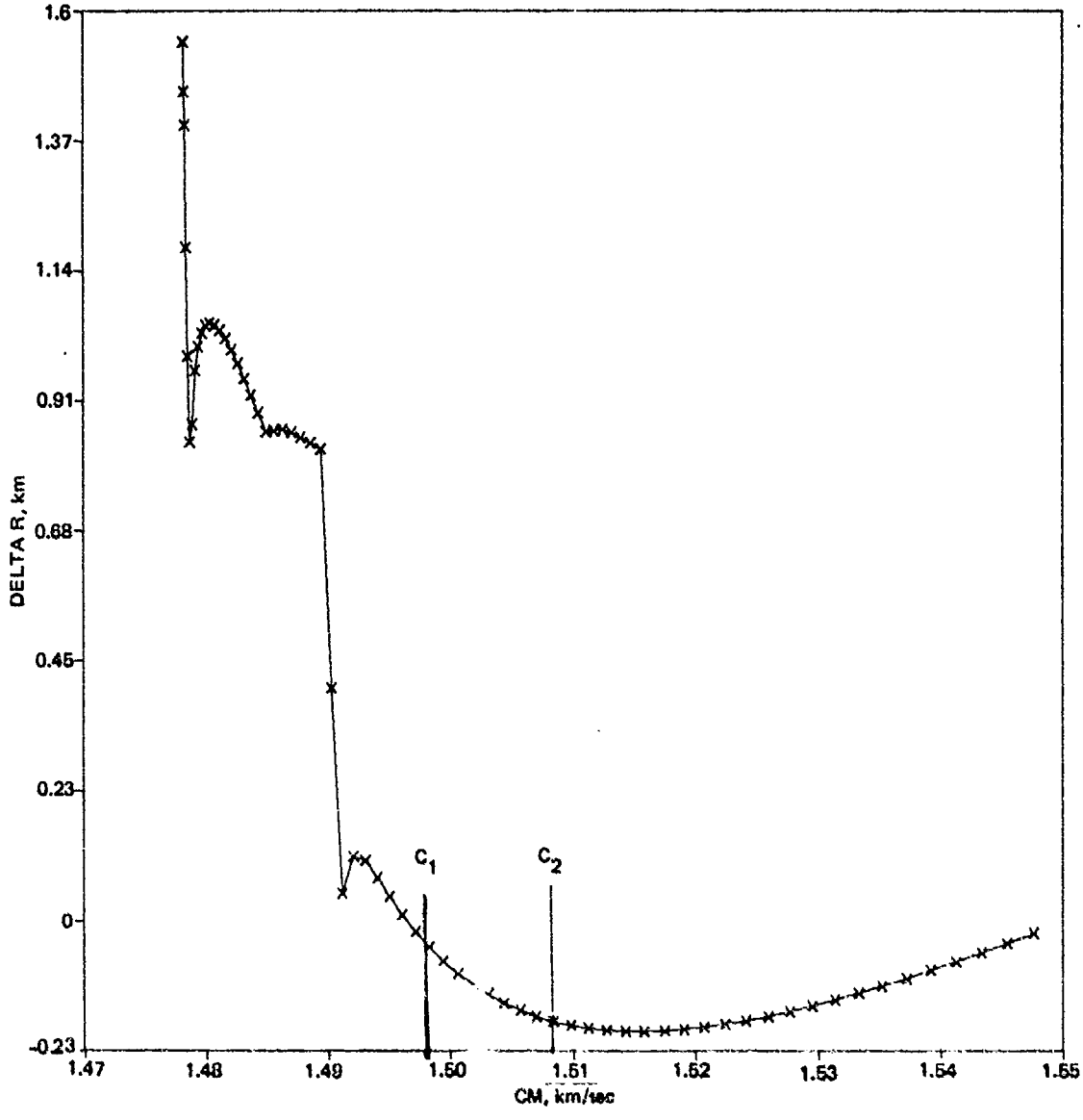


Figure 24. Differences between the cycle range for the deepwater profile and for the seamount profile.

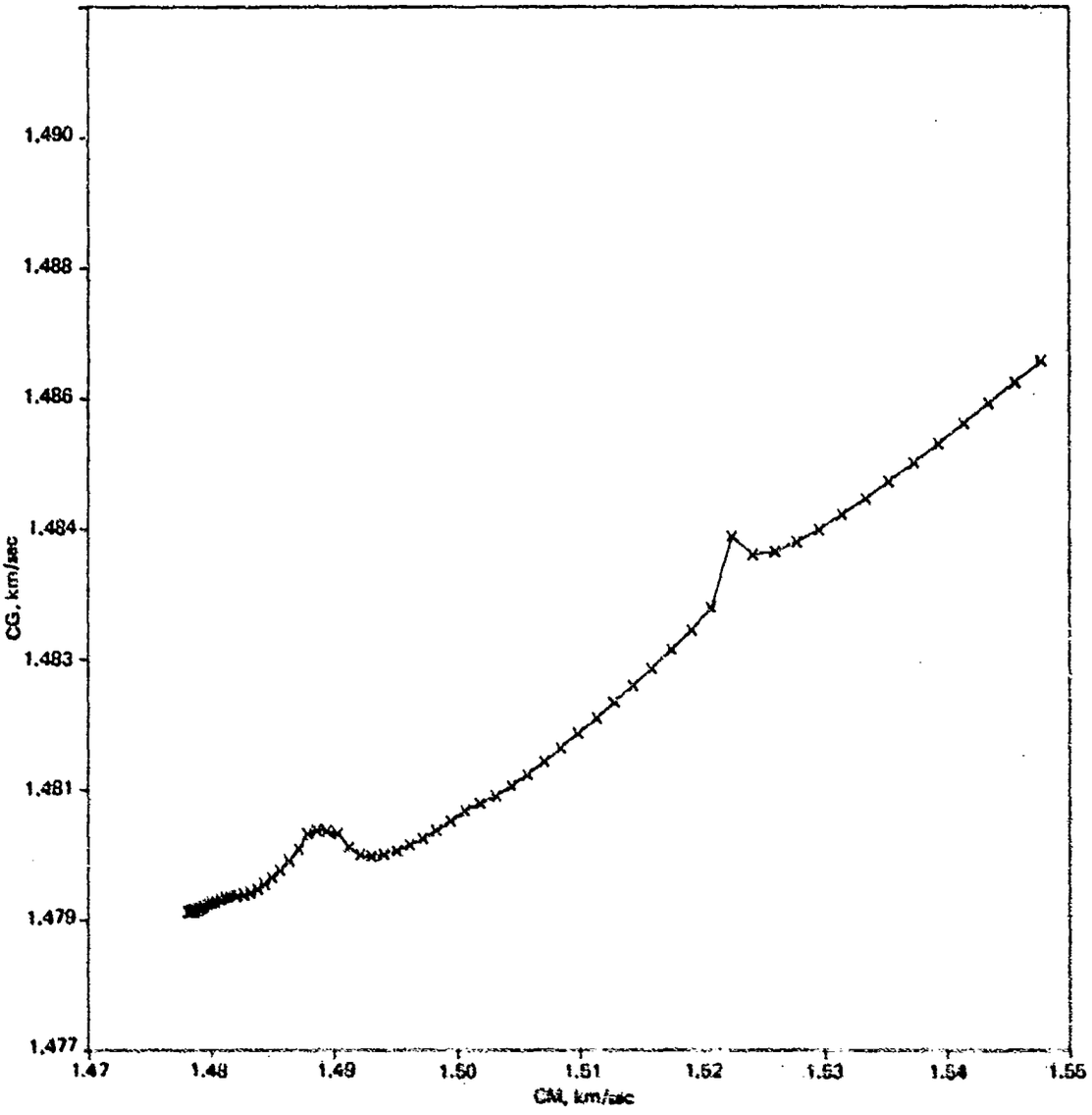


Figure 25. Counterpart of Fig. 23 for the group velocity.

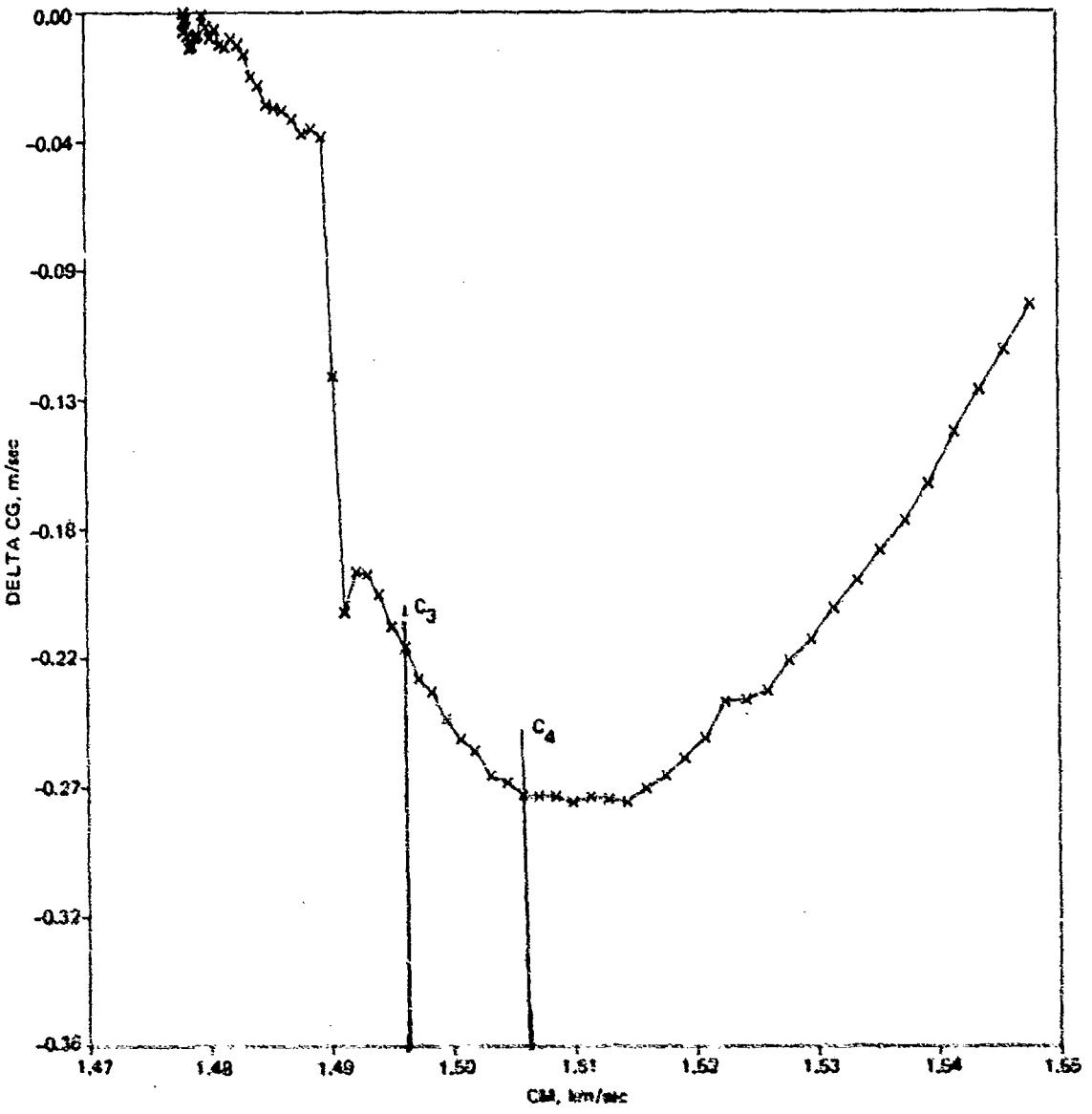


Figure 26. Counterpart of Fig. 24 for the group velocity.

## OTHER DESIRABLE STUDIES

This section discusses some valuable follow-up analysis on the CAPER data. First it should be reiterated that the present report is regarded as preliminary and in no sense represents a complete analysis. Indeed one of the major purposes of this report is to point out the value of the CAPER data and its potential for more detailed analysis.

Some of the items to follow were prescribed in Ref. 1. However because of cost overruns, reprogramming of funds for higher priority items, and other factors the reduction, analysis and reporting of the data were not completed.

### REPORTING OF CW DATA

MPL has reduced all of the CW data taken at 104 Hz for Runs A through D. Data are available for 12 receiver depths. These data are of excellent quality, and MPL presently plans to produce a data report on propagation loss and coherence.

### COMPARISON OF THE CW DATA WITH PROPAGATION LOSS MODELS

Reference 1 called for CAPER data to be provided to AESD for use in the strengthening and evaluation of acoustic propagation models. The CAPER data should be an excellent candidate for further analysis by NORDA Code 320, the successor of AESD. Acoustic ranges are only available for part of Run A. However, as demonstrated in this report, satellite ranges should be adequate. NOSC can provide some limited multipath data at 140 Hz as an aid in the analysis.

In this preliminary report no attempt has been made to calculate propagation loss in the regions of seamount shadowing, which are only ensonified by bottom-reflected paths. An important feature of further analysis by NORDA would be the inclusion of bottom-reflected propagation to determine how well models can predict the propagation loss measured in the regions of seamount shadowing.

### REDUCTION, ANALYSIS, AND REPORTING OF SURFACE DECOUPLING DATA

The third major objective of the CAPER exercise was to investigate surface decoupling (image interference), which causes an increase in propagation loss as a source of receiver approaches the ocean surface. This phase of the exercise is discussed in more detail in Ref. 1. Measurements were made at 104 Hz on receivers at 3, 6, 12, 24, and 36 m as well as on seven deeper receivers over the range interval from 173.8 to 4.1 km. This covers the first three convergence zones as well as the bottom-reflection regions between zones.

MPL has reduced selected samples of these data and they appear to be of excellent quality. Differences of 10 dB are typical between the propagation loss at 3 m and that at 36 m. There are no plans at present to complete the reduction and analysis of this data. However this data set is unique and would provide an excellent opportunity for verifying the theoretical treatment and operational consequences of the surface decoupling effect as presented in Ref. 8.

## ANALYSIS OF BACK REFLECTIONS FROM STODDARD SEAMOUNT

Over a range interval just prior to passing over Stoddard seamount, the MPL records at 104 Hz showed a distinctive up-doppler arrival, which Dr. Morris identified as back reflection from the seamount. As the seamount was traversed this up-doppler arrival merges with the normal down-doppler arrival. Subsequent examination of the NOSC pulsed data at 140 Hz shows two distinct arrivals separated in travel time. These arrivals merge as the seamount is traversed. These data represent an opportunity to determine more precisely the characteristics of back reflection. Additional data reduction is necessary. MPL needs to develop a more rigorous determination of signal levels in the presence of variable doppler shifts. NOSC needs to carefully process all relevant pulsed data, measuring all propagation losses and travel time differences. The analysis of these data would combine ray theory calculations, seamount contours, acoustic propagation losses, acoustic travel times and travel time differences, and doppler shifts to produce a consistent model of reflection.

## CONCLUSIONS

The conclusions are divided into four groups: general, navigation and ranging, seamount shadowing, and sound-speed profiles.

### GENERAL

This initial acoustic assessment of CAPER demonstrates that the exercise was well conceived, planned, and executed. The major experimental goals of the exercise were achieved. The excellent quality of the acoustic and supporting environmental data warrants further analysis. Areas of further analysis include a comparison of detailed experimental propagation loss data with sophisticated range-dependent models that include bottom-reflected paths, a comparison of experimental data on near-surface receivers with the theory of surface decoupling, and the use of experimental measurements of propagation loss, doppler shifts, and travel time differences to produce a consistent model of backscattering and reflection from a seamount slope.

The success of the exercise can be attributed in large part to detailed planning. The impact of several unanticipated equipment casualties at sea was minimized by careful exercise design, which provided for redundancy or backup. Moreover the initial design was examined to determine the sensitivity to navigational errors. As a result of this examination the design was adjusted so that the acoustic result on various runs would be most insensitive to navigational error or other unanticipated changes in the test conditions.

### NAVIGATION AND RANGING

Comparison of the differences between acoustic and satellite ranges showed a mean difference of 117 m with a standard deviation of 272 m. Statistical tests showed that this mean difference was not highly significant. The maximum difference was −726 m, while 88 percent of the differences fell within ±366 m.

Initial comparison of the differences between acoustic and satellite ranges showed a highly significant bias of −234 m. There was also a slight tendency for the differences to become more negative with increasing range. However a geodetic constant of 60 nautical miles per degree of latitude had been used to calculate the satellite ranges. The correction of this value to account for the dependence in latitude removed the range trend as well as 279 m of the bias.

Statistical tests show no significant difference between the accuracy of ranges at satellite fixes and the accuracy of ranges between satellite fixes. The additional error introduced by interpolating between fixes is small compared to the error in the fixes themselves.

The shallowest receiver (94 m) and the receiver (3508 m) just shallower than the critical depth provided excellent travel time data for ranging purposes. The convergence zones for these two depths covered most ranges until the seamount was traversed. Thereafter the seamount intercepted rays to the deep receiver and reliable travel times were available only over small intervals on the shallow receiver.

In situations where the ship speed and course were nearly constant, the technique of calculating apparent ship speed from successive observations of range is a sensitive, practical technique for detecting erroneous range data.

## SEAMOUNT SHADOWING

The receiver depths utilized during the seamount shadowing experiment can be divided into three groups on the basis of detailed ray tracing, which takes into account the receiver-seamount geometry and the bathymetry. For the first group, consisting of six receiver depths between 94 and 844 m, some rays will always clear the peak of the seamount without bottom reflection. For the second group, consisting of three receiver depths between 3396 and 3480 m, no rays can clear the peak of the seamount without reflecting from the seamount. For the third group, consisting of three receiver depths between 4251 and 4363 m, most rays will reflect from the abyssal hills which lie between the receiver and the seamount.

The design and execution of the various seamount shadowing runs well satisfy the goals of the exercise. Once past the seamount, Run A has a lateral displacement of less than 1.8 km. Run A corresponds closely to maximum range shadowing behind the seamount. Traverse Runs D and E are both well positioned for shallow receivers. Near-maximum azimuthal shadowing occurs along Run D. Run E represents minimum shadowing in that rays can always pass over the seamount regardless of azimuth. Traverse Run B is not well positioned with respect to the 94-m receiver depth as the run meanders in and out of the shadow zone between convergence zone 7 and convergence zone 8. However Run B lies in the ensonified region for the 844-m receiver depth.

The effect of the seamount is to intercept the leading portion of the convergence zone. Consider for example the range interval of the fifth convergence zone for a 122-m source and a 94-m receiver. This was 266.7 to 281.7 km for maximum shadowing along the bearing line joining the receiver to the seamount peak and was 241.6 to 281.7 km along bearings which completely clear the seamount. This is an unanticipated result because the effect of shallowing a flat bottom is to reduce the trailing edge of the convergence zone rather than affect the leading edge. This result can be attributed to the fact that the steepest ray, which is the bottom-limited ray, is the first to clear the seamount.

Stoddard Seamount appears ideal for the purpose of investigating seamount shadowing. The dimensions and slopes of Stoddard and its isolated position surrounded by deep abyssal hills create relatively simple conditions for analysis.

## SOUND-SPEED PROFILES

A simple modification to ray calculations for range-independent sound-speed profiles was utilized to assess the effect of horizontal changes in sound-speed profile. Although not rigorous, this method -- called the composite profile method -- accounts for first-order effects.

Significant horizontal changes in the sound-speed profiles were measured. Maximum differences of 9.6 m/sec were measured at a depth of 125 m. Comparison of ray calculations for the receiver profile regime with only those of the composite profile method that include four profile regimes showed significant differences in acoustic results. For example, for a 122-m source and a 94-m receiver the range of the leading edge of the eighth convergence zone was 403.1 and 389.9 km for the receiver only and composite profiles, respectively.

The effect of profile differences was least for configurations involving steeper rays and greatest for those involving less steep rays. Thus profile differences produced less change in the trailing edge of convergence zones and greatest change in the leading edge. Also profile differences produced less change for a deep receiver near the critical depth than for a receiver located at lower sound speeds in the thermocline.

The predicted profile proved to be more than adequate for planning the exercise, despite the fact that the sound speeds at depths above 50 m were significantly lower (as much as 5 m/sec) than any of the four measured profile regimes. Indeed the theoretical results for the predicted profile in many cases agreed better with those of the composite profile than did those based on the measured profile at the receiver. This occurred because the source and receiver were located in the critical thermocline region. In this region the predicted profile was more representative of the composite profile than was the profile regime in which the receiver was located.

Sound speeds within 18.5 km of the seamount peak were about 0.22 m/sec higher than those in the surrounding ocean for depths from 1000 to 2500 m. Bounds on the effect of these increased sound speeds were estimated from ray calculations. These bounds were -200 m on calculated ray theory ranges and 9 m in ranges as determined from measured travel times.

A new method of treating range-dependent profiles, which uses a single profile obtained by averaging the profiles with weights proportioned to the range over which the profiles apply, was tested. The results agreed favorably with the composite profile approach. For example, the leading edge of the eighth convergence zone was 403.1 km for the composite profile and 402.1 km for the weighted average profile. This method is awkward to apply because a new profile (new weights) must be generated for each convergence zone. However the method might be useful to investigators who are restricted to the use of ray programs treating depth dependence only.

## RECOMMENDATIONS

1. Consider further analysis of the CAPER data in the areas of comparison with sophisticated propagation loss models, evaluation of the surface decoupling effect, and investigation of the mechanisms of backscattering and reflection from a seamount slope.

2. Dispense with acoustic ranging on sea tests and rely upon careful satellite navigation unless range accuracies of better than ±450 m are required.

3. The composite method of treating the horizontal change in sound-speed profile should be compared with more rigorous methods to determine conditions under which the composite method is or is not adequate.

4. In experiments where the effect of seamounts or ridges is critical, the deep sound-speed profile should be well sampled to determine modification due to bathymetry. This pertains not only to water masses over the seamounts or ridges themselves but also to the surrounding open-ocean masses so that accurate open-ocean average values can be established for use as controls.

5. Use a latitude-dependent geodetic parameter rather than the nominal 60 nautical miles per degree of latitude in calculating ranges based on satellite fixes as the accuracy of the satellite fixes warrants use of this refinement.

6. In designing exercises, test the sensitivity of the predicted acoustic result to changes in input and adjust the exercise so that these results are least sensitive to changes in test conditions.

7. For acoustic ranging purposes, use a pair of receivers -- one shallow and one at the critical depth -- to obtain maximum coverage by non-bottom-reflected paths.

8. Calculate apparent ship speed from successive range measurements to detect erroneous range data.

## REFERENCES


1. G. B. Morris and C. B. Bishop, Exercise Plan for Combined Acoustic Propagation in Eastpac Region (Exercise CAPER), Marine Physical Laboratory MPL-U-63/74, July 1974.

2. R. W. Bannister et al., "The Effect of Seamounts on Sound Channel Propagation," J. Acoust. Soc. Am., 55, No. 2, 417(A), Feb 1974.

3. E. R. Anderson and P. G. Hansen, Combined Acoustic Propagation in Eastpac Region (Exercise CAPER: Source-Speed Profiles), Naval Undersea Center, NUC TP 485, Sep 1975.

4. R. T. Bachman, Navigation and Bathymetric Data from Exercise CAPER, Naval Undersea Center, NUC TN 1627, Dec 1975.

5. M. A. Pedersen and D. F. Gordon, "Comparison of Curvilinear and Linear Profile Approximation in the Calculation of Underwater Sound Intensities by Ray Theory," J. Acoust. Soc. Am. 41:419–438, Feb 1967.

6. E. D. Bronson, "Three-Point Anchoring in the Deep Ocean," U. S. Naval Institute Proceedings, Vol. 101, No. 2, pp 100–104, Feb 1975.

7. J. R. Lovett, "Merged Seawater Sound Speed Equations," J. Acoust. Soc. Am. 63:1713-1718, June 1978.

8. M. A. Pedersen, D. F. Gordon, and D. White, Low-Frequency Propagation Effects for Sources or Receivers Near the Ocean Surface, Naval Undersea Center, NUC TP 488, Sep 1975.

## INITIAL DISTRIBUTION

ASSISTANT SECRETARY OF THE NAVY (RE&S)
WASHINGTON, DC 20301
ATTN: GA CANN (1)

CHIEF OF NAVAL OPERATIONS
DEPARTMENT OF THE NAVY
WASHINGTON, DC 20350
ATTN: NOP-095 (1)
NOP-951 (1)
NOP-955 (1)

COMMANDER IN CHIEF, PACIFIC (1)
CAMP SMITH, HI 96861

COMMANDER IN CHIEF, PACIFIC FLEET (2)
PO BOX 3
PEARL HARBOR, HI 96860
ATTN: CDR JT HANKINS

COMMANDER THIRD FLEET (6)
PEARL HARBOR, HI 96860
ATTN: CAPT PA VEATCH

COMMANDER SEVENTH FLEET (2)
FPO SAN FRANCISCO 96601
ATTN: CAPT JT TALBERT

COMMANDER SUBMARINE FORCE (2)
US PACIFIC FLEET
PEARL HARBOR, HI 96860
ATTN: DR T CURRY

COMMANDER (2)
SUBMARINE GROUP SEVEN
BOX 50
FPO SEATTLE 98762
ATTN: CAPT J MC NISH
CDR NW SHRIVER

COMMANDER (2)
OCEANOGRAPHIC SYSTEM, PACIFIC
BOX 1390
PEARL HARBOR, HI 96860
ATTN: CDR RC LEAVITT

COMMANDER PATROL AND (2)
RECONNAISSANCE FORCE,
SEVENTH FLEET
BOX F
FPO SEATTLE 98768
ATTN: CDR P O'CONNOR

COMMANDER US NAVAL FORCES,
MARIANAS
FPO SAN FRANCISCO 96630
ATTN: LCDR DL WETHERELL (1)

COMMANDER (1)
OCEANOGRAPHIC DEVELOPMENT
SQUADRON EIGHT
NAVAL AIR STATION
PATUXENT RIVER, MD 20670

CHIEF OF NAVAL MATERIAL
NAVY DEPARTMENT
WASHINGTON, DC 20360
ATTN: NMAT-08T1 (J PROBUS) (1)

COMMANDER (1)
NAVAL AIR DEVELOPMENT CENTER
WARMINSTER, PA 18974

COMMANDER IN CHIEF US (1)
ATLANTIC FLEET
NORFOLK, VA 23511

CHIEF OF NAVAL RESEARCH (1)
ARLINGTON, VA 22217
ATTN: ONR-102-OS (DR JB HERSEY) (1)

DIRECTOR
NAVAL RESEARCH LABORATORY
WASHINGTON, DC 20375
ATTN: CODE 8100 (1)
CODE 8160 (1)
CODE 2627 (1)

OCEANOGRAPHER OF THE NAVY
HOFFMAN II
200 STOVALL ST
ALEXANDRIA, VA 22332
ATTN: CDR ET YOUNG (1)

COMMANDER
NAVAL AIR SYSTEMS COMMAND
WASHINGTON, DC 20360
ATTN: PMA-264 (1)

COMMANDER
NAVAL ELECTRONIC SYSTEMS COMMAND
WASHINGTON, DC 20360
ATTN: PME-124-41 (1)
NELEX-320 (1)
NELEX-035 (1)

COMMANDER (1)
NAVAL SEA SYSTEMS COMMAND
WASHINGTON, DC 20362
ATTN: NSEA-06H1 (1)

DIRECTOR (1)
STRATEGIC SYSTEMS PROJECT OFFICE (PM-1)
DEPARTMENT OF THE NAVY
WASHINGTON, DC 20376

PROJECT MANAGER (2)
ANTI-SUBMARINE WARFARE SYSTEMS
PROJECT (PM-4)
DEPARTMENT OF THE NAVY
WASHINGTON, DC 20360

COMMANDER
NAVAL OCEAN SYSTEMS CENTER
SAN DIEGO, CA 92152
ATTN: MR AKERS (2)
DR RA WAGSTAFF (1)
DR EB TUNSTALL (1)
DR RR GARDNER (1)

OFFICER IN CHARGE (1)
NEW LONDON LABORATORY
NAVAL UNDERWATER SYSTEMS CENTER
NEW LONDON, CT 06320
ATTN: RL MARTIN (4)

COMMANDER (1)
NAVAL OCEANOGRAPHIC OFFICE
NSTL STATION
BAY ST LOUIS, MS 39522
ATTN: CODE 3143 (JL KERLING) (1)

CENTER FOR NAVAL ANALYSIS
1401 WILSON BLVD
ARLINGTON, VA 22209
ATTN: DIRECTOR FOR NAVAL MATTERS (1)
CE WOODS (1)

COMMANDING OFFICER
NAVAL OCEAN RESEARCH AND
DEVELOPMENT ACTIVITY
NSTL STATION, MS 39529
ATTN: CODE 110 (1)
CODE 200 (1)
CODE 300 (1)
CODE 320 (1)
CODE 340 (1)
CODE 400 (1)
CODE 500 (1)
CODE 600 (3)

OFFICE OF NAVAL RESEARCH
ARLINGTON, VA 22217
ATTN: NORDA LIAISON OFFICE (2)
(KW LACKIE)

DEFENSE ADVANCED RESEARCH (1)
PROJECTS AGENCY
1400 WILSON BOULEVARD
ARLINGTON, VA 22209

APPLIED PHYSICS LABORATORY
JOHNS HOPKINS UNIVERSITY
JOHNS HOPKINS ROAD
LAUREL, MD 20810
ATTN: DR GL SMITH (1)

APPLIED RESEARCH LABORATORY
UNIVERSITY OF TEXAS
PO BOX 8029
AUSTIN, TX 78712
ATTN: GE ELLIS (1)
DR LD HAMPTON (1)

ARTHUR D LITTLE, INC
15 ACORD PARK
CAMBRIDGE, MA 02140
ATTN: WG SYKES (1)

BOLT, BERANEK AND NEWMAN (1)
1701 N FORT MYER DRIVE
SUITE 1001
ARLINGTON, VA 22209

BELL TELEPHONE LABORATORIES (1)
1 WHIPPANY ROAD
WHIPPANY, NJ 07981

DANIEL H WAGNER ASSOCIATES (1)
STATION SQUARE ONE
PAOLI, PA 19301

DAUBIN SYSTEMS CORPORATION (1)
104 CRANDON BLVD
SUITE 315
KEY BISCAYNE, FL 33149

GENERAL ELECTRIC CORPORATION
REENTRY ENVIRONMENTAL SYSTEMS DIVISION
3198 CHESTNUT ST
PHILADELPHIA, PA 19101
ATTN: O KLIMA (1)

OPERATIONS RESEARCH, INC
1400 SPRING ST
SILVER SPRING, MD 20910
ATTN: DR JI BOWEN (1)

PALISADES GEOPHYSICAL INSTITUTE, INC (1)
131 ERIE ST
PO BOX 396
BLAUVELT, NY 10913

PLANNING SYSTEMS, INC
7900 WESTPARK DRIVE
MC LEAN, VA 22101
ATTN: DR LP SOLOMON (1)

RAYTHEON COMPANY
SUBMARINE SIGNAL DIVISION
PO BOX 360
PORTSMOUTH, RI 02871
ATTN: DR BA BECKEN (1)

SCIENCE APPLICATIONS, INC
4422/8400 WESTPARK DRIVE
MC LEAN, VA 22101
ATTN: DR JS HANNA (1)

SUTRON CORPORATION
1921 N LYNN ST
SUITE 700
ALEXANDRIA, VA 22209
ATTN: CH DABNEY (1)

TETRA TECH, INC
1911 FORT MYER DRIVE
ARLINGTON, VA 22209
ATTN: WE SIMS (1)

TEXAS INSTRUMENTS, INC
PO BOX 6015
DALLAS, TX 75222
ATTN: A KIRST, JR (1)

TRACOR, INC
6500 TRACOR LANE
AUSTIN, TX 78721
ATTN: DR AF WITTENBORN (1)

TRACOR, INC
1601 RESEARCH BLVD
ROCKVILLE, MD 20850
ATTN: JT GOTTWALD (1)

TRW SYSTEMS GROUP
7600 COLSHIRE DRIVE
MC LEAN, VA 22101
ATTN: RT BROWN (1)
IB GEREBEN (1)

UNDERSEA RESEARCH CORPORATION
7777 LEESBURG PIKE, SUITE 306
FALLS CHURCH, VA 22043
ATTN: VF ANDERSON (1)

UNDERWATER SYSTEMS, INC
WORLD BUILDING
8121 GEORGIA AVENUE
SILVER SPRING, MD 20910
ATTN: DR MS WEINSTEIN (1)

WESTERN ELECTRIC COMPANY (1)
2400 REYNOLDS ROAD
WINSTON-SALEM, NC 27106

WOODS HOLE OCEANOGRAPHIC INSTITUTION
WOODS HOLE, MA 02543
ATTN: EE HAYS (1)

XONICS, INC
6837 HAYVENHURST AVE
VAN NUYS, CA 91406
ATTN: S KULEK (1)

DEFENSE DOCUMENTATION CENTER
CAMERON STATION
ALEXANDRIA, VA 22314 (1)

**DEPARTMENT OF THE NAVY**
OFFICE OF NAVAL RESEARCH
875 NORTH RANDOLPH STREET
SUITE 1425
ARLINGTON VA 22203-1995

IN REPLY REFER TO:

5510/1
Ser 321OA/011/06
31 Jan 06

MEMORANDUM FOR DISTRIBUTION LIST

Subj: DECLASSIFICATION OF LONG RANGE ACOUSTIC PROPAGATION PROJECT (LRAPP) DOCUMENTS

Ref: (a) SECNAVINST 5510.36

Encl: (1) List of DECLASSIFIED LRAPP Documents

1. In accordance with reference (a), a declassification review has been conducted on a number of classified LRAPP documents.

2. The LRAPP documents listed in enclosure (1) have been downgraded to UNCLASSIFIED and have been approved for public release. These documents should be remarked as follows:

   Classification changed to UNCLASSIFIED by authority of the Chief of Naval Operations (N772) letter N772A/6U875630, 20 January 2006.

   DISTRIBUTION STATEMENT A: Approved for Public Release; Distribution is unlimited.

3. Questions may be directed to the undersigned on (703) 696-4619, DSN 426-4619.

BRIAN LINK
By direction

Subj: DECLASSIFICATION OF LONG RANGE ACOUSTIC PROPAGATION PROJECT (LRAPP) DOCUMENTS

DISTRIBUTION LIST:

NAVOCEANO (Code N121LC – Jaime Ratliff)
NRL Washington (Code 5596.3 – Mary Templeman)
PEO LMW Det San Diego (PMS 181)
DTIC-OCQ (Larry Downing)
ARL, U of Texas
Blue Sea Corporation (Dr.Roy Gaul)
ONR 32B (CAPT Paul Stewart)
ONR 321OA (Dr. Ellen Livingston)
APL, U of Washington
APL, Johns Hopkins University
ARL, Penn State University
MPL of Scripps Institution of Oceanography
WHOI
NAVSEA
NAVAIR
NUWC
SAIC

# Declassified LRAPP Documents

| Report Number | Personal Author | Title | Publication Source (Originator) | Pub. Date | Current Availability | Class. |
|---|---|---|---|---|---|---|
| DASC 012-C-77 | Unavailable | LRAPP PACIFIC DYNAMIC ARCHIVE (U) SEPTEMBER 1976 | Daniel Analytical Services Corporation | 770201 | NS; ND | U |
| SAI-78-527-WA | Spofford, C. W. | NELANT DATA ASSESSMENT APPENDIX III-MODELING REPORT | Science Applications, Inc. | 770225 | ND AVA047680 | U |
| PSI TR 036049 | Barnes, A. E., et al. | OCEAN ROUTE ENVELOPES | Planning Systems Inc. | 770419 | ND | U |
| Unavailable | Unavailable | TAP II BEAMFORMING SYSTEM SOFTWARE FINAL REPORT | Bunker-Ramo Corp. Electronic Systems Division | 770501 | ADC011789 | U |
| S01037C8 | Unavailable | TAP 2 PROCESSING SYSTEM FINAL REPORT HARDWARE DOCUMENTATION (U) | Bunker-Ramo Corp. Electronic Systems Division | 770501 | ADC011790; NS; ND | U |
| Unavailable | Weinberg, H. | GENERIC FACT | Naval Underwater Systems Center | 770601 | ADB019907 | U |
| Unavailable | Unavailable | TASSRAP II OB SYSTEM TEST | Analysis and Technology, Inc. | 770614 | ADA955352 | U |
| Unavailable | Unavailable | LRAPP TECHNICAL SUPPORT | Texas Instruments, Inc. | 770624 | ND | U |
| Unavailable | Bessette, R. J., et al. | TASSRAP INPUT MODULE | Analysis and Technology, Inc. | 770729 | ADA955340 | U |
| Unavailable | Unavailable | TAP-II PHASE II FINAL REPORT | Bunker-Ramo Corp. Electronic Systems Division | 770901 | ADC011791 | U |
| Unavailable | Unavailable | LONG RANGE ACOUSTIC PROPAGATION PROJECT (LRAPP) | Xonics, Inc. | 770930 | ADA076269 | U |
| SAI78696WA | Unavailable ADA055728 | REVIEW OF MODELS OF BEAM-NOISE STATISTICS (U) | Science Applications Inc. | 771101 | NS; ND | U |
| TRACORT77RV109 C | Unavailable | FINAL REPORT FOR CONTRACT N00014-76-C-0066 (U) | Tracor Sciences and Systems | 771130 | ADC012607; NS; ND | U |
| Unavailable | Unavailable | LONG RANGE ACOUSTIC PROPAGATION PROJECT (LRAPP) | Xonics, Inc. | 771231 | ADB041703 | U |
| Unavailable | Homer, C. I. | SUS SOURCE LEVEL ERROR ANALYSIS ADA055606 | Underwater Systems, Inc. | 780120 | ND | U |
| Unavailable | Fitzgerald, R. M. | LOW-FREQUENCY LIMITATION OF FACT | Naval Research Laboratory | 780131 | ADA054371 | U |
| Unavailable | Unavailable | MIDWATER ACOUSTIC MEASUREMENT SYSTEM - PAR AND ACODAC | Texas Instruments, Inc. | 780228 | ADB039924 | U |
| ORI TR 1245 | Moses, E. J. | OPTIONS, REQUIREMENTS, AND RECOMMENDATIONS FOR AN LRAPP ACOUSTIC ARRAY PERFORMANCE MODEL | ORI, Inc. | 780331 | ND | U |
| Unavailable | Hosmer, R. F., et al. | COMBINED ACOUSTIC PROPAGATION IN EASTPAC REGION (EXERCISE CAPER): INITIAL ACOUSTIC ANALYSIS | Naval Ocean Systems Center | 780601 | ADB032496 | U |
| LRAPPRC78023 | Watrous, B. A. | LRAPP EXERCISE ENVIRONMENTAL DATA INVENTORY, JUNE 1978 (U) | Naval Ocean R&D Activity | 780601 | NS; ND | U |
| TR052085 | Solomon, L. P., et al. | HISTORICAL TEMPORAL SHIPPING (U) | Planning Systems Inc. | 780628 | NS; ND | U |



ENCL (1)